ISSN 1881-7831 Online ISSN 1881-784X

DD&T

Drug Discoveries & Therapeutics

Volume 18, Number 6
December, 2024

IRCA BSSA
IACMHR

www.ddtjournal.com

DD&T
Drug Discoveries & Therapeutics

ISSN: 1881-7831
Online ISSN: 1881-784X
CODEN: DDTRBX
Issues/Year: 6
Language: English
Publisher: IACMHR Co., Ltd.

Drug Discoveries & Therapeutics is one of a series of peer-reviewed journals of the International Research and Cooperation Association for Bio & Socio-Sciences Advancement (IRCA-BSSA) Group. It is published bimonthly by the International Advancement Center for Medicine & Health Research Co., Ltd. (IACMHR Co., Ltd.) and supported by the IRCA-BSSA.

Drug Discoveries & Therapeutics publishes contributions in all fields of pharmaceutical and therapeutic research such as medicinal chemistry, pharmacology, pharmaceutical analysis, pharmaceutics, pharmaceutical administration, and experimental and clinical studies of effects, mechanisms, or uses of various treatments. Studies in drug-related fields such as biology, biochemistry, physiology, microbiology, and immunology are also within the scope of this journal.

Drug Discoveries & Therapeutics publishes Original Articles, Brief Reports, Reviews, Policy Forum articles, Case Reports, Communications, Editorials, News, and Letters on all aspects of the field of pharmaceutical research. All contributions should seek to promote international collaboration in pharmaceutical science.

Editorial Board

Editorial and Head Office:

Pearl City Koishikawa 603,
2-4-5 Kasuga, Bunkyo-ku,
Tokyo 112-0003, Japan
E-mail: office@ddtjournal.com

Drug Discoveries & Therapeutics

Editorial and Head Office

Pearl City Koishikawa 603, 2-4-5 Kasuga, Bunkyo-ku,
Tokyo 112-0003, Japan

E-mail: office@ddtjournal.com
URL: www.ddtjournal.com

Editorial Board Members

CONTENTS

Volume 18, Number 6, 2024

Review

Original Article

Brief Report

Letter to the Editor

Review

DOI: 10.5582/ddt.2024.01087

Kampo medicine inducing drug-induced liver injury: A case report and systematic review

Akane Hoshi[1,2], Haruki Funakoshi[1,2], Yumi Otoyama[3], Hitoshi Yoshida[3], Kenji Momo[2,*]

[1] Department of Pharmacy, Showa University Hospital, Tokyo, Japan;
[2] Department of Hospital Pharmaceutics, School of Pharmacy, Showa University, Tokyo, Japan;
[3] Department of Medicine, Division of Gastroenterology, School of Medicine, Showa University, Tokyo, Japan.

SUMMARY Kampo medicine, comprising various conventional crude drug products, poses challenges in identifying adverse event causality. We present a case of severe liver injury following the administration of Saibokuto and attempted to identify the likely causative crude drug inducing liver injury through a systematic literature review. A 29-year-old woman developed severe liver injury approximately two months after Saibokuto administration, necessitating steroid pulse therapy for recovery. The literature search was conducted on February 15, 2023 in Japan. Using PubMed and the "Igaku Chuo Zasshi (ICHUSHI) database," two individuals independently selected studies published between January 1997 and February 15, 2023. The search focused on studies involving human subjects, published in either English or Japanese, and specifically investigated Kampo medicines categorized as over-the-counter or prescription drugs suspected as causative agents of drug-induced liver injury (DILI). Studies on health supplements, discontinued Kampo medicines, and autoimmune hepatitis, were excluded. As it is ethically impossible to rechallenge drugs that cause liver injury, this review primarily relied on case report literature. Through the review, 37 cases (men/women: 12/25, including present case) were analyzed, including 32 reports (36 cases) from 3,055 studies that met the inclusion criteria. Notably, 65.9% of cases were associated with Scutellariae radix, with onset occurring within 45 (1-730) days and recovery within 35 (7-184) days. Our case study and literature review underscore a prevalent association between liver injury and Kampo medicines containing Scutellariae radix. Vigilant liver function monitoring, particularly within the first 2 months of administration, is recommended, especially for formulations containing Scutellariae radix.

Keywords Kampo medicine, drug-induced liver injury, scutellariae radix, Saibokuto

1. Introduction

Recently, there has been a growing demand for complementary and alternative medicine (CAM) in the field of life sciences (*1*). CAM is extensively investigated as an approach to address various concerns related to cancer, such as pain, sleep disorders, fatigue, and relaxation, with practices such as yoga and meditation being widely utilized (*2,3*). Additionally, CAM therapies such as acupuncture and Ayurveda therapy have garnered significant attention for managing migraine headaches (*4*).

Among these alternative therapies, Kampo medicine holds a long history of use, particularly in Asian countries. In recent years, pharmaceutical companies have been marketing Kampo medicines as medicinal products, contributing to their growing utilization in the U.S. and other countries (*5,6*). In Japan, the use of Kampo medicines has evolved beyond the traditional "constitution-based" approaches to include evidence-based practices, integrating them into medical settings akin to Western medicine. Recent evidence indicated the widespread employment of Kampo medicine, including the use of "Yokukansan" for managing behavioral and psychological symptoms of dementia (BPSD) (*7*), "Daikenchuto" for post-abdominal surgery ileus (*8*), and "Kakkonto" for Coronavirus disease 2019 (COVID-19) (*9*). In 2021, out of 9.18 trillion yen in pharmaceutical production in Japan, approximately 208 billion yen was attributed to Kampo medicines and other related products. Since 2017, the overall production of Kampo medicines and related products, including those for general use, has increased by 21.7%, reflecting the recognition of their utility (*10,11*).

As the scope of indications for Kampo medicine continues to expand, patients from diverse backgrounds are receiving treatment. Consequently, adverse events not previously associated with Kampo medicine, such as interstitial lung disease (*12*), mesenteric phlebosclerosis (*13*), congestive heart failure (*14*), and drug-induced liver injury (DILI) (*15–17*), have been reported. This underscores the importance of updating safety information for Kampo medicines from a pharmacovigilance perspective.

In our recent experience, we encountered a patient who developed severe liver injury following the administration of Kampo medicine. In this manuscript, we present a case and provide a systematic review of information related to Kampo medicine-induced liver injury, aiming to comprehensively report our findings.

2. Materials and Methods

2.1. Ethics approval

The study was exempt from approval by the Institutional Review Board of Showa University, but written informed consent was obtained from patients for publication of this report in accordance with the journal's patient consent policy.

2.2. Literature survey

The literature search was conducted on February 15, 2023, at 6:00 PM in Japan. Two individuals independently selected relevant studies. The search focused on studies involving human subjects (adults or older), published in either English or Japanese, and specifically investigated Kampo medicines categorized as over-the-counter or prescription drugs suspected as the causative agents of DILI. The selected studies provided the patient information, admission examination findings, and treatment details related to drug-induced liver injuries. Kampo medicines are formulations that contain two or more crude drugs. Studies related to homeopathy, health supplements, herbal mixtures containing non-natural-derived components as primary ingredients, illegal drugs, recreational drugs, discontinued Kampo medicines, topical Kampo medicines, concomitant viral hepatitis, and autoimmune hepatitis were excluded. In addition, to limit liver injury caused by Kampo medicines, drugs that cause liver injury – anti-allergic agents, gout suppressants, hypoglycemic agents, anti-bacterial agents, anticonvulsants, antineoplastic agents, non-steroidal anti-inflammatory drugs, hydroxymethylglutaryl-CoA reductase inhibitors and acetaminophen, and liver injury associated with COVID-19 – were excluded.

Using PubMed and the "Igaku Chuo Zasshi (ICHUSHI) database," we conducted a literature search for studies published between January 1997 and February 15, 2023. The search terms for formula in PubMed were as follows: (((traditional chinese herb medicine) OR (traditional Chinese medicine) OR (Kampo) OR ("Medicine, East Asian Traditional"[Mesh])) AND ((Drug-induced liver injury)) OR ("Chemical and Drug Induced Liver Injury"[Mesh])) AND ((humans[Filter]) AND (1997/1/1:2022/12/31[pdat]) AND (English[Filter] OR Japanese[Filter]) AND (all adult[Filter]))NOT ("Anti-Allergic Agents"[Mesh]) NOT ("Gout Suppressants"[Pharmacological Action])NOT ("Hypoglycemic Agents"[Mesh]) NOT ("Anti-Bacterial Agents"[Mesh]) NOT ("Anticonvulsants"[Mesh]) NOT ("Antineoplastic Agents"[Mesh]) NOT ("Anti-Inflammatory Agents, Non-Steroidal"[Mesh]) NOT ("Hydroxymethylglutaryl-CoA Reductase Inhibitors"[Mesh]) NOT ("Acetaminophen"[Mesh]) NOT ("Antirheumatic Agents"[Mesh]) NOT ("COVID-19"[Mesh]). The search terms for formula in ICYUSHI database were as follows; Medical Database "ICYUSHI": ((((Liver diseases/TH or Hepatic disorder/AL)) and ((Kampo medicine/TH or Kampo medicine/AL))) and (DT=1997:2022 and LA=Japanese, English and PT=Original article, Excluding conference proceedings and (CK=Humans) and (CK=Adult (19-44), Middle-aged (45-64), Elderly (65 and over)))).

2.3. Analysis of cases collected through literature survey

We conducted a systematic review and analyzed the timeline of liver injury manifestations in the cases that we encountered, classifying them into three types: hepatocellular injury, cholestatic, and mixed type (*18*). The time to onset and the time to recovery of liver injury were divided into intervals of 1, 2, 3, 4, and 5 months.

Furthermore, we compiled a list of the Kampo medicines taken by the patients under investigation and categorized them according to their constituent components. We visually analyzed the relationship between the severity of liver injury using total bilirubin (T-bil), alanine aminotransferase (ALT), and alkaline phosphatase (ALP) values, and the components of Kampo medicine. To identify the potential components responsible for DILI, we calculated the proportion of cases with T-bil and ALT at grade 4, and ALP at grade 2 or higher, as assessed by Common Terminology Criteria for Adverse Events version 5.0 (CTCAE ver. 5.0).

3. Results

3.1. Case presentation

In September 2021, a 29-year-old woman was diagnosed with gastroesophageal reflux disease (GERD) and initiated treatment with vonoprazan. In July 2022, she sought care at a local clinic due to persistent pharyngeal discomfort and fullness, prompting the addition of Saibokuto to her medication regimen alongside

vonoprazan. By September 2022, she experienced sudden fatigue and difficulty walking, leading to a visit to the emergency department, where the cause remained unidentified. Subsequently, Rikkunshito was incorporated into her treatment regimen. The next day, feeling generally unwell, she revisited her local clinic, and further sulpiride was added to her medication regimen.

In October 2022, while still adhering to vonoprazan, Saibokuto, Rikkunshito, and sulpiride, the patient developed jaundice and brownish urine. Concerned about potential liver injury, she consulted her primary care physician, who immediately admitted her to the hospital on October 5th. Upon admission (day 1), her blood test results showed elevated levels of ALP at 103 U/L, aspartate aminotransferase (AST) at 1,476 U/L, ALT at 1,263 U/L, T-bil at 11.6 mg/dL, direct bilirubin (D-bil) at 6.8 mg/dL, and a prolonged prothrombin time (PT) at 73%. These results indicated grade 4 severity for ALT, AST, T-bil, and D-bil, according to CTCAE ver. 5.0. DILI was suspected to be the cause of severe hepatic dysfunction, prompting discontinuation of vonoprazan, Saibokuto, Rikkunshito, and sulpiride. Despite extensive examinations, including abdominal ultrasonography and computed tomography, the specific cause of liver injury remained unidentified.

On day 7, her blood test results showed improvements in ALP (84 U/L), AST (1,075 U/L), ALT (1,021 U/L), T-bil (17 mg/dL), and D-bil (12.6 mg/dL), with PT at 68%. On day 8, the patient was transferred to Showa University Hospital. Upon admission, she presented with generalized jaundice, yellowing of the skin, and yellowing of the eyes. Her blood test results at Showa University Hospital showed ALP at 91 U/L, AST at 969 U/L, ALT at 1,007 U/L, T-bil at 19.1 mg/dL, D-bil at 14.4 mg/dL, and PT at 60%. Based on the Roussel-Uclaf Causality Assessment Method (RUCAM) (*19*) scoring of diagnostic criteria for DILI (*18*), she received a score of 9 points, raising suspicion of DILI of the hepatocellular injury type. In addition, a drug-induced lymphocyte stimulation test (DLST) and liver biopsy were performed using the suspected drugs vonoprazan, Saibokuto, Rikkunshito, and sulpiride. On day 9, she received a steroid pulse (methylprednisolone injection 1,000 mg/body) for 3 days, and on day 13, her laboratory findings showed improvements with AST at 56 U/L, ALT at 218 U/L, T-bil at 3.9 mg/dL, and D-bil at 1.6 mg/dL. On day 15, the DLST results indicated a stimulation index of 9.4 for Saibokuto, leading to a diagnosis of DILI due to Saibokuto. On day 18, her condition improved further with AST at 55 U/L, ALT at 125 U/L, T-bil at 3.3 mg/dL, and D-bil at 0.7 mg/dL, and she was discharged. At her first outpatient visit on day 23 after discharge, her blood test results showed AST at 40 U/L, ALT at 67 U/L, T-bil at 2.6 mg/dL, D-bil at 0.5 mg/dL, and overall improvement of jaundice (Figure 1).

3.2. Systematic review results and background of study patients

A total of 3,055 articles were extracted, including 2,663 articles from PubMed, and 390 articles from the "ICYUSHI database", and 2 articles from a manual search. Among them, 12 articles were excluded due to duplication between PubMed and "ICYUSHI database", 2,809 articles were excluded based on their titles, and an additional 173 articles were excluded based on their abstracts (Figure 2). The remaining articles were evaluated by two reviewers for publication year, patient characteristics (age, sex, and medical history), number of days until liver injury manifestation, severity of liver injury, suspected Kampo medicines, sources of Kampo medicines, and number of days until recovery. Following this assessment, 32 case reports/case series studies and our presented cases involving 37 patients including present case were selected for the final analysis (Table 1).

The limitation of this systematic review is that re-administration of the drug causing liver injury may lead to anaphylaxis, and prospective clinical trials are difficult to conduct; thus, the results of the literature review focused on case reports.

3.3. Types of liver injury and days to liver injury manifestation in study patients

The median age of the patients (12 men and 25 women) was 53 years (range: 29–78 years). Their medical history included hypertension, diabetes, and cholecystolithiasis. The median number of days until liver injury manifestation for all patients was 45 (range: 1–730), and the median time to recovery was 35 days (range: 7–184) (Table 1). Among the patients, 18 had hepatocellular injury-type liver injury, 8 had cholestatic injury, and 11 had mixed injury. Patients who developed liver injury within one month after initiation of suspected Kampo medicines had the highest frequency, accounting for 37.8% of the total cases. For the hepatocellular injury type, the majority of patients developed liver injury within 1 month, whereas for the cholestatic type, 100% developed liver injury within 3 months. There were no significant differences in the time period from Kampo medicine intake to liver injury manifestation in the mixed type (Figure 3). Most patients recovered within 2 months of treatment after discontinuing Kampo medicine, accounting for 83.8% of all patients. The percentages of patients who recovered after more than 2 months were 2.7, 5.4, and 8.1% for the hepatocellular injury, cholestatic, and mixed types, respectively (Figure 3).

3.4. Liver injury severity and characteristics of constituent components in Kampo medicines

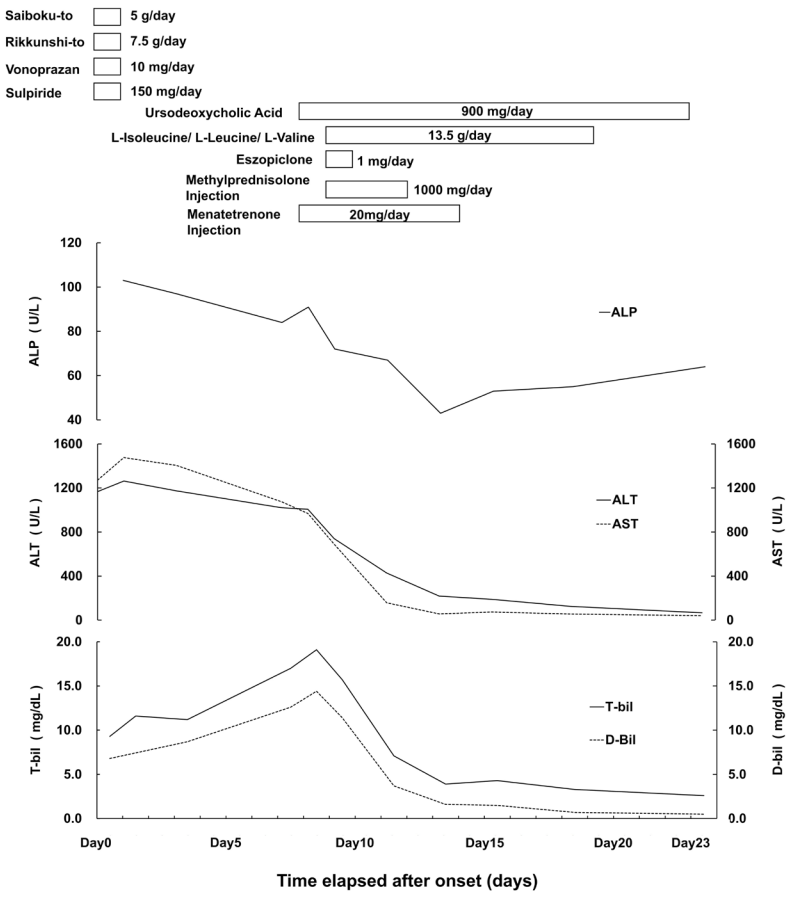

Figure 1. Clinical course of the present case. Description of the liver function laboratory values and medication history of a 29-year-old woman after hospital admission.

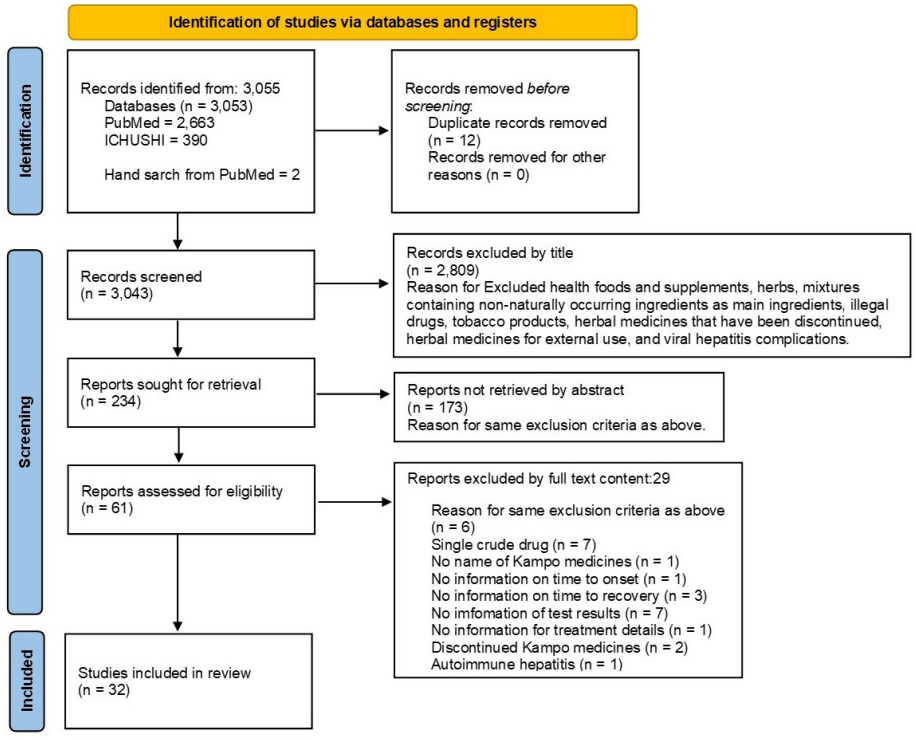

Figure 2. Systematic review of PRISMA flow diagram. Flowchart showing the literature survey on Kampo medicine-induced liver injury from PubMed and ICYUSHI databases.

Table 1. Kampo medicines inducing liver injury from literature survey

Author	Year	Age (years)	Gender	Medical history	Suspect drug source	Suspect drug	Type of DILI	Time to onset of DILI (days)	The Grade of T-bil / ALT/ALP/	Time to recovery from DILI (days)	Treatment
Yoshikubo, *et al.* (*20*)	1997	31	Female	12 weeks of pregnancy	Prescription drug	Bukuryoingohangekobokuto	Hepatocellular injury type	42	4/4/0	37	Suspect drug stopped, Plasma exchange, hemodialysis and mPSL 1000 mg/day 2 days
Matsuda, *et al.* (*21*)	1997	65	Male	Diabetes	Prescription drug	Daisaikoto	mixed type	50	1/4/2	50	Suspect drug stopped
Shiota, *et al.* (*22*)	1997	78	Female	Rheumatoid arthritis	Over-the-counter drugs	Hangeshoshinto	Cholestatic type	10	0/2/1	57	Suspect drug stopped
Takeshima, *et al.* (*23*)	1997	49	Female	Duodenal ulcer	Prescription drug	Shosaikoto	Mixed type	100	0/4/2	30	Suspect drug stopped
Nakai, *et al.* (*24*)	1998	71	Male	None	Over-the-counter drugs	Shakuyakukanzoto	cholestatic type	21	4/3/3	45	Suspect drug stopped, UDCA, and GA
Okada, *et al.* (*25*)	1999	60	Male	Hypertension	Prescription drug	Hangeshoshinto	Cholestatic type	60	0/2/2	60	Suspect drug stopped and GA
Nagai, *et al.* (*26*)	1999	49	Female	Internal hemorrhoid	Prescription drug	Otsujito	Hepatocellular injury type	101	0/4/2	28	Suspect drug stopped and GA
Kamioka, *et al.* (*27*)	1999	46	Female	None	Over-the-counter drugs	Unseiin	Hepatocellular injury type	300	0/4/1	25	Suspect drug stopped and GA
Kurai, *et al.* (*28*)	2000	48	Female	None	Prescription drug	Otsujito	Hepatocellular injury type	69	1/4/2	93	Suspect drug stopped, UDCA, and GA
Ozawa, *et al.* (*29*)	2001	46	Female	Hypertension	Prescription drug	Bofutsusyosan	Mixed type	425	4/3/1	80	Suspect drug stopped, Plasma exchange, Hemodialysis, UDCA, GA, and mPSL 1000 mg/day 3 days
Ishii, *et al.* (*30*)	2001	64	Male	Myocardial infarction	Over-the-counter drugs	Pian tze huang	Mixed type	305	0/3/1	28	Suspect drug stopped, UDCA, and GA
Kamigaki, *et al.* (*31*)	2001	66	Male	Hypertension	Prescription drug	Kakkonto	Mixed type	10	2/2/1	51	Suspect drug stopped, UDCA, and GA
Tani, *et al.* (*32*)	2001	57	Male	None	Prescription drug	Saibokuto	Cholestatic type	9	2/1/2	36	Suspect drug stopped, UDCA, GA, and PSL 30 mg/day tapered off.
Gabriella, *et al.* (*33*)	2002	48	Male	Psoriasis	Over-the-counter drugs	Fu Fang Qing Dai Wan	Hepatocellular injury type	30	2/4/2	56	Suspect drug stopped.
Yamamoto, *et al.* (*34*)	2003	35	Male	None	Prescription drug	Bofutsusyosan	Hepatocellular injury type	215	4/4/3	36	Suspect drug stopped and UDCA
Hosonuma, *et al.* (*35*)	2003	42	Female	None	Over-the-counter drugs	Saikokeishikankyoto	Hepatocellular injury type	30	1/4/2	31	Suspect drug stopped.
Hosonuma, *et al.* (*35*)	2003	42	Female	None	Prescription drug	Nyoshinsan	Hepatocellular injury type	1	0/4/2	14	Suspect drug stopped.
Li-Ming, *et al.* (*36*)	2006	52	Female	Cholecystolithiasis	Prescription drug	Shosaikoto	Hepatocellular injury type	45	1/4/1	54	Suspect drug stopped.

UDCA: Ursodeoxycholic acid, GA: glycyrrhizin acid, T-bil: total bilirubin, ALT: alanine aminotransferase, ALP: alkaline phosphatase.

Table 1. Kampo medicines inducing liver injury from literature survey (continued)

Author	Year	Age (years)	Gender	Medical history	Suspect drug source	Suspect drug	Type of DILI	Time to onset of DILI (days)	The Grade of T-bil / ALT/ALP/	Time to recovery from DILI (days)	Treatment
Uchiyama, *et al.* (*37*)	2007	54	Male	Diabetes, Hypertension, Myocardial infarction	Prescription drug	Hangeshoshinto	Hepatocellular injury type	4	4/4/3	59	Suspect drug stopped, UDCA, and PSL 40 mg/day followed by mPSL 1000 mg/day 3 days
Motoyama, *et al.* (*38*)	2008	37	Female	None	Over-the-counter drugs	Bofutsusyosan	Hepatocellular injury type	60	4/4/3	20	Suspect drug stopped, GA, and PSL 40 mg/day
Irie, *et al.* (*39*)	2008	55	Female	None	Prescription drug	Nyoshinsan, Saffron	Mixed type	94	4/4/3	35	Suspect drug stopped and UDCA
Sannomiya, *et al.* (*40*)	2009	54	Female	Hypertension	Prescription drug	Bofutsusyosan	Hepatocellular injury type	21	2/4/1	15	Suspect drug stopped and GA
Sannomiya, *et al.* (*40*)	2009	52	Female	Basedow's disease	Prescription drug	Bofutsusyosan	Hepatocellular injury type	120	2/4/2	36	Suspect drug stopped, UDCA, and GA
Tanaka, *et al.* (*41*)	2011	32	Male	None	Over-the-counter drugs	Bofutsusyosan	Cholestatic type	60	4/4/3	20	Suspect drug stopped.
Futenma, *et al.* (*42*)	2012	68	Female	Knee osteoarthritis	Prescription drug	Boiogito	Mixed type	35	0/2/1	35	Suspect drug stopped.
Futenma, *et al.* (*42*)	2012	72	Female	Hypertension	Prescription drug	Boiogito	Cholestatic type	21	2/2/2	7	Suspect drug stopped
Negishi, *et al.* (*43*)	2014	57	Male	None	Prescription drug	Hochuekkito	Cholestatic type	7	4/3/2	184	Suspect drug stopped, UDCA, and GA
Maruyama, *et al.* (*44*)	2014	61	Female	Diabetes, Dyslipidemia, Hypertension	Prescription drug	Saireito	Mixed type	29	1/4/3	120	Suspect drug stopped
Dohmen, *et al.* (*45*)	2015	43	Female	Anxiety neurosis, Dyslipidemia, Sinusitis	Prescription drug	Shin'iseihaito	Mixed type	75	2/4/3	42	Suspect drug stopped
Oikawa, *et al.* (*46*)	2015	58	Female	None	Prescription drug	Saikokeishikankyoto	Mixed type	7	0/2/1	14	Suspect drug stopped
Ozeki, *et al.* (*47*)	2017	51	Female	None	Prescription drug	Bofutsusyosan	Hepatocellular injury type	60	2/4/2	9	Suspect drug stopped
Shimada, *et al.* (*48*)	2018	67	Female	Cholecystolithiasis	Prescription drug	Shosaikoto	Cholestatic type	4	1/2/1	15	Suspect drug stopped
Shimada, *et al.* (*48*)	2018	68	Female	Cholecystolithiasis	Prescription drug	Saikokeishikankyoto	Hepatocellular injury type	21	1/4/2	33	Suspect drug stopped
Shinohara, *et al.* (*49*)	2019	60s	Male	Atrial fibrillation, Cerebral infarction	Over-the-counter drugs	Ryutanshakanto	Hepatocellular injury type	730	1/4/2	12	Suspect drug stopped, UDCA, and GA
Yamamoto, *et al.* (*50*)	2020	36	Female	Irritable bowel syndrome	Prescription drug	Keishakuchimoto, Kamikihito	Mixed type	112	0/1/0	77	Suspect drug stopped
Funakoshi, *et al.* (*17*)	2021	59	Female	Lung cancer	Prescription drug	Hanshiren, Zenshikunshito, Ninjin'yoeito	Hepatocellular injury type	16	2/4/2	14	Suspect drug stopped
Our case	2022	29	Female	None	Prescription drug	Saibokuto	Hepatocellular injury type	76	4/4/1	18	Suspect drug stopped, UDCA, and mPSL 1000 mg/day 3 days

UDCA: Ursodeoxycholic acid, GA: glycyrrhizin acid, T-bil: total bilirubin, ALT: alanine aminotransferase, ALP: alkaline phosphatase.

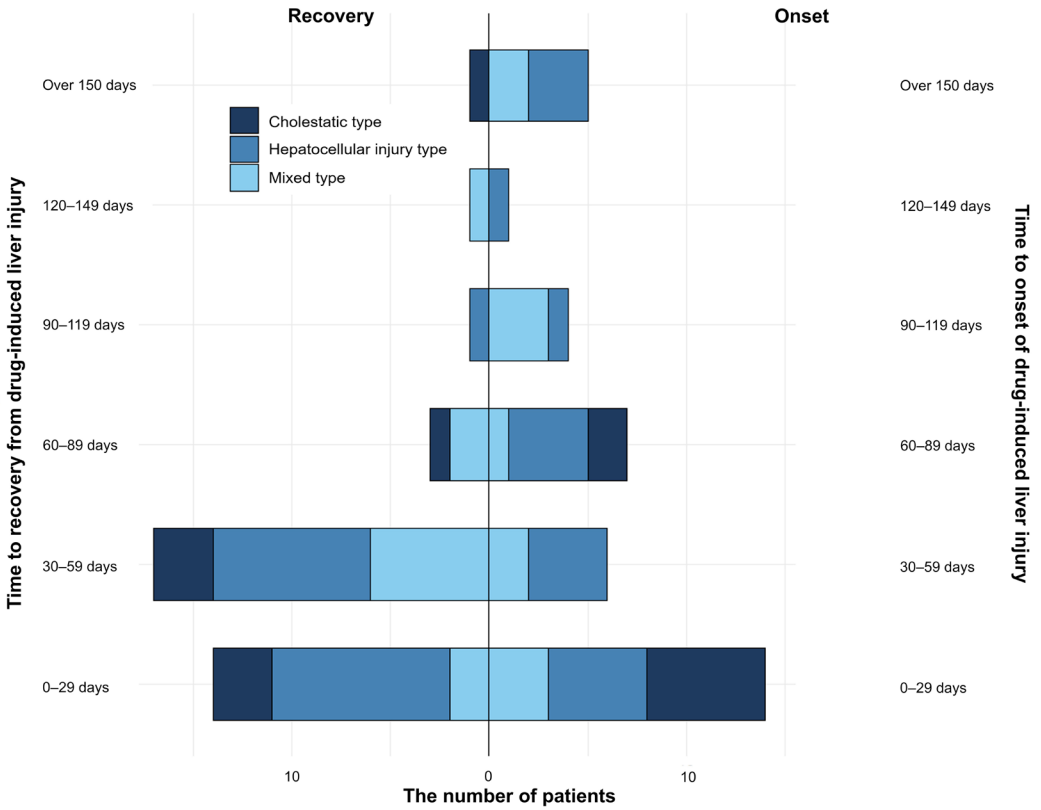

Figure 3. Time to onset and recovery by type of drug-induced liver injury. Time to onset and time to recovery from drug-induced liver injury are shown for cases from the literature survey.

Regarding the suspected Kampo medicines responsible for liver injury in the study patients, Bofutsushosan was reported in 7 cases, whereas Saikokeishikankyoto, Shosaikoto, and Hangeshashinto were each reported in 3 cases. Among these, 28 cases involved Kampo medicines categorized as prescription drugs, and nine cases involved Kampo medicines categorized as over-the-counter drugs. In this systematic review, 41 drugs were suspected in 37 cases investigated. A heatmap was created for each patient to illustrate the constituent components of the suspected Kampo medicines related to liver injury. According to the heatmap for T-bil grade 4 level, Glycyrrhizae radix (24.3%) was most frequently found in suspected Kampo medicines, followed by Scutellariae radix (18.9%) and Zingiberis rhizoma (18.9%) (Figure 4). Similarly, for ALP grade 2 level, the order was Glycyrrhizae radix (43.2%), Scutellariae radix (40.5%), and Zingiberis rhizoma (29.7%) (Figure 4), whereas for ALT grade 4, Scutellariae radix (56.8%) was the most frequently found in suspected Kampo medicines, followed by Glycyrrhizae radix (51.6%), Zingiberis rhizoma (35.1%), and Angelicae radix (35.1%) (Figure 4). Glycyrrhizae radix and Scutellariae radix are commonly found in suspected Kampo medicines associated with liver injury based on T-bil, ALT, and ALP levels.

4. Discussion

In this study, we present cases of severe liver injury associated with Kampo medicine, a traditional medicine widely used in Japan. Additionally, we conducted a systematic review to compile data on Kampo medicine-induced liver injury, focusing on the differences in the types of liver injury and the time of manifestation.

The patients that we encountered had a history of alcohol consumption approximately once every 1 to 2 months. Upon admission, tests for hepatitis A, B, C, and E, cytomegalovirus infection, and Epstein-Barr virus infection were all negative. Antinuclear antibodies were also negative, and liver biopsy did not reveal any abnormalities. DILI can be classified as hepatocellular, cholestatic, and mixed type (*18,51*). In this case, hepatocellular injury with jaundice was present, necessitating hospitalization due to the high risk of severe liver failure and poor outcomes (*52*). This type of hepatocellular injury was the most frequent type of liver injury observed in this systematic review. Furthermore, the time-to-onset of adverse events was consistent with the early onset type.

Treatment of DILI hepatoprotective drugs (*53*). In our cases, improvement was not observed upon discontinuation but was achieved through steroid pulse

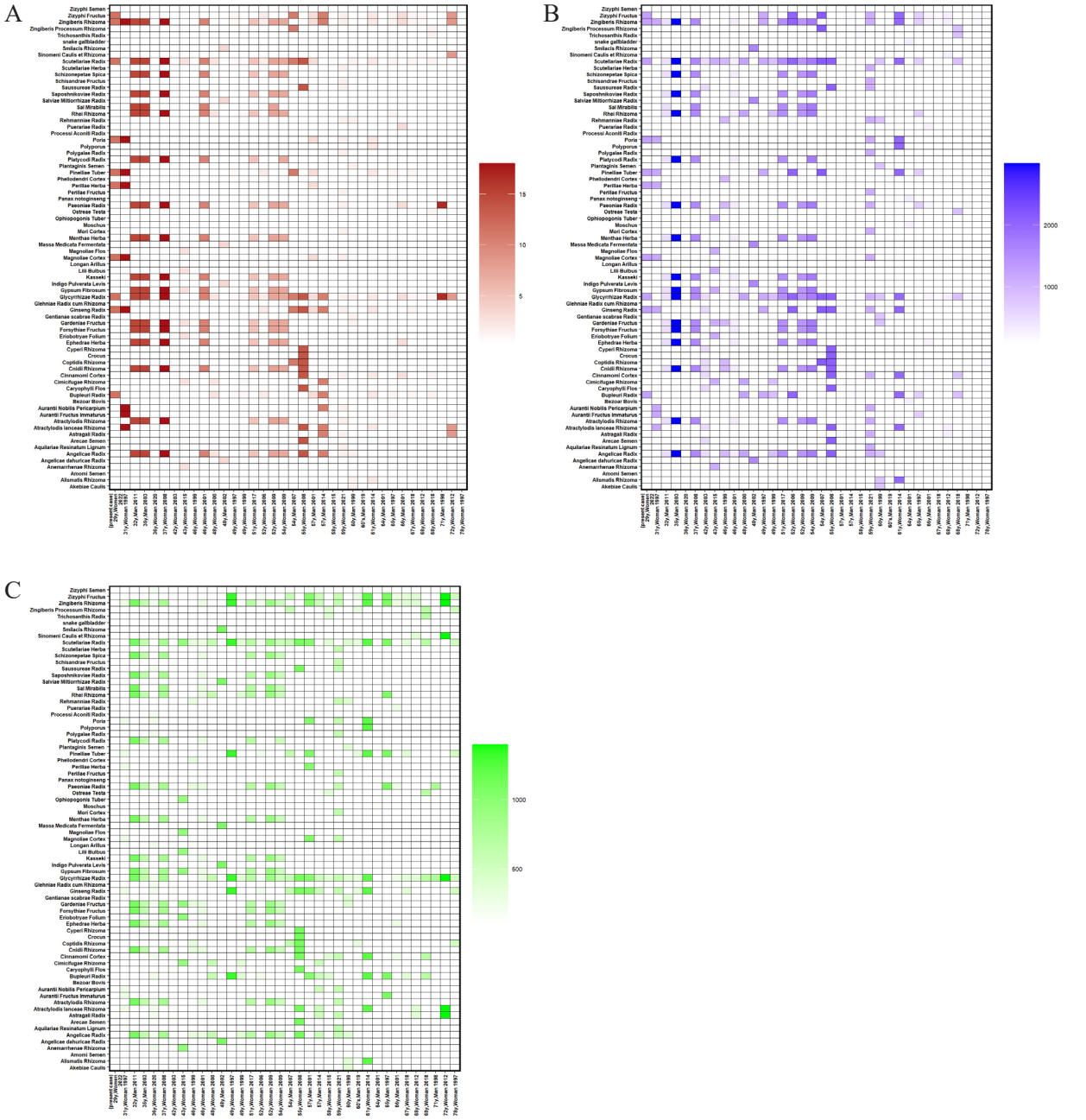

Figure 4. Severity of Kampo medicines inducing liver injury based on cases from literature survey. The correlation between the severity of Kampo medicines and the laboratory values for each patient in the literature survey is displayed in the color shade. (**A**) T-bil, (**B**) ALT, and (**C**) ALP. T-bil: total bilirubin, ALT: alanine aminotransferase, ALP: alkaline phosphatase.

therapy. A systematic review found two cases (*34,49*) of hepatocellular injury requiring plasma exchange and hemodialysis, both with severe liver injury that improved after steroid pulse therapy. However, in both cases, the liver injury improved the day after the steroid pulse, which is similar to the present case. As acute liver failure occurs in severe cases of DILI, steroid pulse therapy may be used to prevent severe disease (*54,55*). Early steroid pulse therapy is believed to inhibit the progression of liver failure by suppressing hepatocyte destruction and microvascular damage via the immune response (*56*), and our patient also recovered quickly and was discharged from the hospital after steroid pulse therapy.

In this systematic review, we primarily relied on case report literature to evaluate the drugs that cause liver injury, the time to onset, the time to recovery, and the severity of the injury that needed to be assessed. According to the results of this systematic review, 41 components of suspected Kampo medicines contained 80.5% Glycyrrhizae radix and 65.9% Scutellariae radix. Glycyrrhizae radix has been frequently reported to cause pseudoaldosteronism, whereas Scutellariae radix is commonly associated with interstitial pneumonia and liver injury. Specifically, Scutellariae radix was found in 27 formulations (65.9%), including Bofutsushosan, Hangeshashinto, Nyoshinsan, Otsujito, Ryutanshakanto,

Saibokuto, Saireito, Shin'iseihaito, and so on. The possibility of Scutellariae radix as a cause of DILI has been considered in previous studies (*57,58*).

Glycyrrhizae radix is present in 73.6% of Japanese medicinal Kampo medicines (*11*). To the best of our knowledge, Glycyrrhizae radix associated DILI has never been reported before. Glycyrrhizin, a major component of Glycyrrhizae radix, and its metabolite glycyrrhetinic acid acts on hepatocyte cell membranes, reducing enzymes release from hepatocytes and exerting a protective effect on hepatocytes (*59*). Furthermore, it has been suggested that baicalin, the major component of Scutellariae radix, may act as a hapten, causing allergic reactions and resulting in cellular damage (*60*). Additionally, in the present case, the patient was administered with Saibokuto, which contains both Glycyrrhizae radix and Scutellariae radix, and Rikkunshito, which contains Glycyrrhizae; however, but the DLST results in this case were positive for Saibokuto. When Rikkunshito was added, the patient was already suffering from fatigue and anorexia, which are early symptoms of liver injury. It has been suggested that careful consideration is required, especially for Kampo medicines containing Scutellariae radix.

Many Kampo medicines contain Scutellariae radix, which is also found in over-the-counter drugs (*57*). Owing to the recent increase in CAM use, the number of suspected cases of DILI caused by Kampo medicine is expected to increase. Since cases involving Scutellariae radix may be severe, as in this case, it is important to confirm the formulation of Kampo medicine, take appropriate action, and instruct the patient to avoid future use of both medical and over-the-counter medications.

Kampo medicines contain multiple active ingredients with diverse therapeutic effects. However, identifying the specific cause becomes challenging (*53*). Moreover, rechallenging patients carries a high risk, the cause of which remains unclear. Therefore, conducting a prospective study is ethically challenging. In addition, the literature review focuses on case reports of liver injury caused by Kampo medicines. It is important to note that the study may be biased due to the small proportion of Kampo medicines used in comparison to Western medicines and the fact that case reports of Kampo medicines are not very common.

5. Conclusions

In this study, we compiled information on Kampo medicine-induced liver injury and highlighted the possibility of different time to onset for each type of liver injury, and the likelihood of Scutellariae radix as a suspected component. In the medical field, particularly when administering Kampo medicines containing Scutellariae radix, monitoring liver function for at least two months from the start of administration may be crucial owing to the potential risk of hepatotoxicity.

Funding: None.

Conflict of Interest: The authors have no conflicts of interest to disclose.

References

1. Eisenberg DM, Davis RB, Ettner SL, Appel S, Wilkey S, Van Rompay M, Kessler RC. Trends in alternative medicine use in the United States, 1990-1997: results of a follow-up national survey. JAMA. 1998; 280:1569-1575.
2. Kristoffersen AE, Wider B, Nilsen JV, Bjelland M, Mora DC, Nordberg JH, Broderstad AR, Nakandi K, Stub T. Prevalence of late and long-term effects of cancer (treatment) and use of complementary and alternative medicine in Norway. BMC Complement Med Ther. 2022; 22:322.
3. Greenlee H, DuPont-Reyes MJ, Balneaves LG, Carlson LE, Cohen MR, Deng G, Johnson JA, Mumber M, Seely D, Zick SM, Boyce LM, Tripathy D. Clinical practice guidelines on the evidence-based use of integrative therapies during and after breast cancer treatment. CA Cancer J Clin. 2017; 67:194-232.
4. Soman A, Venkatram S, Chikkanna U, Ramakrishna KK, Bhargav H, Mailankody P, Varambally S. Ayurveda for management of migraine: A narrative review of clinical evidence. J Fam Med Prim Care. 2022; 11:4228-4235.
5. Ernst E. The efficacy of herbal medicine – an overview. Fundam Clin Pharmacol. 2005; 19:405-409.
6. Ahmad Khan MS, Ahmad I. Herbal Medicine. In: New Look to Phytomedicine. Elsevier; 2019; pp. 3-13. *https://linkinghub.elsevier.com/retrieve/pii/B978012814619400001X*. (accessed January 11, 2023)
7. Mizukami K, Asada T, Kinoshita T, *et al.* A randomized cross-over study of a traditional Japanese medicine (kampo), yokukansan, in the treatment of the behavioural and psychological symptoms of dementia. Int J Neuropsychopharmacol. 2009; 12:191-199.
8. Ishizuka M, Shibuya N, Nagata H, Takagi K, Iwasaki Y, Hachiya H, Aoki T, Kubota K. Perioperative administration of traditional Japanese herbal medicine Daikenchuto relieves postoperative ileus in patients undergoing surgery for gastrointestinal cancer: A systematic review and meta-analysis. Anticancer Res. 2017; 37:5967-5974.
9. Takayama S, Namiki T, Arita R, *et al*. Multicenter, randomized controlled trial of traditional Japanese medicine, kakkonto with shosaikotokakikyosekko, for mild and moderate coronavirus disease patients. Front Pharmacol. 2022; 13:1008946.
10. Production dynamics of Chinese herbal preparations, *etc*. From "Annual Report on the Current State of Pharmaceutical Industry Production" in 2017. Japan Kampo Medicine Manufacturers Association; 2019. *https://www.nikkankyo.org/serv/movement/h29/all.pdf* (accessed December 20, 2023). (in Japanese)
11. Production dynamics of Chinese herbal preparations, *etc*. From "Annual Report on the Current State of Pharmaceutical Industry Production" in 2021. Japan Kampo Medicine Manufacturers Association; 2023. *https://www.nikkankyo.org/serv/movement/R03/all. pdf* (accessed December 20, 2023). (in Japanese)
12. Enomoto Y, Nakamura Y, Enomoto N, Fujisawa T, Inui N, Suda T. Japanese herbal medicine-induced pneumonitis: A

review of 73 patients. Respir Investig. 2017; 55:138-144.
13. Nagata Y, Watanabe T, Nagasaka K, Yamada M, Murai M, Takeuchi S, Murase M, Yazaki T, Murase T, Komatsu K, Kaizuka M, Sano M, Asano K, Ando C, Taniuchi N. Total dosage of gardenia fruit used by patients with mesenteric phlebosclerosis. BMC Complement Altern Med. 2016; 16:207.
14. Washino M, Oguri M, Kamiya H. A case of congestive heart failure caused by pseudoaldosteronism. Heart. 2017; 49:476-480. (in Japanese)
15. Jing J, Teschke R. Traditional Chinese medicine and herb-induced liver injury: Comparison with drug-induced liver injury. J Clin Transl Hepatol. 2018; 6:57-68.
16. Navarro VJ, Khan I, Björnsson E, Seeff LB, Serrano J, Hoofnagle JH. Liver injury from herbal and dietary supplements. Hepatol Baltim Md. 2017; 65:363-373.
17. Funakoshi H, Momo K, Kashima A, Ida H, Miyata Y, Sagara H, Sasaki T. Liver injury by the traditional Chinese medicine Hanshirento, Zenshikunshito, and Ninjin'yoeito in a patient with lung cancer: Probable causality assessed by the updated Roussel Uclaf Causality Assessment Method. Integr Cancer Ther. 2021; 20:15347354211004734.
18. Takikawa H, Morikazu O, Takamori Y, Murata Y, Taniguchi H, Ito T, Masaaki W, Minoru A, Naoto M, Minoru N, Hiroyuki M, Shigeru O, Akiko H, Tomonori S. Proposal of diagnostic criteria of drug induced hepatic injury in DDW-J2004 workshop. Acta Hepatologica Japonica. 2005; 46:85-90. (in Japanese)
19. Danan G, Teschke R. RUCAM in Drug and Herb Induced Liver Injury: The Update. Int J Mol Sci. 2015; 17:14.
20. Yoshikubo S, Kimura K, Mizutari K, Kamo S, Maeda K. A case of drug-induced liver injury due to bukuryo-in-go-hange-koboku-to. Nihon Shokakibyo Gakkai Zasshi. 1997; 94:564-568. (in Japanese)
21. Matsuda R, Takahashi D, Chiba E, Kawana I, Tomiyama M, Ebira H, Ikegami T, Kitamura H, Ishii M. A case of drug induced hepatitis and interstitial pneumonia caused by a herbal drug, Dai-saiko-to. Nihon Shokakibyo Gakkai Zasshi. 1997; 94:787-791. (in Japanese)
22. Shiota G, Oyama K, Mitsuda A, Idobe Y, Tomie Y, Harada K, Kishimoto Y. A case of drug-induced liver injury due to Hangeshashinto. New Horiz Med. 1997; 29:3041-3043. (in Japanese)
23. Takeshima F, Omagari K, Oda H, Mizuta Y, Makiyama K, Kouno S. A case of liver injury induced by a herbal drug (Sho-saiko-to). Gastroenterology. 1997; 24:579-582. (in Japanese)
24. Nakai T, Kioka K, Sano K, Aoki T, Moriyoshi Y, Kurai O, Nebiki H, Okawa K, Oka H, Harihara S, Ohba H, Sou K, Kuroki T. A case of drug-induced liver injury by Chinese digestive medicine. Nihon Shokakibyo Gakkai Zasshi. 1998; 95:1374-1377. (in Japanese)
25. Okada H, Watanabe K, Suzuki S, Suzuki K, Ito T, Muranushi A, Kuramochi S, Tsuchimoto K, Ishino S, Hanawa T. A case of hepatitis and interstitial pneumonitis induced by Hangeshashin-to and Shosaiko-to. Kampo Med. 1999; 50:57-65. (in Japanese)
26. Nagai K, Hosaka H, Ishii K, Shinohara M, Sumino Y, Nonaka H, Akima M, Yamamuro W. A Case by Report: Acute Hepatic lnjury lnduced by Formula secundarius-haemorrhoica. J Med Soc Toho. 1999; 46:311-317.
27. Kamioka R, Kamioka T, Kitauchi S, Shiotani A, Nakata H, Hara T, Kawai J, Ito H, Nishioka S. A case of drug-induced liver injury caused by Unseiin. Gastroenterology. 1999; 29:231-236. (in Japanese)
28. Kurai O, Kawasaki Y, Kioka K, Oka H, Harihara S. A case of drug-induced hepatitis with severe intrahepatic cholestasis due to Otsuji-to. Gastroenterology. 2000; 31:68-473. (in Japanese)
29. Ozawa T, Watanabe H, Okuyama Y, Okumura K, Tsuchiya T, Tanji N, Anzai Y, Unakami M. A case of drug induced liver injury caused by a herbal drug, bofu-tsu-sho-san. Nihon Shokakibyo Gakkai Zasshi. 2001; 98:416-420. (in Japanese)
30. Ishii Y, Uemura M, Kojima H, Yasu S, Sakurai S, Fukui H. A case of drug-induced liver damage caused by Gya-tan in a Pain Zi Huang. Acta Hepatologica Japonica. 2001; 42:455-459. (in Japanese)
31. Kamigaki M, Nakazawa I, Kumei Y, Hayashi N, Takasugi Y. A case of drug-induced liver injury due to Kakkonto. Intern Med. 2001; 87:801-803.
32. Tani M, Hayashi Y, Okamoto S, Yokohama S, Inaba M, Kubota H, Nakamura K. Rapid improvement of icterus and pruritus by the oral administration of colestimide in two cases of drug-induced hepatitis. Intern Med. 2001; 40:1098-1103.
33. Gabriella V, Leonardo C, Luciano A, Francesco C. Acute hepatitis induced by traditional Chinese herbs used in the treatment of psoriasis. J Gastroenterol Hepatol. 2002; 17:1342-1343.
34. Yamamoto H, Tanaka A, Kitagawa S, Suzuki K, Fujita Y, Maruyama M. A case with acute hepatic failure during long administration of "Bofu-Tsusyosan." Acta Hepatologica Japonica. 2003; 44:579-485. (in Japanese)
35. Hoshonuma K, Yuasa K, Yamada S, Takagi H, Mori M. A case of reproducible hepatic injury induced by three kinds of herbal medicine. Acta Hepatologica Japonica. 2003; 44:32-36. (in Japanese)
36. Hsu LM, Huang YS, Tsay SH, Chang FY, Lee SD. Acute hepatitis induced by Chinese hepatoprotective herb, xiao-chai-hu-tang. J Chin Med Assoc. 2006; 69:86-88.
37. Uchiyama M, Ogata K, Hara S, Irie M, Sakisaka S, Futagami K. A Severe Case of Hepatitis lnduced by a Herbal Medicine Hangeshashinto. Nihon Byoin Yakuzaishikai Zasshi. 2007; 43:1182-1185. (in Japanese)
38. Motoyama H, Enomoto M, Yasuda T, Fujii H, Sawako K, Shuji I, Hiroyasu M, Tadashi T, Akihiro T, Hiroki S, Norifumi K. Drug-induced liver injury caused by an herbal medicine, bofu-tsu-sho-san. Nihon Shokakibyo Gakkai Zasshi. 2008; 105:1234-1239. (in Japanese)
39. Irie M, Fukushima K, Matsumoto T, *et al.* A case of the drug-induced hepatic injury by Nyoshin-san and Saffron-K. Acta Hepatologica Japonica. 2008; 49:166-170. (in Japanese)
40. Sannomiya N, Matsusita T, Takahashi Y, Ito Y, Nakamura T, Goto H, Takaaki A. Two cases of liver damage thought to be caused by Bofutsushosan. Gifu Sekijuji Byoin Igaku Zasshi. 2009; 21:17-24. (in Japanese)
41. Tanaka H, Koga F, Baba S. A case of drug-induced liver injury due to jaundice caused by over-the-counter drug Bofu-Tsusho-San. Jpn J Clin Exp Med. 2011; 88:883-886. (in Japanese)
42. Futenma C, Uehara T, Kikuzato N, Shimabukuro Y. Discussion of drug-induced liver injury due to Boiogito. Pain and Kampo Med. 2012; 22:91-94.
43. Negishi R, Ichikawa T, Yoshiyuki T, Akira F, Sayo T, Akira T, Kimika A, Masataka K, Hiroshi S, Sae O, Nobuaki M, Yuh F, Itaru O, Masayuki F. Liver injury and hepatic encephalopathy induced by the herbal medicine

Hochuekkito. Nihon Shokakibyo Gakkai Zasshi. 2014; 111:1149-1156. (in Japanese)
44. Maruyama Y, Yoshizawa K, Tsuruta F, Maruyama M, Fujimori K, Shigeno S, Mana F, Takeshi U, Susumu M, Satoshi S, Takeji U, Eiji T. A case of repeated liver injury induced by different herbal medicines containing the same components. Acta Hepatologica Japonica. 2014; 55:214-220. (in Japanese)
45. Dohmen K, Tanaka H, Haruno M, Shimoda S, Aishima A. A case of drug-induced liver injury caused by Keishi-karyukotsu-boreito and Shin-i-seihaito. Nihon Shokakibyo Gakkai Zasshi. 2015; 112:1054-1059. (in Japanese)
46. Oikawa T, Gono Y, Fukuda T, Horikawa T, Hotta H, Mori Y, Kawanabe T, Ishige T, Odaguchi H, Wakasugi A, Okutomi T, Hanawa T. Three asymptomatic cases of suspected drug-induced liver injury possibly caused by Scutellariae radix. Kampo Med. 2015; 66:212-217. (in Japanese)
47. Ozeki N, Arakawa T, Nishio Y, Takeda K, Muroi K, Okufuji M, Yanagida Y. A case of drug-induced liver injury due to Bofutsushosan. Science of Kampo Med. 2017; 41:53-55. (in Japanese)
48. Shimada Y, Fujimoto M, Nogami T, Watari H, Kitahara H, Misawa H, Kimbara Y, Kita K ichiro. Recurrent drug-induced liver injury caused by the incidental readministration of a Kampo formula containing Scutellariae radix. Intern Med. 2018; 57:1733-1740.
49. Shinohara T, Ichikawa Y, Minowa Y, Ogiwara J, Shimazaki T, Yui N, Masayuki K, Keiji T, Kunihiko O. A case of suspected fluminant hepatitis induced by over-the-counter Ryutanshakanto. J Jpn Soc Emer Med. 2019; 22:64-68. (in Japanese)
50. Yamamoto M, Kitada R, Jokoji R, Kondo M, Koyama T, Nakamura M, Arisaka Y. A case of liver injury induced by a Chinese herbal formula containing a herbal medicine with a heat-clearing action. Kampo & the Newest Ther. 2020; 29:195-197.
51. Chalasani NP, Maddur H, Russo MW, Wong RJ, Reddy KR, Practice Parameters Committee of the American College of Gastroenterology. ACG clinical guideline: Diagnosis and management of idiosyncratic drug-induced liver injury. Am J Gastroenterol. 2021; 116:878-898.
52. Zimmerman HJ. Hepatotoxicity: The adverse effects of drugs and other chemicals on the liver. Lippincott Williams & Wilkins, Philadelphia, USA, 1999; pp. 848.
53. Li M, Luo Q, Tao Y, Sun X, Liu C. Pharmacotherapies for drug-induced liver injury: A current literature review. Front Pharmacol. 2021; 12:806249.
54. Hisanaga T, Hidaka I, Sakaida I, Nakayama N, Ido A, Kato N, Takikawa Y, Inoue K, Shimizu M, Genda T, Terai S, Tsubouchi H, Takikawa H, Mochida S. Analysis of the safety of pretransplant corticosteroid therapy in patients with acute liver failure and late-onset hepatic failure in Japan. J Gastroenterol Hepatol. 2021; 5:428-433.
55. Wree A, Dechêne A, Herzer K, Hilgard P, Syn WK, Gerken G, Canbay A. Steroid and ursodesoxycholic acid combination therapy in severe drug-induced liver injury. Digestion. 2011; 84:54-59.
56. Fujiwara K, Hida S, Yasui S, Yokosuka O, Oda S. Corticosteroid might reduce serum levels of pro-inflammatory cytokines in fulminant hepatitis: A case series. Hepatol Res Off J Jpn Soc Hepatol. 2018; 48:106-112.
57. Terada M, Kitazawa H, Kawakami J. Pharmacoepidemiology of interstitial pneumonia and liver dysfunction associated with Kampo medicine. Iryo Yakugaku. 2002; 28:425-434. (in Japanese)
58. Shimada Y. Adverse effects of Kampo medicines. Intern Med. 2022; 61:29-35.
59. Conn JW, Rovner DR, Cohen EL. Licorice-induced pseudoaldosteronism. Hypertension, hypokalemia, aldosteronopenia, and suppressed plasma renin activity. JAMA. 1968; 205:492-496.
60. Makino T, Hishida A, Goda Y, Mizukami H. Comparison of the major flavonoid content of S. baicalensis, S. lateriflora, and their commercial products. J Nat Med. 2008; 62:294-299.

Received December 6, 2024; Revised December 23, 2024; Accepted December 24, 2024.

*Address correspondence to:
Kenji Momo, Department of Hospital Pharmaceutics, School of Pharmacy, Showa University, Hatanodai 1-5-8, Shinagawa-ku, Tokyo 142-8555, Japan.
E-mail: k.momo@pharm.showa-u.ac.jp

Released online in J-STAGE as advance publication December 29, 2024.

Original Article

DOI: 10.5582/ddt.2024.01086

Long-term renoprotective effect of luseogliflozin in type 2 diabetes patients: CHikushi Anti-diabetes mellitus Trial-Lusefi (CHAT-Lu)

Yosuke Takamiya[1,*], Chiyori Imanaga[1], Ichiro Abe[2], Kunihisa Kobayashi[2], Amane Ike[1], Akira Kawamura[1], Hidenori Urata[1]

[1] Department of Cardiovascular Diseases, Fukuoka University Chikushi Hospital, Fukuoka, Japan;
[2] Department of Endocrinology and Diabetes Mellitus, Fukuoka University Chikushi Hospital, Fukuoka, Japan.

SUMMARY Several sodium-glucose cotransporter 2 (SGLT2) inhibitors are known to have beneficial effects on renal function in patients with type 2 diabetes. However, the long-term effects of luseogliflozin, an SGLT2 inhibitor, remain uncertain in real-world settings. This multicenter, open-label, prospective observational study evaluated the long-term effects of luseogliflozin on renal function in Japanese patients with type 2 diabetes. Fifty-four outpatients initiated on luseogliflozin at Fukuoka University Chikushi Hospital or associated clinics were enrolled from April 2018 to December 2019, with 46 patients included in the final analysis set. The primary outcome was the change in estimated glomerular filtration rate (eGFR) from baseline to 104 weeks, and secondary outcomes included the change in eGFR at week 52 and changes in body weight and blood and urinary parameters at 52 and 104 weeks. The mean duration of diabetes was 8.1 years. Baseline eGFR was 75.8 ± 17.4 mL/min/1.73m^2, and no decline in eGFR was observed from baseline to 104 weeks. Decline in eGFR was suppressed in the two groups stratified by baseline eGFR (< 60 and ≥ 60 mL/min/1.73m^2). No changes were noted in urinary albumin excretion rate. Blood glucose, body weight, blood pressure, liver function, and uric acid levels showed significant improvements. There were four adverse events, but no serious adverse events closely related to luseogliflozin treatment. In type 2 diabetes patients, 2-year treatment with luseogliflozin provided beneficial metabolic effects and improved the rate of decline in eGFR, suggesting a renal protective effect.

Keywords Sodium-glucose cotransporter 2 inhibitor, renal function, multifaceted effects, practicing physician

1. Introduction

Many epidemiological analyses have shown that better glycemic control in patients with type 2 diabetes can suppress the onset and progression of microangiopathy more effectively. However, as shown in the United Kingdom Prospective Diabetes Study (UKPDS) 80, the post-trial monitoring of the UKPDS, the use of conventional sulfonylureas drugs and insulin does not improve mortality rates significantly compared to standard treatment unless the treatment is continued for ten years (*1*). Biguanides, pioglitazone, and α-glucosidase inhibitor drugs have demonstrated favorable effects on the short-term prognosis of macroangiopathy (*2-4*). However, until recently, there were no substantial reports on improved renal function in type 2 diabetes patients with diabetic nephropathy, and there is no clear evidence on whether conventional drugs improve renal prognosis. In the EMPA-REG study, the sodium-glucose cotransporter 2 (SGLT2) inhibitor empagliflozin improved the short-term prognosis of macroangiopathy, except for nonfatal stroke (*5*). Several large-scale studies (*5-8*) have also shown the effects of empagliflozin, dapagliflozin, and canagliflozin on improving renal prognosis. This study aimed to investigate whether luseogliflozin, an SGLT2 inhibitor, exhibits a class effect in protecting renal function. We also investigated whether there are differences in renal protective effects depending on the baseline estimated glomerular filtration rate (eGFR). We prospectively administered luseogliflozin to patients with type 2 diabetes, including those with renal dysfunction, to investigate the long-term renal prognosis.

2. Patients and Methods

2.1. Patients

Participants were patients with type 2 diabetes aged 20

years or older who were treated at the outpatient clinic of Fukuoka University Chikushi Hospital or by local physicians registered in the Chikushi Cardiovascular Clinical Research Network, who had provided written consent and who had been prescribed luseogliflozin (hemoglobin A1c [HbA1c] 6.5% or more but less than 10%, including those currently undergoing treatment), and whose eGFR immediately before starting treatment was 30-90 mL/min/1.73m^2.

Patients were excluded if they had any of the following conditions: severe ketosis, diabetic coma or precoma, type 1 diabetes, severe infection, preoperative/postoperative state, severe trauma, pregnancy or possible pregnancy (for women), breastfeeding, or known hypersensitivity to any of the ingredients of luseogliflozin. In addition, patients were excluded if they had taken SGLT2 inhibitors within 6 months before starting luseogliflozin treatment or were deemed unsuitable for any other reason by the study investigators.

Patients were discontinued from the study if they withdrew consent, experienced adverse events, including severe hypoglycemia that prevented them from continuing treatment, missed outpatient visits, or if a physician deemed it inappropriate for them to continue in the study.

This study was approved by the Kyoto Prefectural University of Medicine Clinical Research Review Board (file number: 201822). The study protocol and patient informed consent forms were included in the ethics committee application documents, and written consent was obtained from each patient before enrollment. The study was conducted in accordance with the Declaration of Helsinki (as revised in 2013). The study was registered in the Japan Registry of Clinical Trials (registration number: jRCTs051180060).

2.2. Evaluation endpoints

The primary endpoints were changes in eGFR from baseline to 104 weeks overall, further stratified by baseline eGFR (eGFR < 60 mL/min/1.73m^2 or eGFR ≥ 60 mL/min/1.73m^2). Secondary endpoints were changes in eGFR from baseline to week 52, changes in resting double product (calculated as systolic blood pressure × pulse rate) at week 52 and week 104, and changes in body weight, blood test values (*e.g.*, hemoglobin, HbA1c, hepatic biomarkers, lipids, and uric acid) and urine test values (*e.g.*, urinary albumin excretion rate) at week 52 and week 104. Safety endpoints included type, severity, and causality of adverse events.

2.3. Diabetes mellitus, hypertension, dyslipidemia and obesity

Diabetes, hypertension, and dyslipidemia were determined based on prescription status or according to Japanese guidelines (*9-11*). Obesity was defined according to Japanese standards as a body mass index of 25 kg/m^2 or higher.

2.4. Statistical analysis

Statistical analysis was performed at Fukuoka University with IBM SPSS Statistics version 23 (IBM Corp., Armonk, NY, US). Significant differences were tested using the Student's *t*-test for items with normal variation and the Mann-Whitney test for items without normality. Equality of variance was tested with the Levene test, and when equal variance was not assumed, Welch's test was performed. Correlations were tested with Spearman's rank correlation coefficient. Numerical results are presented as mean ± standard deviation (SD), median with interquartile range (IQR), or frequency ratio. A *P*-value of less than 0.05 was considered significant.

3. Results

Between April 2018 and December 2019, 54 patients were enrolled across five facilities. Three patients discontinued luseogliflozin due to adverse events, two patients deviated from the protocol, and three patients dropped out. The remaining 46 patients continued luseogliflozin up to week 104 and were included in the analysis (Figure 1). Reported adverse events included death, cerebral infarction, elevated blood glucose (with luseogliflozin continued), and skin rash in one patient each. The dosage of luseogliflozin at week 104 was 2.5 mg/day in 30 patients, 5 mg/day in 15 patients, and 1.25 mg/day in one patient.

Table 1 presents the background characteristics of participants. The mean age was 66.2 years, and the mean duration of diabetes was 8.1 years. The proportion of obese patients was high, with a mean body mass index of 27 kg/m^2. Approximately 60% of patients had hypertension and dyslipidemia as comorbidities. Dipeptidyl peptidase 4 inhibitors were the most commonly used oral hypoglycemic drugs (37%), followed by biguanides (26%). Renin-angiotensin-

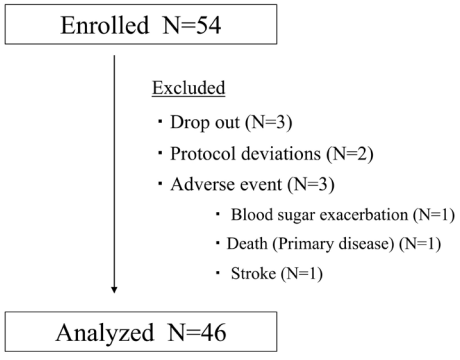

Figure 1. Participant flow in the study.

aldosterone system (RAS) inhibitors were used in approximately 46% of patients.

Figure 2 shows the changes in eGFR over time. Overall eGFR (mL/min/1.73m^2) was 75.8 ± 17.4 at baseline, 75.4 ± 20.7 at week 52, and 75.8 ± 20.8 at week 104, with no significant decline observed during the study period. To assess changes in eGFR, patients were divided into two groups based on baseline eGFR (≥ 60 mL/min/1.73m^2 and < 60 mL/min/1.73m^2). Patients with renal dysfunction (eGFR < 60 mL/min/1.73m^2) accounted for 8.7% of the total. No significant decline in eGFR was observed in either group.

Table 1. Patient characteristics

Characteristics	N (%)
N	46
Mean age (SD), y (*n* = 46)	66.2 ± 13.2
Male (*n* = 46)	27 (58.6)
Duration, y (*n* = 45)	8.1 ± 6.8
Body mass index, kg/m^2 (*n* = 46)	27 ± 3.7
Clinical presentation	
Hypertension (*n* = 43)	29 (67.4)
Dyslipidemia (*n* = 43)	28 (65.1)
Hyperuricemia (*n* = 43)	6 (14.0)
Smoking (*n* = 46)	23 (50.0)
Drinking (*n* = 46)	28 (60.9)
Ischemic heart disease (*n* = 43)	4 (9.3)
Previous stroke (*n* = 43)	1 (2.3)
Diabetic microangiopathy (*n* = 43)	1 (2.3)
Medication	
Antidiabetic drugs	
DPP4 inhibitors (*n* = 46)	17 (37.0)
Biguanides (*n* = 46)	12 (26.0)
Sulfonylureas (*n* = 46)	7 (15.2)
α-Glucosidase inhibitors (*n* = 46)	0 (0)
Glinides (*n* = 46)	0 (0)
Thiazolidinediones (*n* = 46)	2 (4.3)
Insulin (*n* = 46)	1 (2.2)
GLP1 RAs (*n* = 46)	0 (0)
Antihypertensive drugs (*n* = 46)	29 (63.0)
Renin-angiotensin system inhibitors (*n* = 46)	21 (45.7)
Antidyslipidemic drugs (*n* = 46)	18 (39.1)
Antithrombotic agents (*n* = 46)	4 (8.7)

Data are presented as numbers (%) or means ± standard deviation. DPP4, dipeptidyl peptidase 4; GLP1 RAs, glucagon-like peptide-1 receptor agonists, SD, standard deviation.

Secondary endpoints are shown in Table 2. No significant change was observed in urinary albumin excretion rate over time. Baseline HbA1c was 7.5% and was significantly decreased at week 52 and week 104 (week 52, 7.0%; week 104, 7.0%; $P < 0.01$ for each). Body weight significantly decreased by 3.6 kg at week 52, and this effect was maintained at week 104. Systolic and diastolic blood pressure significantly decreased at week 52, and diastolic blood pressure also significantly decreased at week 104. Hepatic biomarkers significantly improved at week 52 and week 104. Serum uric acid levels significantly decreased at week 104.

As shown in Figure 3, eGFR demonstrated no significant decrease over time regardless of urinary albumin excretion rate or use of RAS inhibitors.

Table 3 shows the correlation matrix table for each parameter at week 104. Changes in eGFR did not correlate with changes in HbA1c, body weight, or blood pressure. The only parameter negatively correlating with eGFR changes at week 104 was uric acid.

4. Discussion

This multicenter study conducted in local residents demonstrated that administering luseogliflozin, an SGLT2 inhibitor, to patients with type 2 diabetes in clinical practice provides long-term renal protective effects. Several large-scale studies (*5-8*) have shown that dapagliflozin, empagliflozin, and canagliflozin improve renal prognosis. While primary endpoints of large-scale clinical trials often include end-stage renal

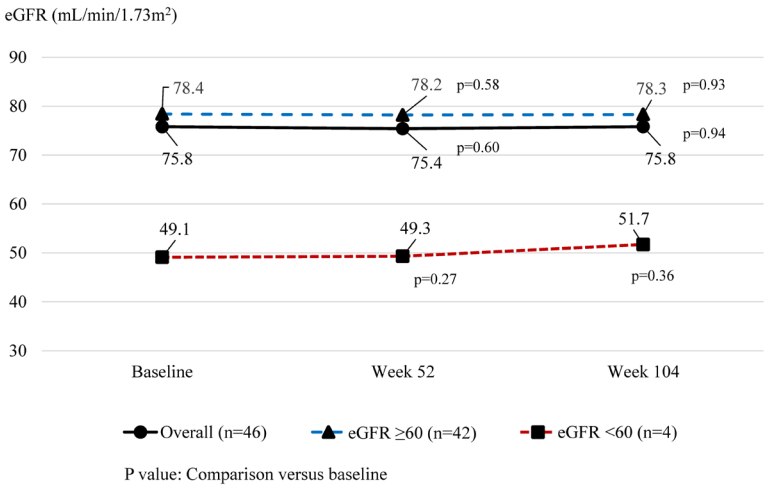

Figure 2. Change of eGFR. Week 52, after 52 weeks of treatment; week 104, after 104 weeks of treatment. eGFR, estimated glomerular filtration rate; G ≥ 60, eGFR ≥ 60 mL/min/1.73m^2; G < 60, eGFR < 60 mL/min/1.73 m^2.

Table 2. Changes in parameters at week 52 and week 104

	Week 0	Week 52	*P*-value *vs.* Week 0	Week 104	*P*-value *vs.* Week 0
Body weight, kg (*n* = 44)	70.6 ± 12.7	67.0 ± 12.0	< 0.01	66.8 ± 12.5	< 0.01
SBP, mmHg (*n* = 45)	133.1 ± 13.0	129.5 ± 9.7	0.02	130.0 ± 10.2	0.18
DBP, mmHg (*n* = 45)	76.2 ± 8.4	73.8 ± 8.6	< 0.01	73.8 ± 9.5	0.02
HR, bpm (*n* = 40)	74.3 ± 10.0	73.2 ± 8.9	0.27	73.6 ± 8.3	0.46
Double product (*n* = 41)	9982 ± 1696	9607 ± 1350	0.12	9572 ± 1202	0.14
HbA1c, % (*n* = 46)	7.5 ± 0.6	7.0 ± 0.7	< 0.01	7.0 ± 0.6	< 0.01
Glucose, mg/dL (*n* = 46)	176.7 ± 56.0	148.3 ± 36.6	< 0.01	141.9 ± 37.4	< 0.01
LDL-C, mg/dL (*n* = 42)	115.7 ± 32.0	115.6 ± 29.1	0.22	110.7 ± 26.2	< 0.01
HDL-C, mg/dL (*n* = 41)	50.8 ± 12.8	54.2 ± 14.8	< 0.01	53.0 ± 13.2	0.05
Triglyceride, mg/dL (IQR) (*n* = 43)	162 (110-233)	153 (111-203)	0.18	155 (107-221.5)	0.19
AST, U/L (IQR) (*n* = 43)	24 (21-35)	21 (17-26)	< 0.01	22 (17-26.5)	< 0.01
ALT, U/L (IQR) (*n* = 43)	29 (21-43)	23 (15-27)	< 0.01	22 (16.5-27.5)	< 0.01
γ-GTP, U/L (IQR) (*n* = 43)	35 (24-50)	27 (18-37)	< 0.01	27 (21-36.5)	< 0.01
UA, mg/dL (*n* = 43)	5.3 ± 1.3	5.0 ± 1.1	0.06	4.9 ± 1.2	0.01
WBC,×10^3 /μL (*n* = 42)	6.5 ± 1.4	6.1 ± 1.3	0.10	6.3 ± 1.5	0.39
Ht, % (*n* = 42)	42.4 ± 3.6	43.5 ± 4.1	0.02	43.1 ± 3.6	0.50
Plt, ×10^4/μL (*n* = 42)	23.0 ± 5.9	22.7 ± 6.0	0.14	22.7 ± 6.3	0.10
ALB, mg/dL (*n* = 32)	4.2 ± 0.3	4.3 ± 0.3	0.60	4.3 ± 0.3	0.90
Na, mmol/L(*n* = 43)	140.1 ± 2.5	140.3 ± 2.4	0.07	140.0 ± 2.1	1.00
K, mmol/L(*n* = 43)	4.2 ± 0.4	4.3 ± 0.4	0.48	4.2 ± 0.4	0.68
Urinary albumin/urinary creatinine (mg/g • Cr) (*n* = 34)	18.0 (8.0-61.2)	20.5 (8.4-58.4)	0.99	14.5 (6.6-43.2)	0.48

Data are presented as means ± standard deviation or medians (interquartile range). Week 0, 0 week (baseline); week 52, after 52 weeks of treatment; week 104, after 104 weeks of treatment. γ-GTP, gamma-glutamyl transpeptidase; ALB, albumin; ALT, alanine transaminase; AST, aspartate transaminase; DBP, diastolic blood pressure; HbA1c, hemoglobin A1c; HDL-C, high-density lipoprotein cholesterol; HR, heart rate; Ht, hematocrit; IQR, interquartile range; LDL-C, low-density lipoprotein cholesterol; Plt, platelets; SBP, systolic blood pressure; UA, uric acid; WBC, white blood cells.

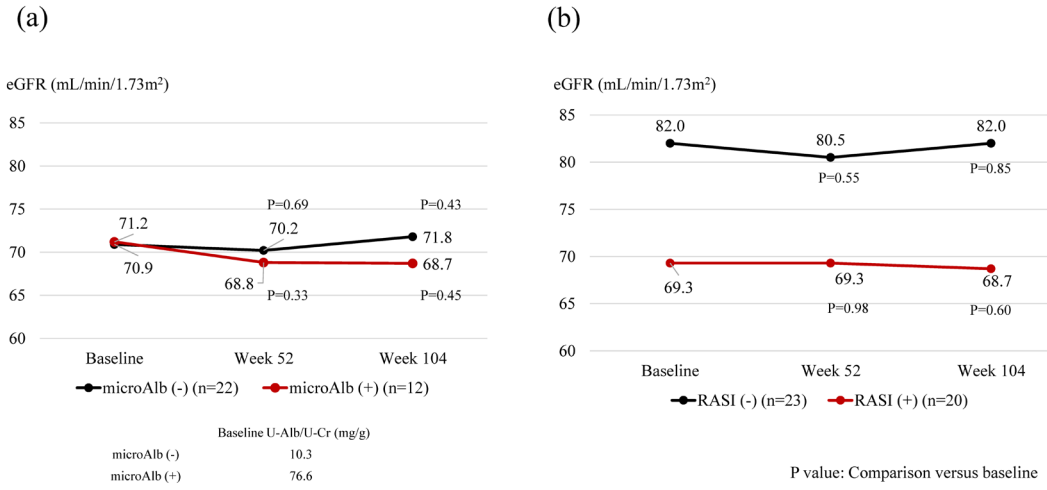

Figure 3. Change of eGFR with or without microalbuminuria (a) and renin-angiotensin-aldosterone system inhibitors (b) at baseline. Week 52, after 52 weeks of treatment; week 104, after 104 weeks of treatment. eGFR, estimated glomerular filtration rate; microAlb, microalbuminuria; RASI, renin-angiotensin system inhibitor; U-Alb, urinary albumin; U-Cr, urinary creatinine.

disease, renal death, and cardiovascular death, the evaluation of these endpoints requires a large sample size of around several thousand participants. It would be difficult to conduct such large clinical trials in routine clinical settings; for this reason, we focused on the eGFR slope following long-term treatment with SGLT2 inhibitors. The eGFR slope is associated with renal prognosis, and a decline of 0.5-1.0 mL/min/1.73m^2/year in eGFR has been reported as a surrogate endpoint for the progression of renal disease (*12*). The average annual decline in eGFR in Japanese patients is 0.36 mL/min/1.73m^2 (*13*), and the annual decline in eGFR in patients with type 2 diabetes has been reported to be as high as 1.67 mL/min/1.73m^2 in a large-scale study (*14*). This accelerated decline indicates diabetes as a factor that worsens renal prognosis.

This study aimed to demonstrate the renal protective effects of luseogliflozin, which has not been shown to improve renal prognosis in large-scale studies. In this study, no significant decline in eGFR was

Table 3. Correlation between amounts of change in each parameter at week 104

	ΔeGFR	ΔHbA1c	ΔDBP	ΔBW	ΔLDL-C	ΔHDL-C	ΔAST	ΔALT	ΔγGTP	ΔUA
ΔeGFR										
ΔHbA1c	*r* = -0.03 *P* = 0.85									
ΔDBP	*r* ≤ 0.01 *P* = 0.97	*r* = 0.35 *P* = 0.82								
ΔBW	*r* = 0.15 *P* = 0.34	*r* = 0.21 *P* = 0.18	*r* = 0.29 *P* = 0.053							
ΔLDL-C	*r* = 0.06 *P* = 0.75	*r* = 0.22 *P* = 0.19	***r = 0.41*** ***P = 0.01***	*r* = 0.24 *P* = 0.16						
ΔHDL-C	*r* = 0.14 *P* = 0.37	*r* = 0.01 *P* = 0.95	*r* = 0.25 *P* = 0.11	*r* = -0.29 *P* = 0.06	*r* = 0.29 *P* = 0.91					
ΔAST	*r* = -0.15 *P* = 0.35	*r* = -0.72 *P* = 0.65	*r* = -0.25 *P* = 0.12	*r* ≤ -0.01 *P* = 0.99	***r = -0.38*** ***P = 0.02***	*r* = -0.30 *P* = 0.056				
ΔALT	*r* = -0.20 *P* = 0.21	*r* = 0.27 *P* = 0.87	*r* = -0.21 *P* = 0.19	*r* = 0.06 *P* = 0.72	*r* = -0.30 *P* = 0.07	***r = -0.31*** *P* = 0.05	***r = 0.91*** ***P < 0.01***			
ΔγGTP	*r* = -0.05 *P* = 076	*r* = -0.29 *P* = 0.06	*r* = -0.24 *P* = 0.13	*r* = -0.14 *P* = 0.36	*r* = -0.09 *P* = 0.61	***r = -0.36*** ***P = 0.02***	***r = 0.41*** ***P < 0.01***	***r = 0.42*** ***P < 0.01***		
ΔUA	***r = -0.32*** ***P = 0.04***	*r* = 0.29 *P* = 0.053	*r* = -0.22 *P* = 0.17	*r* = -0.02 *P* = 0.92	*r* = -0.09 *P* = 0.58	*r* = -0.12 *P* = 0.44	*r* = 0.17 *P* = 0.28	*r* = 0.17 *P* = 0.30	***r = 0.32*** ***P = 0.04***	

ΔeGFR = (estimated glomerular filtration rate at week 104 - estimated glomerular filtration rate at baseline), ΔHbA1c = (hemoglobin A1c at week 104 - hemoglobin A1c at baseline), ΔDBP = (diastolic blood pressure at week 104 - diastolic blood pressure at baseline), ΔBW = (body weight at week 104 - body weight at baseline), ΔALT=(alanine transaminase at week 104 - alanine transaminase at baseline), ΔAST = (aspartate transaminase at week 104 - aspartate transaminase at baseline), Δγ-GTP = (gamma-glutamyl transpeptidase at week 104 - gamma-glutamyl transpeptidase at baseline), ΔHDL-C = (high-density lipoprotein cholesterol at week 104 - high-density lipoprotein cholesterol at baseline), ΔLDL-C = (low-density lipoprotein cholesterol at week 104 - low-density lipoprotein cholesterol at baseline), ΔUA = (uric acid at week 104 - uric acid at baseline).

observed in the two years after starting luseogliflozin treatment. eGFR remained stable, and the group with reduced renal function (eGFR < 60 mL/min/1.73m^2) showed an increase in eGFR of 2.6 mL/min/1.73m^2. Among patients with type 2 diabetes, administration of luseogliflozin did not result in decreased eGFR or increased urinary albumin excretion rate, suggesting its potential to improve renal prognosis. Among the six SGLT2 inhibitors available in Japan, luseogliflozin has the lowest prescribed dose (*15*). A previous *in vivo* study revealed that luseogliflozin has a high renal transfer rate (*16*), which may enable luseogliflozin's pharmacological effects to be exerted efficiently. Luseogliflozin utilizes multiple metabolic pathways, which means there are minimal changes in plasma exposure even in patients with hepatic or renal dysfunction (*17,18*), thus reducing the risk of side effects. These characteristics suggest that luseogliflozin has at least equal or greater efficacy than that of other SGLT2 inhibitors. The results of this study suggest that the renal protective effect of SGLT2 inhibitors, including luseogliflozin, is a class effect, supporting the findings of Suzuki *et al.* (*19*). Large-scale studies have reported that SGLT2 inhibitors improve renal function to a greater extent in patients with reduced renal function than in patients with normal renal function (*7,8*). In this study, over 90% of patients had an eGFR of 60 mL/min/1.73m^2 or higher, and 65% (22 of 34 patients) were in the normoalbuminuric phase. In patients with normal renal function, luseogliflozin suppressed decreases in eGFR and increases in urinary albumin, demonstrating a renal protective effect. In the normoalbuminuric phase, glycemic control was initially insufficient, with an HbA1c of 7.5%, and it is said that diabetic nephropathy develops 10 years after the onset of diabetes (*20*). In this study, the mean duration of diabetes was approximately 8 years, so this patient population is considered to be at high risk of progressing to the microalbuminuria phase. In view of this, it may be beneficial to administer SGLT2 inhibitors to all patients with type 2 diabetes, including those before the onset of nephropathy, unless use is contraindicated for some reason.

SGLT2 inhibitors inhibit the sodium-glucose cotransporter 2 in the kidneys, suppressing the reabsorption of Na and glucose. As one of the renal protective mechanisms of SGLT2 inhibitors in type 2 diabetes, the inhibition of SGLT2 suppresses Na reabsorption in the proximal tubule, increasing Na delivery to the macula densa surrounding the distal tubule; this causes the afferent arteriole to constrict, reducing hyperfiltration and lowering intraglomerular pressure, thus preventing glomerular injury (*21*). At the cellular level, it has been reported that SGLT2 inhibitors improve energy metabolism in proximal tubule cells, suppress Na/K ATPase consumption on the vascular side of the proximal tubule, and protect tubule cells (*22*), and that increased expression of SGLT2 leads to injury in glomerular epithelial cells (podocytes) (*23*). In this study, luseogliflozin not only improved glycemic

control but also reduced body weight, diastolic blood pressure, liver function parameters, and uric acid at week 52, and these effects were maintained at week 104. The changes in eGFR at weeks 52 and 104 showed no correlation with baseline HbA1c or with the amount of HbA1c reduction over the 2-year period, suggesting that the renal protective effect of luseogliflozin is independent of glycemic control. The pleiotropic effects of luseogliflozin were weight loss, diuresis, uric acid reduction, and blood pressure reduction, which did not show a direct correlation with renal function, except for uric acid reduction. However, it is already known that hypertension, hyperglycemia, and worsening uric acid can cause renal dysfunction (*24,25*); thus, improvements in these factors may have contributed synergistically to renal protection.

In patients with type 2 diabetes, angiotensin II type 1 (AT1) receptor expression is increased in efferent arterioles compared to afferent arterioles, and RAS inhibitors dilate efferent arterioles more, lowering intraglomerular pressure (*26*). Combining the use of RAS inhibitors with SGLT2 inhibitors may provide additional correction of intraglomerular pressure. On the other hand, there is a concern that this combination may reduce eGFR. In this study, there was no decrease in eGFR regardless of RAS inhibitor use, suggesting that combined use with RAS inhibitors does not excessively reduce intraglomerular pressure and continues to provide renal protection, and further suggests that luseogliflozin offers a renal protective effect independent of RAS inhibitor treatment.

Patients with type 2 diabetes have a high rate of nonalcoholic fatty liver disease (approximately 70%) (*27*), and the incidence of hypertension is twice as high as that of nondiabetic patients (*28*). Obesity contributes to hyperinsulinemia, which can lead to the onset of diabetes and elevated blood glucose. In this study, luseogliflozin reduced body weight, lowered diastolic blood pressure, improved liver damage, and reduced uric acid levels, resulting in long-term improvement of lifestyle-related conditions commonly associated with diabetes. This suggests that luseogliflozin may also be useful in improving and maintaining comprehensive health.

Adverse events occurred in four patients. One adverse event was death due to malignant brain lymphoma which was not related to luseogliflozin. There was no evidence of urinary ketone bodies or lactic acidosis, indicating that luseogliflozin was safe for long-term use.

A limitation of this study is that it was a single-arm, open-label study, and a placebo effect could not be ruled out.

In this multicenter, prospective, observational study conducted in a real-world clinical setting by general practitioners, luseogliflozin demonstrated renal protective effects in patients with type 2 diabetes regardless of the baseline eGFR value or the presence or absence of microalbuminuria. The study showed that luseogliflozin demonstrates multifaceted favorable effects on blood glucose, liver function, body weight, and uric acid.

Acknowledgements

We thank the following members of the Chikushi Cardiovascular Research Network for recruiting participants for this study: Takehiko Kodera (Kodera Internal Clinic), Tadasu Matsuzaki (Matsuzaki Clinic), Takatoshi Otonari (Otonari Clinic), and Masanori Shimizu (Shimizu Clinic).

Funding: The authors received financial support from Taisho Pharmaceutical Co., Ltd. (17-P16).

Conflict of Interest: The principal investigator of the study has received financial support from Taisho Pharmaceutical Co., Ltd. The other authors have no conflict of interest to disclose. The funder was not involved in the study design, the collection, analysis, and interpretation of data, in the writing of the report, or in the decision to submit the paper for publication.

References

1. Holman RR, Paul SK, Bethel MA, Neil HA, Matthews DR. Long-term follow-up after tight control of blood pressure in type 2 diabetes. N Engl J Med. 2008; 359:1565-1576.
2. Dormandy JA, Charbonnel B, Eckland DJ, *et al*. Secondary prevention of macrovascular events in patients with type 2 diabetes in the PROactive Study (PROspective pioglitAzone Clinical Trial In macroVascular Events): a randomised controlled trial. Lancet. 2005; 366:1279-1289.
3. Holman RR, Paul SK, Bethel MA, Matthews DR, Neil HA. 10-year follow-up of intensive glucose control in type 2 diabetes. N Engl J Med. 2008; 359:1577-1589.
4. Chiasson JL, Josse RG, Gomis R, Hanefeld M, Karasik A, Laakso M. Acarbose treatment and the risk of cardiovascular disease and hypertension in patients with impaired glucose tolerance: the STOP-NIDDM trial. JAMA. 2003; 290:486-494.
5. Zinman B, Wanner C, Lachin JM, Fitchett D, Bluhmki E, Hantel S, Mattheus M, Devins T, Johansen OE, Woerle HJ, Broedl UC, Inzucchi SE. Empagliflozin, cardiovascular outcomes, and mortality in type 2 diabetes. N Engl J Med. 2015; 373:2117-2128.
6. Neal B, Perkovic V, Mahaffey KW, de Zeeuw D, Fulcher G, Erondu N, Shaw W, Law G, Desai M, Matthews DR. Canagliflozin and cardiovascular and renal events in type 2 diabetes. N Engl J Med. 2017; 377:644-657.
7. Mosenzon O, Wiviott SD, Cahn A, *et al.* Effects of dapagliflozin on development and progression of kidney disease in patients with type 2 diabetes: an analysis from the DECLARE-TIMI 58 randomised trial. Lancet Diabetes Endocrinol. 2019; 7:606-617.
8. Perkovic V, Jardine MJ, Neal B, *et al.* Canagliflozin and renal outcomes in type 2 diabetes and nephropathy. N

Engl J Med. 2019; 380:2295-2306.
9. Araki E, Goto A, Kondo T, Noda M, Noto H, Origasa H, Osawa H, Taguchi A, Tanizawa Y, Tobe K, Yoshioka N. Japanese Clinical Practice Guideline for Diabetes 2019. J Diabetes Investig. 2020; 11:1020-1076.
10. Kinoshita M, Yokote K, Arai H, *et al*. Japan Atherosclerosis Society (JAS) Guidelines for Prevention of Atherosclerotic Cardiovascular Diseases 2017. J Atheroscler Thromb. 2018; 25:846-984.
11. Umemura S, Arima H, Arima S, *et al.* The Japanese Society of Hypertension Guidelines for the Management of Hypertension (JSH 2019). Hypertens Res. 2019; 42:1235-1481.
12. Levey AS, Gansevoort RT, Coresh J, *et al*. Change in albuminuria and GFR as end points for clinical trials in early stages of CKD: A scientific workshop sponsored by the National Kidney Foundation in collaboration with the US Food and Drug Administration and European Medicines Agency. Am J Kidney Dis. 2020; 75:84-104.
13. Imai E, Horio M, Yamagata K, Iseki K, Hara S, Ura N, Kiyohara Y, Makino H, Hishida A, Matsuo S. Slower decline of glomerular filtration rate in the Japanese general population: a longitudinal 10-year follow-up study. Hypertens Res. 2008; 31:433-441.
14. Wanner C, Inzucchi SE, Lachin JM, Fitchett D, von Eynatten M, Mattheus M, Johansen OE, Woerle HJ, Broedl UC, Zinman B. Empagliflozin and progression of kidney disease in type 2 diabetes. N Engl J Med. 2016; 375:323-334.
15. Seino Y, Sasaki T, Fukatsu A, Ubukata M, Sakai S, Samukawa Y. Efficacy and safety of luseogliflozin as monotherapy in Japanese patients with type 2 diabetes mellitus: a randomized, double-blind, placebo-controlled, phase 3 study. Curr Med Res Opin. 2014; 30:1245-1255.
16. Kakinuma H, Oi T, Hashimoto-Tsuchiya Y, *et al.* (1S)-1,5-anhydro-1-[5-(4-ethoxybenzyl)-2-methoxy-4-methylphenyl]-1-thio-D-glucitol (TS-071) is a potent, selective sodium-dependent glucose cotransporter 2 (SGLT2) inhibitor for type 2 diabetes treatment. J Med Chem. 2010; 53:3247-3261.
17. Samukawa Y, Sata M, Furihata K, Ito T, Ueda N, Ochiai H, Sakai S, Kumagai Y. Luseogliflozin, an SGLT2 inhibitor, in Japanese patients with mild/moderate hepatic impairment: A pharmacokinetic study. Clin Pharmacol Drug Dev. 2017; 6:439-447.
18. Samukawa Y, Haneda M, Seino Y, Sasaki T, Fukatsu A, Kubo Y, Sato Y, Sakai S. Pharmacokinetics and pharmacodynamics of luseogliflozin, a selective SGLT2 inhibitor, in Japanese patients with type 2 diabetes with mild to severe renal impairment. Clin Pharmacol Drug Dev. 2018; 7:820-828.
19. Suzuki Y, Kaneko H, Okada A, Matsuoka S, Fujiu K, Michihata N, Jo T, Takeda N, Morita H, Node K, Nangaku M, Yasunaga H, Komuro I. Kidney outcomes in patients with diabetes mellitus did not differ between individual sodium-glucose cotransporter-2 inhibitors. Kidney Int. 2022; 102:1147-1153.
20. Adler AI, Stevens RJ, Manley SE, Bilous RW, Cull CA, Holman RR. Development and progression of nephropathy in type 2 diabetes: the United Kingdom Prospective Diabetes Study (UKPDS 64). Kidney Int. 2003; 63:225-232.
21. DeFronzo RA, Reeves WB, Awad AS. Pathophysiology of diabetic kidney disease: impact of SGLT2 inhibitors. Nat Rev Nephrol. 2021; 17:319-334.
22. Vallon V, Richter K, Blantz RC, Thomson S, Osswald H. Glomerular hyperfiltration in experimental diabetes mellitus: potential role of tubular reabsorption. J Am Soc Nephrol. 1999; 10:2569-2576.
23. Cassis P, Locatelli M, Cerullo D, Corna D, Buelli S, Zanchi C, Villa S, Morigi M, Remuzzi G, Benigni A, Zoja C. SGLT2 inhibitor dapagliflozin limits podocyte damage in proteinuric nondiabetic nephropathy. JCI Insight. 2018; 3:e98720.
24. Boris Bikbov, Carrie Purcell, Andrew S Levey, *et al*. Global, regional, and national burden of chronic kidney disease, 1990-2017: A systematic analysis for the Global Burden of Disease Study 2017. Lancet. 2020; 395:709-733.
25. Tsai CW, Lin SY, Kuo CC, Huang CC. Serum uric acid and progression of kidney disease: A longitudinal analysis and mini-review. PLoS One. 2017; 12:e0170393.
26. Kobori H, Nangaku M, Navar LG, Nishiyama A. The intrarenal renin-angiotensin system: from physiology to the pathobiology of hypertension and kidney disease. Pharmacol Rev. 2007; 59:251-287.
27. Lomonaco R, Godinez Leiva E, Bril F, *et al*. Advanced liver fibrosis is common in patients with type 2 diabetes followed in the outpatient setting: The need for systematic screening. Diabetes Care. 2021; 44:399-406.
28. Iimura O. Insulin resistance and hypertension in Japanese. Hypertens Res. 1996; 19 Suppl 1:S1-8.

Received December 2, 2024; Revised December 21, 2024; Accepted December 22, 2024.

**Address correspondence to:*
Yosuke Takamiya, Department of Cardiovascular Diseases, Fukuoka University Chikushi Hospital, 1-1-1, Zokumyoin, Chikushino-shi, Fukuoka, 818-8502, Japan.
E-mail: takamiya2011@cis.fukuoka-u.ac.jp

Released online in J-STAGE as advance publication December 27, 2024.

Original Article

DOI: 10.5582/ddt.2024.01066

Shenling Guchang prescription ameliorates intestinal barrier inflammation in gestational diabetes rats *via* TLR4/NF-κB pathway

Manling Li[1,2,§], Lisha Li[3,4,5,§], Xingman Liu[1,2], Tao Yang[1], Jingyun Gao[1], Anqin Wu[1], Zhaozhao Hua[1,*], Ling Wang[6,*]

[1] Department of Obstetrics, The Second Affiliated Hospital of Guizhou University of Chinese Medicine, Guiyang, Guizhou, China;
[2] Guizhou University of Traditional Chinese Medicine (TCM), Guiyang, China;
[3] Laboratory for Reproductive Immunology, Obstetrics and Gynecology Hospital of Fudan University, Shanghai, China;
[4] The Academy of Integrative Medicine of Fudan University Shanghai, China;
[5] Shanghai Key Laboratory of Female Reproductive Endocrine-related Diseases, Shanghai, China;
[6] Department of Obstetrics and Reproductive Immunology, Shanghai East Hospital, Tongji University School of Medicine, Shanghai, China.

SUMMARY Gestational diabetes mellitus (GDM) is linked to a greater risk of various maternal and fetal complications, including the possibility of long-term metabolic issues in offspring. Our initial research suggests that the Traditional Chinese Medicine formula, Shenling Guchang prescription (SLGP), may have an impact on the gut microbiota. However, the specific mechanisms through which it affects intestinal barrier inflammation in GDM are still not fully understood. This study explored SLGP's mechanisms in GDM. Firstly, network pharmacology predicted key bioactive constituents targeting toll-like receptor 4 (TLR4)/nuclear factor-kappa B (NF-κB), guiding experimental design. Subsequently, the pregnant female rats were induced with GDM through intraperitoneal streptozotocin injection and then divided into control, model, metformin, and SLGP treatment groups. Blood samples were collected for ELISA analysis to measure levels of inflammatory markers, intestinal tissues were examined histologically using hematoxylin-eosin (HE) staining, and western blot analysis was conducted to evaluate TLR4 and NF-κB expression. Relative to control rats, model group animals exhibited significant increases in the levels of inflammatory markers (IL-1β, IL-6, TNF-α, TGF-β, CRP), as well as enhanced TLR4 and p-NF-κB p65 expression, along with intestinal histopathological changes. Treatment with SLGP notably reduced inflammatory markers and protein expression in the colonic tissue of GDM rats, leading to a decrease in histopathological damage. Overall, SLGP was found to modulate the TLR4/NF-κB pathway, resulting in enhancements in insulin resistance and a reduction in inflammatory responses in GDM rats, thereby providing protection for the intestines. This study demonstrates the potential therapeutic effectiveness of SLGP in addressing intestinal inflammation linked to GDM.

Keywords Gestational diabetes mellitus, intestinal inflammation, inflammatory marker, toll-like receptor 4, nuclear factor-kappa B

1. Introduction

Obesity is a pressing global health issue that has fueled a rise in gestational diabetes mellitus (GDM) incidence, which now impacts approximately 4-16.5% of pregnant women globally (*1*), exposing both the mother and the fetus to health risks that can persist even after the perinatal period ends (*2-4*). The precise causes of GDM are incompletely understood, but key drivers of this condition include inflammation, oxidative stress, and insulin resistance (*5,6*). The gut microbiome, a complex assembly of diverse microorganisms in the gastrointestinal tract, plays a central role in shaping host immune activity and metabolic functionality (*7,8*). Recent studies suggest that gut dysbiosis are linked to GDM incidence (*9,10*). The disruption of normal microbial homeostasis within the gut can lead to the production of a variety of signaling molecules and metabolites that can modulate the function of the intestinal barrier (*11,12*). Such disturbances can be linked to an increase in gut permeability such that lipopolysaccharide (LPS) and other compounds can access the bloodstream and trigger

TLR4/MyD88/NF-κB pathway-mediated inflammation (*13*). The consequent oxidative stress and systemic inflammation can lead to the onset of insulin resistance associated with GDM (*14*).

At present, the outcomes associated with common treatments for GDM such as exercise, dietary changes, and pharmacological interventions remain highly variable (*15*). There is thus a clear need to devise new treatment options that are more efficacious. Traditional Chinese medicine (TCM) has been established as a promising approach to the treatment of GDM, although the mechanisms through which TCM prescriptions exert their effects are incompletely understood, particularly as they pertain to the TLR4/NF-κB pathway (*16*).

This study was developed to assess the impact of Shenling Guchang prescription (SLGP), a TCM formula, a traditional Chinese medicine formula has been used to treat various gastrointestinal diseases in clinical practice, and its potential benefits in controlling GDM. To deeply understand SLGP's therapeutic potential, network pharmacology was first utilized to predict its active components and relevant targets. Following this, a GDM rats model was implemented to explore the mechanisms of action. By merging network pharmacology with vivo experimentation, the study aimed to clarify SLGP's role in GDM's pathophysiological processes.

2. Materials and Methods

2.1. Network pharmacology

2.1.1. Collection of chemical composition and target prediction of SLGP

The chemical composition and target prediction of SLGP were conducted using Chinese traditional medicine. Active ingredients from Pseudostellaria heterophylla, Atractylodes Macrocephalae Koidz, Poria cocos, Coicis Semen, Dioscorea opposita Thunb, Crataegi Folium, Puerariae Lobatae Radix, Agrimoniae Herba, and Glycyrrhizae Radix et Rhizoma were retrieved based on criteria from the Traditional Chinese Medicine Database and Analysis Platform (TCMSP, *https://tcmsp-e.com/*), specifically targeting compounds with oral bioavailability (OB) ≥ 30% and medicinal likeness (DL) ≥ 0.18. After sorting, Uniprot (*https://www.uniprot.org/*) data were used to standardize gene names by removing non-human genes and eliminating duplicate targets.

2.1.2. Acquisition of GDM-related targets

Targets associated with Gestational Diabetes Mellitus (GDM) were obtained by que-rying GeneCards (*https://www.genecards.org/*) and OMIM (*https://www.omim.org/*) databases using the keyword "GDM". Integrated database entries were scrutinized in Excel to remove duplicate genes and validate gene information against the Uniprot database.

2.1.3. Drug-disease target prediction results

Drug component targets and disease targets were mapped, and a Venn diagram was created to identify intersecting genes. The Drug-Ingredient-Target network was sub-sequently constructed using Cytoscape 3.7.2 software.

2.1.4. Construction of target protein interaction network

To investigate the protein-protein interactions of SLGP in treating GDM, drug-intersecting genes were uploaded to the STRING database (*https://string-db.org/*) to construct a Protein-Protein Interaction (PPI) network. Species specificity was set to "Homo sapiens", and a minimum interaction score of 0.7 was applied to ensure study credibility. Results were exported in TSV format and analyzed in Cytoscape 3.7.2. Node size and color reflected Degree centrality, while edge thickness indicated CombineScore, highlighting core targets in the network diagram.

2.1.5. GO enrichment analysis and KEGG pathway analysis

Intersection genes were imported into the Drug_Disease.txt file, and their symbols were converted to EntrezIDs using the org.Hs.eg.db package in RStudio. GO enrichment and KEGG pathway analyses were performed using the clusterProfiler package, with human species specified and significance threshold set at $P < 0.05$. The top 10 results were visualized using the ggplot2 package, elucidating the role of SLGP target proteins in GDM treatment across Biological Processes (BP), Cellular Components (CC), and Molecular Functions (MF). Additionally, KEGG pathway enrichment analysis provided further insights into the therapeutic targets of SLGP in GDM treatment.

2.2. Animals

In total, 62 specific-pathogen-free (SPF) healthy female Sprague-Dawley (SD) rats (8 weeks old, 200 ± 20 g) and 36 SPF healthy male SD rats of a similar age and weight were purchased from Changsha Tianqin Biotechnology Co., Ltd. (experimental animal qualification certificate number SCXK (Xiang) 2021-0005). These rats were individually housed at the Animal Experiment Center of Guizhou University of Chinese Medicine with free food and water access under controlled conditions (22 ± 1°C, 12 h light/dark cycle). The Guizhou University of Chinese Medicine approved all animal studies, and efforts were made to minimize animal suffering wherever possible.

2.3. Pregnant rat preparation

After allowing 1 week for acclimatization, the 62 female rats were fasted overnight with free access to water, followed by analyses of their blood glucose levels, with levels < 6.1 mmol/L being sufficient for inclusion in this study. The 62 enrolled rats that met these criteria were allowed to acclimate for an additional week, after which they were co-housed for one week with male rats at a 1.5:1 ratio. In the morning, rats were examined for vaginal plugs, with the day that a plug was observed was set as day 0.5 of pregnancy. Blood glucose was measured on day 0.5 to exclude any potential for pre-gestational diabetes. After one week, any rats who did not conceive were excluded from this analysis. In total, 48 rats successfully became pregnant.

2.4. GDM modeling and treatment

The 48 pregnant female rats were further subdivided at random into 6 groups (n = 8/group), including a blank control group in which rats received a normal diet. The remaining 40 rats underwent GDM modeling by administering a high-fat/high-sugar diet (59% regular feed, 18% lard, 20% sugar, and 3% egg yolk; Ke Ao Xie Li, Beijing, China) for 5 days. After this 5-day period, all pregnant rats underwent overnight fasting with free access to water, followed by the measurement of their body weight and fasting blood glucose (*17*). Rats in the modeling groups were then administered freshly prepared STZ (35 mg/kg; Solarbio, Beijing, China, batch number is S8050-100mg) once per day for 3 days, whereas the rats in the blank control group were injected with a similar volume of vehicle control (0.1 mmol/L sodium citrate buffer). At 24, 48, and 72 h post-administration, fasting blood glucose levels in these rats were analyzed, with modeling being considered successful if the rats exhibited blood glucose levels above 11.1 mmol/L on three consecutive days. Body weights were again measured after successful modeling.

The 40 rats that had undergone GDM modeling were further divided with a random number table into model, metformin, and SLGP treatment (low-, medium-, or high-dose) groups. Per the "Laboratory Animals" dosage conversions, a dose equivalent to the daily dose for a 60 kg adult was calculated. SLGP was obtained from The Intelligent Granule Pharmacy of the Second Affiliated Hospital of Guizhou University of Chinese Medicine, and consisted of 15 g Pseudostellaria heterophylla, 15 g Atractylodes Macrocephalae Koidz, 15 g Poria cocos, 20 g Coicis Semen, 30 g Atractylodis Dioscorea opposita Thunb, 15 g Crataegi Folium, 15 g Puerariae Lobatae Radix, 15 g Agrimoniae Herba, and 6 g Glycyrrhizae Radix et Rhizoma (Table 1). Square granules from Sichuan New Green Medicine Industry (Batch numbers: 20110141, 21080031, 21080103, 21060067, 21050095, 21040030, 20080222, 21020023, 20080229, and 21070040) were administered *via* gavage to rats in the low-, medium-, and high-dose treatment groups at 4.5, 9, and 18 mg/kg. Metformin (500 mg/tablet; Tianfang Pharmaceutical, Xi'an, China) was obtained from the Western Medicine Pharmacy of the same hospital and was administered to rats in the appropriate group at 52.5 mg/kg *via* gavage. Rats in the model and blank groups instead received an equal volume of 0.9% saline. Treatment was repeated once per day for 2 weeks, after which all rats were euthanized following food and water deprivation for 12 h. Blood glucose and body weight values were measured for rats in each group, after which samples of blood and colon tissue were harvested for analysis.

2.5. ELISAs

After allowing blood samples to stand for 30 min at room temperature, they were centrifuged (15 min, 2,000 rpm; radius: 5 cm), and serum was then stored at -80°C. Serum levels of insulin (Elabscience, Wuhan, Hubei, China), C-reactive protein (CRP, eBioscience, Wuhan, Hubei, China), IL-1β, IL-6 (MultiSciences, Shanghai, China), lipopolysaccharide (LPS, MSKBIO, Wuhan, China), TGF-β, tumor necrosis factor-α (TNF-α), TLR-4 (Bioswamp, Wuhan, Hubei, China), and phospho-NF-κB p65 (MSKBIO, Wuhan, Hubei, China).

2.6. Histopathological staining

Samples of colon tissue from the same location in each rate were fixed for 48 h in 4% paraformaldehyde,

Table 1. Composition of SLGP

English name	Chinese name	Content (g)	Main components
Pseudostellaria heterophylla	Taizishen	15	Polysaccharides, amino acids, trace elements
Atractylodes Macrocephalae Koidz	Baizhu	15	Starch, triterpenoids, flavonoids
Poria cocos	Fulin	20	Lignans, polysaccharides, alkaloids
Coicis Semen	Yiyiren	20	Polysaccharides, proteins, amino acids
Dioscorea opposita Thunb	Shanyao	30	Starch, glycoproteins, saponins
Crataegi Folium	Shanzhaye	15	Flavonoids, triterpenoids, sterols
Puerariae Lobatae Radix	Gegeng	15	Saponins, flavonoids, polysaccharides
Agrimoniae Herba	Xianhecao	15	Alkaloids, flavonoids, tannins
Glycyrrhizae Radix et Rhizoma	Gancao	6	Glycyrrhizin, flavonoids, polysaccharides

paraffin-embedded, and cut into 4-6 μm sections. These sections were then deparaffinized, rehydrated, and stained with hematoxylin and eosin (H&E) solution (Servare,Wuhan,Hubei,China) as directed, followed by imaging with a microscope.

2.7. Western immunoblotting

Colon tissue samples were collected from the same location in rats from each group and stored at -80°C for analysis. RIPA buffer (Kangwei Century,Qingdao,China) was used to homogenize these colon tissue samples, which were then centrifuged (5 min, 15,000 rpm), and supernatants were collected. After measuring the total protein content in these supernatants, 30 μg per sample was separated *via* SDS-PAGE and transferred to a PVDF membrane (Millipore,Shanghai,China) with a semi-dry transfer technique. Blocked membranes were incubated overnight with primary antibodies specific for TLR4 (Bioswamp), p-NF-κB p65 (CST, Shanghai, China), and GAPDH (Abcam,Shanghai,China) at 4°C. After a 1 h incubation with secondary antibodies (Kangwei Century), a chemiluminescent substrate was used for membrane development. ImageJ was used for densitometric analyses of protein bands, with GAPDH as a loading control.

2.8. Statistical analysis

GraphPad Prism 8.0 and SPSS 19.0 were used to analyze all data, which are reported as means ± standard deviations (SD). Results were compared with one-way ANOVAs and multiple comparisons testing as appropriate. $P < 0.05$ was selected as the cut-off to define significance.

3. Results

3.1. Acquisition of active compounds and its targets in SLGP

Following removal of ineffective components and criteria of OB ≥ 30% and DL ≥ 0.18, the following components were collected: 6 from Pseudostellariae Radix, 5 from Radix Pseudostellariae, 4 from Radix Pseudostellariae, 6 from Hawthorn Leaf, 88 from Licorice, 6 from Poria Poria, 12 from Yam, 4 from Pueraria Root, and 9 from Coix Seed. In total, 122 ingredients were identified from all pharmaceutical ingredients. Collecting all disease targets of these 122 active compounds, a components-targets network was constructed. The top five components identified were MOL000098 (quercetin), MOL000422 (kaempferol), MOL000006 (luteolin), MOL000449 (stigmasterol), and MOL000392 (formononetin).

3.2. PPI network analysis of core targets

Using a Relevance Score > 5 as the criterion for inclusion from GeneCards, 2,636 targets were included, and an additional 522 targets were obtained from the OMIM database. After deduplication, 3,056 GDM-related targets were identified. Intersection of GDM target genes and drug target genes yielded 134 overlapping genes, representing potential interaction targets for GDM treatment (Figure 1A). After intersection of all drug and GDM targets, 134 overlapping genes were identified and analyzed using the String database (*https://string-db.org/*) for protein-protein interaction prediction in Homo sapiens, with a confidence threshold of 0.7. The resulting network file was saved in TSV format and imported into Cytoscape 3.7.2 to construct a protein interaction network. Nodes with Degree > 5 were selected for topology analysis, revealing 104 nodes and 2230 edges. The top 20 target genes including *IL6*, *TP53*, *STAT3*, *AKT1*, *IL1B*, *TNF*, *EGFR*, *JUN*, *CASP3*, *MMP9*, *PTGS2*, *MYC*, *BCL2*, *IL10*, *CXCL8*, *HIF1A*, *ESR1*, *MAPK3*, *FOS*, and *STAT1* were screened using the cytohuba plug-in (Table 2, Figure 1B).

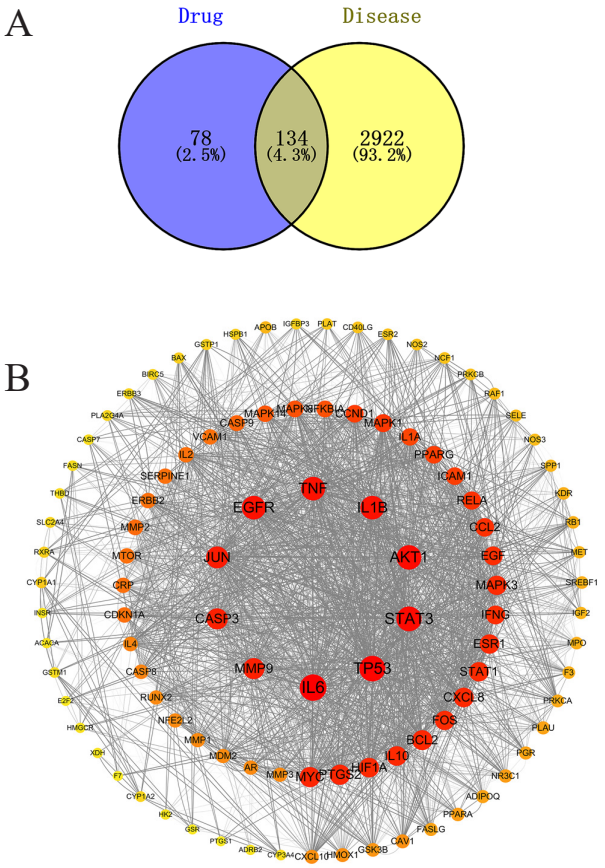

Figure 1. Components and targets analysis of SLGP in treating GDM. (A) The core regulatory genes of SLGP in treating GDM. (B) PPI network showed the protein relationship between SLGP and GDM. The network was re-edited by Cytoscape. The node's color is marked from red to yellow according to the degree value in descending order.

Table 2. Top 20 target genes of SLGP

Rank	Gene	Protein name	Score
1	*IL6*	Interleukin-6	63
2	*TP53*	Cellular tumor antigen p53	60
3	*STAT3*	Signal transducer and activator of transcription 3	57
4	*AKT1*	RAC-alpha serine/threonine-protein kinase	56
5	*IL1B*	Interleukin-1 beta	53
6	*TNF*	Tumor necrosis factor	53
7	*EGFR*	Epidermal growth factor receptor	53
8	*JUN*	Jun proto-oncogene	47
9	*CASP3*	Caspase-3	44
10	*MMP9*	Matrix metalloproteinase-9	44
11	*PTGS2*	Prostaglandin G/H synthase 2	41
12	*MYC*	Myelocytomatosis oncogene	41
13	*BCL2*	B-cell lymphoma-2	40
14	*IL10*	Interleukin-10	39
15	*CXCL8*	C-X-C motif chemokine ligand 8	39
16	*HIF1A*	Hypoxia-inducible factor 1-alpha	39
17	*ESR1*	Estrogen receptor	38
18	*MAPK3*	Mitogen-activated protein kinase 3	38
19	*FOS*	Proto-oncogene c-Fos	38
20	*STAT1*	Signal transducer and activator of transcription 1	38

3.3. Biological function enrichment analysis

3.3.1. GO enrichment analysis

ClusterProfiler package identified 2,742 enriched GO terms, including 2473 bio-logical processes (BP), 78 cellular components (CC), and 191 molecular functions (MF). Top 10 GO terms for BP, CC, and MF were plotted. BP involved responses to lipopolysaccharides, chemical stress, nutrient levels, reactive oxygen species metabolism, drug responses, oxidative stress, muscle cell proliferation, and cellular response to oxidative stress. CC encompassed membrane rafts, plasma membrane rafts, vesicular lumen, and transcriptional regulatory complexes. MF included nuclear receptor activity, ligand-activated transcription factor activity, DNA-bindintranscription factor binding, and cytokine receptor binding, *etc*. (Figure 2A).

3.3.2. KEGG pathway enrichment analysis

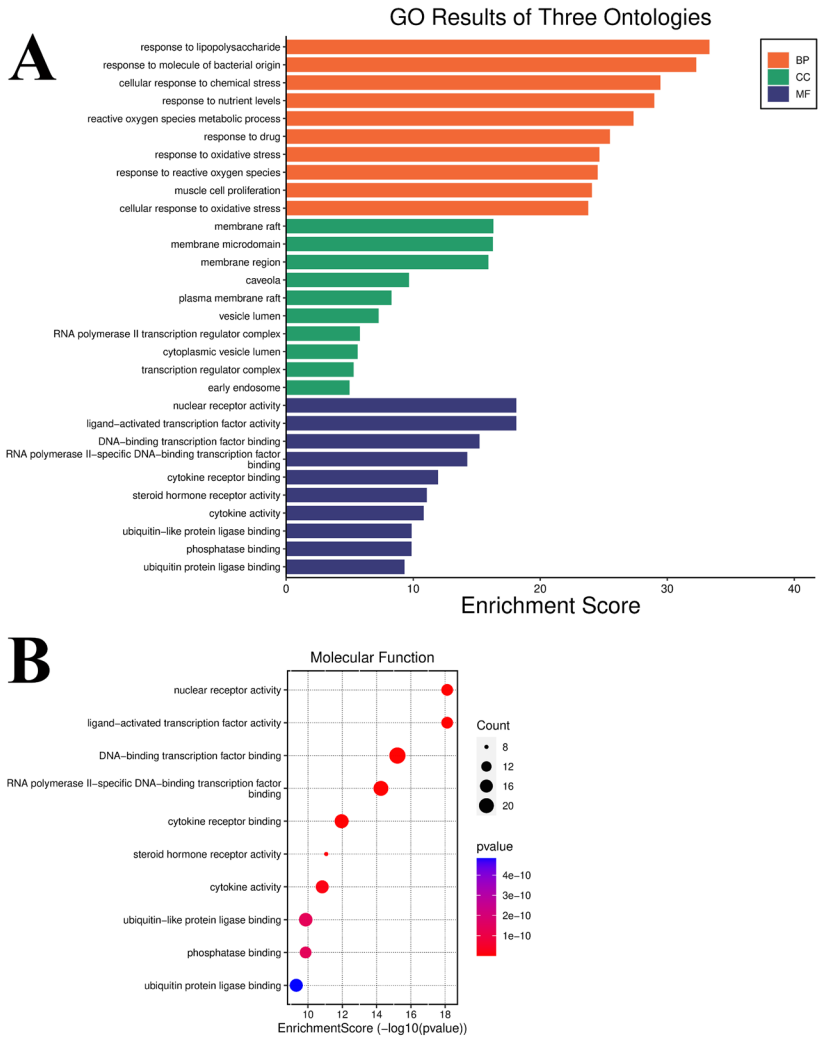

Figure 2. Enrichment analysis of SLGP on GDM. (A) The biological process, cellular component, and molecular function of GO analysis were shown. **(B)** KEGG pathway analysis showed the top 20 enrichment pathways.

KEGG Pathway analysis identified 179 pathways relevant to GDM treatment, with the top 20 pathways selected for mapping. Pathways included lipid and atherosclerosis, AGE-RAGE signaling pathway in complications of diabetes, hepatitis B, fluid shear stress and atherosclerosis, prostate cancer, and others, suggesting potential regulatory mechanisms of Chinese herbal compounds, *etc*. (Figure 2B).

3.4. SLGP treatment improves glucose metabolism in GDM model rats

GDM model rats were gavaged with SLGP (4.5, 9, or 18 mg/kg) or metformin (52.5 mg/kg), while blank and model group rats were instead gavaged with an equal volume of 0.9% saline once per day for two weeks. Relative to blank controls, GDM model groups exhibited significantly elevated insulin levels ($P < 0.01$). Compared with the model group, high-dose SLGP treatment significantly lowered insulin levels in these experimental rats (Table 3, $P < 0.05$).

3.5. SLGP suppresses intestinal barrier-related inflammatory factor production

Relative to blank controls, significant increases in CRP, IL-6, IL-1β, TGF-β, TNF-α, and LPS levels were detected in the model group ($P < 0.05$). SLGP treatment significantly reduced the levels of these inflammatory factors relative to the model group ($P < 0.05$), and similar reductions were observed in the metformin group, albeit without any significant differences in TGF-β and TNF-α levels (Table 4).

Table 3. The impact of SLGP on glycometabolic activity ($\bar{x} \pm s$, $n = 8$)

Groups	*n*	INS/pg·mL^{-1}
Normal	8	115.89 ± 48.66**
GDM	8	239.96 ± 47.97
Low-dose SLGP	8	193.65 ± 93.82
Medium-dose SLGP	8	224.47 ± 55.61
High-dose SLGP	8	137.30 ± 55.26*
Metformin group	8	205.16 ± 20.96

$^{*}P < 0.05$ *vs.* GDM; $^{**}P < 0.01$ *vs.* GDM.

3.6. SLGP modulates serum TLR4 and p-NF-κB p65 levels in rats

Significantly elevated TLR4 and p-NF-κB p65 levels were detected in the model group as compared to the blank group ($P < 0.05$), while these levels were significantly reduced relative to model rats in serum samples from the medium-dose SLGP group (Table 5, $P < 0.05$).

3.7. SLGP treatment alters intestinal barrier histopathology in GDM model rats

Control group rats exhibited a colonic structure that was intact without any apparent evidence of inflammatory cell infiltration or necrosis. Model group rats presented with degenerative changes in the mucosal layer, a congested and edematous submucosal layer, a thinner muscle layer, an enlarged intestinal lumen, and some degree of crypt loss. For rats in the low-, medium-, and high-dose SLGP treatment groups, mucosal degeneration and submucosal congestion and edema were still evident, but the degree of inflammatory cell infiltration was reduced as compared to that observed for GDM model rats. Mucosal and submucosal necrosis were evident in the metformin group, together with mild edema, congestion, and inflammatory cell infiltration (Figure 3).

3.8. SLGP affects colon TLR4, p-NF-κB p65 protein expression

Western immunoblotting revealed significantly elevated TLR4 and p-NF-κB p65 protein levels in the model group as compared to the blank group ($P < 0.05$), while these levels were significantly reduced relative to model rats in colon samples from the medium- and high-dose SLGP groups and the metformin group (Figure 4, $P < 0.05$).

4. Discussion

GDM is a metabolic disorder that frequently arises during pregnancy, exposing both the mother and fetus to substantial health risks. Women diagnosed with GDM also face an elevated risk of subsequently developing postpartum diabetes and cardiovascular

Table 4. The impact of SLGP on inflammatory factors related to the intestinal barrier in rats ($\bar{x} \pm s$, $n = 8$)

Groups	*n*	CRP/ng·mL^{-1}	IL-6/pg·mL^{-1}	IL-1β/pg·mL^{-1}	TGF-β/pg·L^{-1}	TNF-α/ng·L^{-1}	LPS/ng·L^{-1}
Normal	8	262.45 ± 17.87**	42.55 ± 16.71**	75.88 ± 37.77**	30.81 ± 11.46**	159.37 ± 43.08**	37.89 ± 5.97**
GDM	8	326.25 ± 31.81	88.57 ± 11.55	217.48 ± 41.73	55.24 ± 19.38	254.33 ± 84.96	58.26 ± 11.56
Low-dose SLGP	8	284.36 ± 45.45*	30.79 ± 22.69**	139.34 ± 62.27*	31.78 ± 13.44*	210.62 ± 59.41	42.41 ± 11.24**
Medium-dose SLGP	8	267.09 ± 24.45**	24.46 ± 14.25**	130.06 ± 72.32*	35.034 ± 14.09*	163.27 ± 23.93**	43.58 ± 6.33**
High-dose SLGP	8	274.50 ± 40.09**	39.26 ± 15.18**	114.63 ± 41.36**	32.03 ± 56.68*	168.20 ± 24.85*	43.99 ± 7.41**
Metformin	8	271.175 ± 20.96**	34.59 ± 23.36**	141.07 ± 58.72*	38.47 ± 19.60	211.25 ± 58.21	38.68 ± 4.49**

$^{*}P < 0.05$ *vs.* GDM; $^{**}P < 0.01$ *vs.* GDM.

Table 5. The impact of SLGP on signaling pathway molecules in GDM model rats ($\bar{x} \pm s$, $n = 8$)

Groups	*n*	TLR4/ng·mL^{-1}	p-NF-κBp65/pg·mL^{-1}
Normal	8	0.88 ± 0.10*	177.15 ± 70.85*
GDM	8	1.15 ± 0.08	267.23 ± 82.00
Low-dose SLGP	8	0.95 ± 0.26	227.50 ± 32.08
Medium-dose SLGP	8	0.84 ± 0.19**	183.39 ± 54.98*
High-dose SLGP	8	0.99 ± 0.19	223.90 ± 28.37
Metformin	8	1.27 ± 0.17	296.95 ± 77.15

$^{*}P < 0.05$ *vs.* GDM; $^{**}P < 0.01$ *vs.* GDM.

diseases, while their infants are also more likely to develop complications including macrosomia, neonatal hypoglycemia, and respiratory distress syndrome (*18,19*), and they may also develop long-term health issues including childhood obesity and cardiovascular diseases when they reach adulthood (*20,21*). Insulin resistance is a hallmark of GDM and a key driver of the pathogenesis of this condition (*22*). A variety of complex interactions between environmental, inflammatory, and genetic factors underlie GDM development (*23,24*). The gut

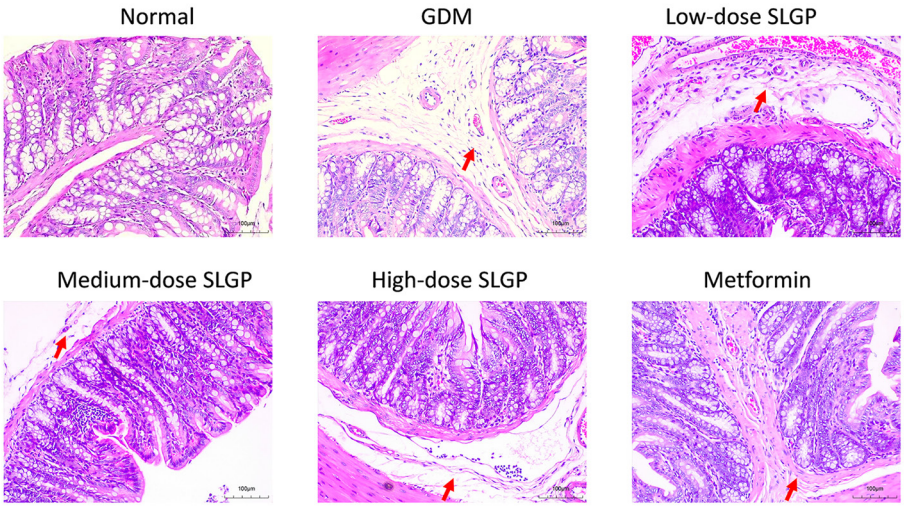

Figure 3. The impact of SLGP on colon tissue pathology in rats (H&E, 100×).

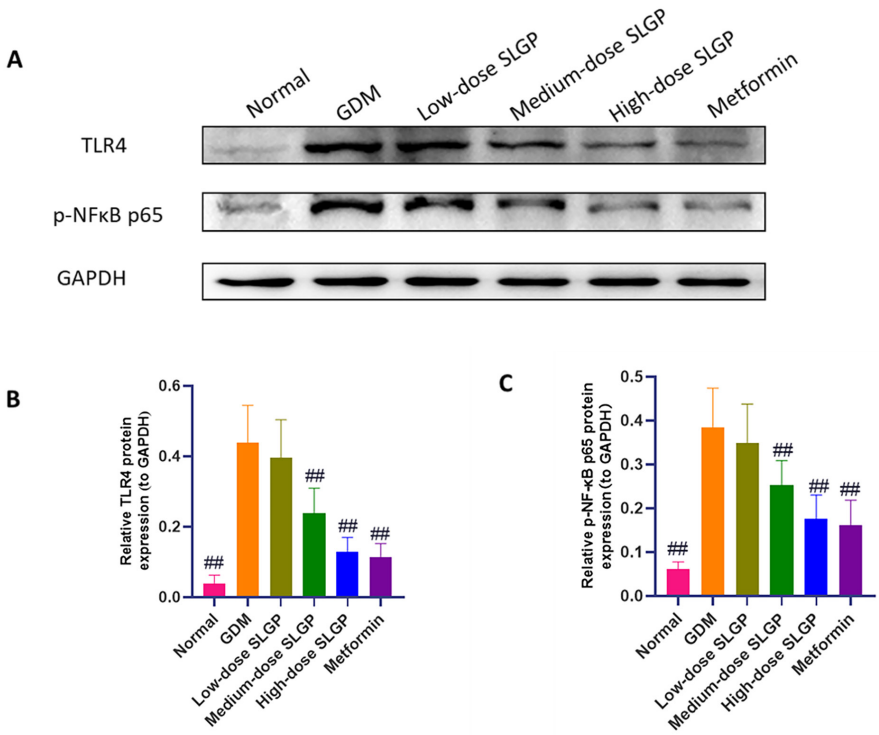

Figure 4. Colon tissue TLR4 and p-NF-κB p65 protein levels in different groups as detected by Western immunoblotting. Data are means ± SD and were compared with one-way ANOVAs and Tukey's post hoc test. $^{\#\#}P < 0.05$ *vs.* GDM group. **(A)** TLR4, p-NF-κB p65, and GAPDH were detected by Western immunoblotting. **(B, C)** Statistical analyses of TLR4/GAPDH **(B)** and p-NF-κB p65/GAPDH **(C)** levels.

microbiome and dysfunction of the intestinal barrier layer have both been demonstrated to be closely associated with GDM onset (*25,26*). Moreover, hyperglycemia has been shown to exert detrimental effects on the intestinal barrier function. The intestinal barrier is crucial for maintaining homeostasis and preventing the translocation of potentially harmful substances from the gut lumen into the circulation. Under high glucose conditions, the intestinal epithelial cells can undergo changes that compromise the integrity of tight junctions and adherens junctions, leading to increased intestinal permeability (*27*). Furthermore, hyperglycemia has been associated with an increase in the risk of enteric infection by compromising the intestinal barrier's ability to control microbial translocation. This was demonstrated in a study where hyperglycemia was shown to drive intestinal barrier dysfunction and risk for enteric infection, potentially leading to a vicious cycle of inflammation and further impairment of barrier function (*28*). Under physiological conditions, the intestinal barrier functions as a key boundary interface between the host and the lumen of the gut which is vital to the maintenance of systemic homeostasis (*29*).

Our network pharmacology analysis precisely identified a select group of target genes pivotal to inflammatory pathways in GDM, including *IL6*, *TNF*, and *IL1β*, represents the cornerstone of the inflammatory response, with well-established roles in immune regulation and pro-inflammatory cytokine production. Furthermore, GDM has been proposed to be related to intestinal mucosal damage that leads to LPS leakage into systemic circulation as a consequence of greater intestinal permeability (*30-32*). This, in turn, triggers inflammatory signaling mediated by TLR4 and other pattern recognition receptors, driving NF-κB pathway activation that culminates in pro-inflammatory cytokine production and the onset and/or exacerbation of insulin resistance (*33,34*).

The gut microflora comprises a complex microecological system that is integral to the control of host immunity and metabolic function. Intestinal dysbiosis has been linked to GDM in the past. Gut microbiota disruptions can affect metabolite and signaling molecule production, thereby compromising the integrity of the intestinal barrier and giving rise to systemic inflammatory activity (*35,36*). The restoration of gut microbiota homeostasis may thus be an effective and novel approach to GDM management (*37-40*).

In this study, a rat model of GDM was employed to study how SLGP affects intestinal barrier inflammation and TLR4/NF-κB pathway signaling. In prior studies, we have found that SLGP offers promise owing to its ability to modulate the composition of the gut microbiome and to improve glycometabolic activity in GDM model rats, possibly through its effects on TLR4/NF-κB signaling induced by LPS. In this study, the precise underlying mechanisms whereby SLGP can treat GDM were explored at length, focusing in particular on TLR4/NF-κB signaling. These analyses ultimately suggest that SLGP can inhibit the stimulatory effects of LPS, thereby helping to reduce inflammation and insulin resistance. Together, these findings suggest that SLGP is capable of enhancing the degree of glycemic control in GDM model rats through the alleviation of inflammation and insulin resistance.

These results suggest that SLGP treatment can strengthen the intestinal barrier in GDM model rats, as evidenced by observed histopathological improvements in the colon tissues from these SLGP-treated rats. These improvements in barrier integrity may help mitigate LPS translocation across the compromised barrier interface. Consistent with such a model, TLR4 and p-NF-κB p65 protein levels were reduced by SLGP treatment with a concomitant reduction in inflammatory factor expression consistent with the suppression of the inflammatory response.

While this study underscores the promising therapeutic utility of SLGP as an approach to GDM management, there are certain limitations to this therapeutic strategy. Firstly, there is a lack of research on the effect of STZ on intestinal barrier, so it is not clear whether STZ has an effect on intestinal barrier. Secondly, the GDM modeling, which induced by STZ, involves the destruction of pancreatic β-cells, results in a form of diabetes that is more akin to type 1 diabetes rather than GDM, which is primarily characterized by insulin resistance during pregnancy. Thirdly, most studies of the efficacy of SLGP-based management of GDM to date have been conducted in animal model systems, while clinical data availability remains limited. Further clinical trials are thus warranted to inform patient treatment. Accordingly, future studies will center on the implementation of large-scale, multi-center, randomized controlled clinical trials based on the present results in order to help bridge the gap between basic preclinical research and clinical utility. This strategy will ultimately help provide an evidence-based foundation for the management of GDM using traditional Chinese medicine.

In summary, these results suggest that SLGP may offer value as a treatment for GDM through its ability to suppress TLR4/NF-κB pathway activity and to restore the integrity and function of the intestinal barrier.

Funding: This work was supported by grants from a project for the Science and Technology Department of Guizhou Province (grant No. Qian Ke He Ji Chu -ZK[2023] General 434), projects under National Natural Science Foundation of China (grant no.82460949 to ZZ Hua, grant no.82374243 to L Wang and grant no. 82304906 to LS Li).

Conflict of Interest: The authors have no conflicts of interest to disclose.

References

1. Sartayeva A, Danyarova L, Begalina D, Nurgalieva Z, Baikadamova L, Adilova G. Gestational diabetes: Prevalence and risks for the mother and child. Georgian Med News. 2022; 328-329:47-52.
2. Lowe WL Jr, Scholtens DM, Lowe LP, *et al*. Association of gestational diabetes with maternal disorders of glucose metabolism and childhood adiposity. JAMA. 2018; 32:1005-1016.
3. Chen T, Qin Y, Chen M, Zhang Y, Wang X, Dong T, Chen G, Sun X, Lu T, White RA 3rd, Ye P, Tun HM, Xia Y. Gestational diabetes mellitus is associated with the neonatal gut microbiota and metabolome. BMC Med. 2021; 19:120.
4. Johns EC, Denison FC, Norman JE, Reynolds RM. Gestational diabetes mellitus: Mechanisms, treatment, and complications. Trends Endocrinol Metab. 2018; 29:743-754.
5. Plows JF, Stanley JL, Baker PN, Reynolds CM, Vickers MH. The pathophysiology of gestational diabetes mellitus. Int J Mol Sci. 2018; 19:3342.
6. Chen T, Liu D. The mystery of exosomes in gestational diabetes mellitus. Oxid Med Cell Longev. 2022; 2022:2169259.
7. Ionescu RF, Enache RM, Cretoiu SM, Gaspar BS. Gut microbiome changesin gestational diabetes. Int J Mol Sci. 2022; 23:12839.
8. Wheeler AE, Stoeger V, Owens RM. Lab-on-chip technologies for exploringthe gut-immune axis in metabolic disease. Lab Chip. 2024; 24:1266-1292.
9. Pheiffer C, Riedel S, Dias S, Adam S. Gestational diabetes and the gut microbiota: Fibre and polyphenol supplementation as a therapeutic strategy. Microorganisms. 2024; 12:633.
10. Sun Z, Pan XF, Li X, *et al*. The gut microbiome dynamically associates with host glucose metabolism throughout pregnancy: Longitudinal findings from a matched case-control study of gestational diabetes mellitus. Adv Sci (Weinh). 2023; 10:e2205289.
11. Yang J, Wang J, Wu W, Su C, Wu Y, Li Q. Xylooligosaccharides ameliorate insulin resistance by increasing *Akkermansia muciniphila* and improving intestinal barrier dysfunction in gestational diabetes mellitus mice. Food Funct. 2024; 15:3122-3129.
12. Tajik N, Frech M, Schulz O, *et al*. Targeting zonulin and intestinal epithelial barrier function to prevent onset of arthritis. Nat Commun. 2020; 11:199.
13. Wang S, Cui Z, Yang H. Interactions between host and gut microbiota in gestational diabetes mellitus and their impacts on offspring. BMC Microbiol. 2024; 24:161.
14. Cortez RV, Taddei CR, Sparvoli LG, Ângelo AGS, Padilha M, Mattar R, Daher S. Microbiome and its relation to gestational diabetes. Endocrine. 2019; 64:254-264.
15. Facchinetti F, Dante G, Petrella E, Neri I. Dietary interventions, lifestyle changes, and dietary supplements in preventing gestational diabetes mellitus: A literature review. Obstet Gynecol Surv. 2014; 69:669-680.
16. Xu YXZ, Xi S, Qian X. Evaluating traditional Chinese medicine and herbal products for the treatment of gestational diabetes mellitus. J Diabetes Res. 2019; 2019:9182595.
17. Gao X, He J, Zhu A, Xie K, Yan K, Jiang X, Xu Y, Li Q, Xu A, Ye D, Guo J. Modelling gestational diabetes mellitus: large animals hold great promise. Rev Endocr Metab Disord. 2021; 22:407-420.
18. Cho NH, Shaw JE, Karuranga S, Huang Y, da Rocha Fernandes JD, Ohlrogge AW, Malanda B. IDF diabetes atlas: Global estimates of diabetes prevalence for 2017 and projections for 2045. Diabetes Res Clin Pract. 2018; 138:271-281.
19. Tarry-Adkins JL, Aiken CE, Ozanne SE. Neonatal, infant, and childhood growth following metformin versus insulin treatment for gestational diabetes: A systematic review and meta-analysis. PLoS Med. 2019; 16:e1002848.
20. Sweeting A, Wong J, Murphy HR, Ross GP. A clinical update on gestational diabetes mellitus. Endocr Rev. 2022; 43:763-793.
21. Perak AM, Lancki N, Kuang A, Labarthe DR, Allen NB, Shah SH, Lowe LP, Grobman WA, Lawrence JM, Lloyd-Jones DM, Lowe WL Jr, Scholtens DM. Associations of maternal cardiovascular health in pregnancy with offspring cardiovascular health in early adolescence. JAMA. 2021; 325:658-668.
22. Lin J, Jin H, Chen L. Associations between insulin resistance and adverse pregnancy outcomes in women with gestational diabetes mellitus: A retrospective study. BMC Pregnancy Childbirth. 2021; 21:526.
23. Alejandro EU, Mamerto TP, Chung G, Villavieja A, Gaus NL, Morgan E, Pineda-Cortel MRB. Gestational diabetes mellitus: A harbinger of the vicious cycle of diabetes. Int J Mol Sci. 2020; 21:5003.
24. Ruszała M, Niebrzydowska M, Pilszyk A, Kimber-Trojnar Ż, Trojnar M, Leszczyńska-Gorzelak B. Novel biomolecules in the pathogenesis of gestational diabetes mellitus. Int J Mol Sci. 2021; 22:11578.
25. Di Tommaso N, Gasbarrini A, Ponziani FR. Intestinal barrier in human health and disease. Int J Environ Res Public Health. 2021; 18:12836.
26. Cui M, Qi C, Yang L, Zhang M, Wang H, She G, Yu R, Miao T, Sun J. A pregnancy complication-dependent change in SIgA-targeted microbiota during third trimester. Food Funct. 2020; 11:1513-1524.
27. Qing Q, Zhang S, Chen Y, Li R, Mao H, Chen Q. High glucose-induced intestinal epithelial barrier damage is aggravated by syndecan-1 destruction and heparanase overexpression. J Cell Mol Med. 2015; 19:1366-1374.
28. Dubois N, Muñoz-Garcia J, Heymann D, Renodon-Cornière A. High glucose exposure drives intestinal barrier dysfunction by altering its morphological, structural and functional properties. Biochem Pharmacol. 2023; 216:115765.
29. Ye D, Huang J, Wu J, Xie K, Gao X, Yan K, Zhang P, Tao Y, Li Y, Zang S, Rong X, Li J, Guo J. Integrative metagenomic and metabolomic analyses reveal gut microbiota-derived multiple hits connected to development of gestational diabetes mellitus in humans. Gut Microbes. 2023; 15:2154552.
30. Odenwald MA, Turner JR. The intestinal epithelial barrier: A therapeutic target? Nat Rev Gastroenterol Hepatol. 2017; 14:9-21.
31. Huang L, Thonusin C, Chattipakorn N, Chattipakorn SC. Impacts of gut microbiota on gestational diabetes mellitus: A comprehensive review. Eur J Nutr. 2021; 60:2343-2360.
32. Zhang H, Qi C, Zhao Y, Lu M, Li X, Zhou J, Dang H, Cui M, Miao T, Sun J, Li D. Depletion of gut secretory immunoglobulin a coated *Lactobacillus reuteri* is associated with gestational diabetes mellitus-related intestinal mucosal barrier damage. Food Funct. 2021; 12:10783-10794.

33. Liu Y, Sun R, Lin X, Wu L, Chen H, Shen S, Li Y, Wei Y, Deng G. Procyanidins and its metabolites by gut microbiome improves insulin resistance in gestational diabetes mellitus mice model *via* regulating NF-κB and NLRP3 inflammasome pathway. Biomed Pharmacother. 2022; 151:113078.
34. Ding S, Xu S, Ma Y, Liu G, Jang H, Fang J. Modulatory mechanisms of the NLRP3 inflammasomes in diabetes. Biomolecules. 2019; 9:850.
35. Feng H, Su R, Song Y, Wang C, Lin L, Ma J, Yang H. Positive correlation between enhanced expression of TLR4/MyD88/NF-κB with insulin resistance in placentae of gestational diabetes mellitus. PLoS One. 2016; 11:e0157185.
36. Medici Dualib P, Ogassavara J, Mattar R, Mariko Koga da Silva E, Atala Dib S, de Almeida Pititto B. Gut microbiota and gestational diabetes mellitus: A systematic review. Diabetes Res Clin Pract. 2021; 180:109078.
37. Wang X, Liu H, Li Y, Huang S, Zhang L, Cao C, Baker PN, Tong C, Zheng P, Qi H. Altered gut bacterial and metabolic signatures and their interaction in gestational diabetes mellitus. Gut Microbes. 2020; 12:1-13.
38. Liang W, Feng Y, Yang D, Qin J, Zhi X, Wu W, Jie Q. Oral probiotics increased the proportion of Treg, Tfr, and Breg cells to inhibit the inflammatory response and impede gestational diabetes mellitus. Mol Med. 2023; 29:122.
39. Hasain Z, Mokhtar NM, Kamaruddin NA, Mohamed Ismail NA, Razalli NH, Gnanou JV, Raja Ali RA. Gut microbiota and gestational diabetes mellitus: A review of host-gut microbiota interactions and their therapeutic potential. Front Cell Infect Microbiol. 2020; 10:188.
40. Homayouni A, Bagheri N, Mohammad-Alizadeh-Charandabi S, Kashani N, Mobaraki-Asl N, Mirghafurvand M, Asgharian H, Ansari F, Pourjafar H. Prevention of gestational diabetes mellitus (GDM) and probiotics: Mechanism of action: A review. Curr Diabetes Rev. 2020; 16:538-545.

Received September 8, 2024; Revised December 1, 2024; Accepted December 4, 2024.

[§]These authors contributed equally to this work.

**Address correspondence to:*
Ling Wang, Department of Obstetrics and Reproductive Immunology, Shanghai East Hospital, Tongji University School of Medicine, No. 1800 Yuntai Road, Shanghai 200120, China.
E-mail: dr.wangling@vip.163.com

Zhaozhao Hua, Department of Obstetrics, The Second Affiliated Hospital of Guizhou University of Chinese Medicine, Guiyang, Guizhou 550002, China.
E-mail: gzyefyzzh1@163.com

Released online in J-STAGE as advance publication December 12, 2024.

Original Article

DOI: 10.5582/ddt.2024.01078

Corticosteroid dose escalation in non-ICU COVID-19 patients with worsening lung lesions reduces lesion severity without improving clinical outcomes

Qingqing Wang, Qing Miao, Yuyan Ma, Yi Su, Jue Pan, Bijie Hu*

Department of Infectious Diseases, Zhongshan Hospital, Fudan University, Shanghai, China.

SUMMARY The effect of increasing corticosteroid doses on clinical outcomes and chest findings in patients with coronavirus disease (COVID-19) pneumonia and lung disease remains unknown. We aimed to investigate the effects of increasing steroid dosage on chest lesion area and clinical outcomes in patients with moderate or severe COVID-19 and progressive lung involvement on chest computed tomography (CT). A total of 105 patients with radiological progression during methylprednisolone (MP) therapy either received an increased MP dose (n = 79) or were maintained on the same MP dose (n = 26). These patients were divided into dose-increment and no-change groups according to the MP dose adjustment strategy. Clinical features, changes in CT severity scores within 7 days after steroid adjustment, and outcomes were compared between the groups. Six (7.6%) and one (3.8%) patients in the dose-increment and no-change groups, respectively, had increasing World Health Organization outcome scores 96 h after MP adjustment (P = 0.678). Length of stay [15 days (IQR: 10-24) *vs.* 14 days (IQR: 10-25); P = 0.994] and in-hospital death rate (7.6% *vs.* 3.8%; P = 0.678) showed no significant differences between the groups. Logistic regression analyses revealed that an increased MP dose was significantly associated with improvement in CT lesion area compared with no change in MP dose, but the CT lesions deteriorated subsequently (79.7% *vs.* 53.8%, P = 0.044). In conclusion, increasing the MP dose in patients with worsening CT findings ameliorates CT lesions but fails to prevent serious adverse outcomes.

Keywords coronavirus disease pneumonia, corticosteroid dosage adjustment, outcome, chest CT deterioration

1. Introduction

The coronavirus disease 2019 (COVID-19) epidemic, caused by severe acute respiratory syndrome coronavirus 2 (SARS-CoV-2), in China occurred in December 2019 (*1*). Antiviral agents (*2*), immunomodulators (*3,4*), and antithrombotic drugs (*5,6*) are alternative agents for heterogeneous patients hospitalized for COVID-19 pneumonia.

Corticosteroids are strong anti-inflammatory drugs used to treat various types of pneumonia, such as influenza and SARS. These drugs were recommended for patients with COVID-19 requiring oxygen supplementation in management guidelines, mainly according to the results of the RECOVERY trial (a randomized, controlled, open-label platform trial, named Randomised Evaluation of COVID-19 Therapy) (*7-9*). In this clinical trial, the dose and duration of dexamethasone administration (6 mg/day for 10 days) were based on previous experience of safely using corticosteroids for asthma and chronic obstructive pulmonary disease (*10,11*). Only patients requiring oxygen supplementation had slightly decreased all-cause mortality in hospitals. The influence of corticosteroid treatment on clinical symptoms and lung lesions remains unknown, but it is correlated with the severity of illness and mortality (*12-14*). Moreover, the optimal dose and duration of corticosteroid therapy have not yet been determined, especially in patients with worsening clinical symptoms or lung lesions.

The RECOVERY trial also assessed the benefit of high- and low-dose dexamethasone administration in patients requiring respiratory support (*15*). This study showed that higher doses of corticosteroids significantly increased the risk of death compared with low doses of corticosteroids. Taboada *et al.* (*16*) showed that treatment with a high dose of dexamethasone reduced clinical worsening, including an increased need for FiO_2 or a score > 4 on the 10-point World Health Organization (WHO) Clinical Progression Scale (*17*).

Patients with COVID-19 require oxygen therapy. However, some studies that used intravenous pulses of methylprednisolone (MP) to treat adults with severe COVID-19 pneumonia showed no decrease in mortality or intubation rate (*18*).

Most studies have focused on investigating the effects of different corticosteroid doses on hypoxic patients by recording the need for oxygen therapy, time free from invasive mechanical ventilation, and mortality. However, the effects of corticosteroid dose adjustment remain undetermined in patients who already received steroid treatment and have aggressive hypoxia or an increased number of lung lesions. The pooled prevalence was 90% for chest computed tomographyn (CT) abnormalities in COVID-19 cases (*19*), with ground-glass opacity, consolidation, septal thickening, crazy-paving pattern, and fibrosis. Chest CT is a potential tool in the diagnosis and prognostication of COVID-19 (*12,14,20*), and the CT severity score is a predictor of mortality and short-term prognosis in these cases (*21,22*). Steroids are thought to reduce pulmonary inflammation in severe pneumonia. However, the effect of steroid treatment to the CT lesions in refractory is undetectable. Here, we aimed to investigate the effects of increasing steroid dose on chest lesion areas and clinical outcomes in patients with moderate or severe COVID-19 and progressive lung involvement on chest CT.

2. Patients and Methods

2.1. Study design

This retrospective clinical cohort study was designed to evaluate the effects of different steroid dose adjustment strategies in patients hospitalized for COVID-19 at Zhongshan Hospital, Fudan University in Shanghai, China.

2.2. Participants

Hospitalized patients were enrolled if they were aged ≥18 years, tested positive for SARS-CoV-2 through real-time polymerase chain reaction, were antigen-positive, had clinically suspected COVID-19 as judged by two experienced attending physicians, had pneumonia, and received corticosteroids between December 14, 2022, and January 26, 2023. The exclusion criteria were failure to undergo chest radiology testing after MP therapy, MP dose reduction after radiological progression, and no radiological progression. The specific inclusion and exclusion criteria are shown in the flowchart (Figure 1).

All patients admitted to our department had moderate or severe illness. Severe illness was defined as SpO_2 < 93%, PaO_2/FiO_2 ratio < 300, respiratory rate ≥ 30 breaths per min, or ≥ 50% lung involvement on chest CT. All patients received standard care, including nirmatelvir/ritonavir (paxlovid) and anticoagulant therapy, according to the current guidelines or evidence at the time of admission. Patients with pneumonia were also administered corticosteroids. Other immunomodulators were rarely used.

All patients underwent chest radiology examinations

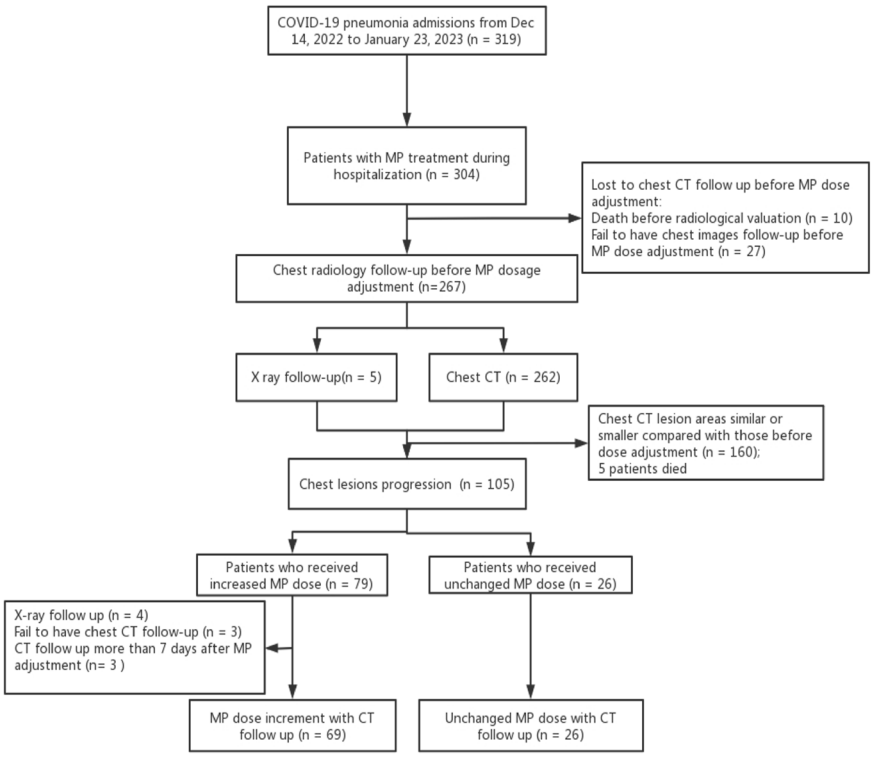

Figure 1. Flow chart.

upon admission and during MP treatment. Progression was defined as lung lesions on chest radiography or CT more than 3 days after MP treatment that were larger than those at admission.

Demographic information, baseline clinical characteristics, complications, and laboratory test results at baseline and follow-up were obtained from the electronic medical records of the patients. Clinical progression was defined as an increase in the level of oxygen supplementation or large chest CT lesions compared with previous ones.

Written informed consent was obtained from all patients before participation in the study. The study was approved by Clinical Research Ethics Committee of Zhongshan Hospital, Fudan University (approval No.: B2023-018).

2.3. CT examination and image evaluation

CT scanning was performed on a 320-slice CT scanner (uCT960+; Shanghai United Imaging Healthcare, Shanghai, China). The CT parameters were as follows: 120 kVp; 300 mAs; detector collimation, 160 × 0.5; pitch, 1.0938; rotation time, 0.5 s; matrix size, 1024 × 1024; field of view, 350 mm; and slice thickness, 1.0 mm, covering the scanning range from the lung apices to the bases.

Most patients underwent chest radiology on admission and every 3-7 days during MP treatment. Two experienced respiratory physicians (with 28 and 22 years of experience), who were blinded to the clinical data, scored and compared the CT findings in consensus. The CT lesions are described using ground-glass opacity, consolidation, patchy consolidation, fibrosis, irregular solid nodules, and interlobular septal thickening (*23*). Meanwhile, the abnormalities including mucoid impactions, focal consolidation, and cavity suggesting bacterial or fungi infection were excluded. The comparison results were divided into three types according to the changes in the lesion area between two adjacent CT images as follows: improvement, no change, and progression. To quantify the extent of lesions, a scoring system was used to assess the abnormal areas. Each of the five lung lobes was scored on a scale of 0 to 5: 0, no involvement; 1, < 5% involvement; 2, 5%–25% involvement; 3, 26%–49% involvement; 4, 50%–75% involvement; and 5, > 75% involvement. Each lobe had a score of 0–5, with a total possible score of 0–25 (*24*).

2.4. Corticosteroid administration

The most common type of steroid was MP; the doses of other types of steroids, such as dexamethasone, were equivalently converted to those of MP. The enrolled participants received MP therapy before or upon admission. The initial dosage was 40–80 mg administered through intravenous injection per day for 10 days, as determined by an experienced physician according to age, complications, hypoxic condition, risk factors, and CT lesion area. Furthermore, the clinicians adjusted the MP dose according to changes in the need for oxygen, breathing rate, symptoms, or CT lesions. Clinical worsening is the worsening of patient condition (increasing need for oxygen and increasing breath rates). The clinicians adjusted the MP dose in patients with clinical worsening or progression of chest CT lesions by increasing the dose by 20–40 mg per day or maintaining the same daily dosage.

2.5. Outcome measures

The primary outcomes of the study were WHO outcome score (WHO Clinical Progression Scale) > 6, length of stay, and in-hospital mortality rate after disease progression (clinical worsening or CT lesion aggression). The WHO outcome scores were assessed for pneumonia aggression 96 h after MP adjustment. This score is based on the level of ventilation required in hospitalized patients, with scores ranging from 4 to 10 (4, room air; 5, oxygen supplementation required; 6, noninvasive positive pressure ventilation usage; 7–9, needing endotracheal intubation; and 10, death). The secondary outcomes of the study were improvement in lung lesion area, reduction in CT severity score within 7 days after MP dose adjustment, and lung lesion reduction, as determined by clinicians.

2.6. Statistical analysis

Categorical data are described using absolute number and percentage, and continuous data are expressed as median (interquartile range [IQR], 25th–75th percentiles), depending on the normality of distribution. Chi-square, Fisher's exact, and Wilcoxon tests were used to measure differences in variables, where appropriate.

The sample size was 69 in group 1 and 26 in group 2, which achieved 77.364% power to result in an odds ratio of the group proportions of 0.297. The proportion in group 1 (treatment group) was assumed to be 0.7530 under the null hypothesis and 0.4752 under the alternative hypothesis. The proportion in group 2 (control group) was 0.7530. The test used was the two-sided Z-Test with unpooled variance. The significance level of the test was 0.05.

A logistic regression model was used to explore the association between the improvement in lung lesions after MP adjustment and the varieties. Multivariate analysis was performed using a multiple logistic regression model that included possible biological variables and varieties at $P < 0.1$. Significance was set at $P < 0.05$, and all tests were two-tailed. Data analyses were performed using SPSS version 25.0.

3. Results

We consecutively included 319 patients with COVID-19 pneumonia; their baseline characteristics are listed in Table S1 (*https://www.ddtjournal.com/action/getSupplementalData.php?ID=232*). The median age was 72 (IQR, 66–82) years; 192 patients (60.2%) were ≥ 70 years, and 207 (64.9%) were men. The most common complications were hypertension (59.2%), diabetes mellitus (35.1%), cardiovascular disease (25.7%), malignancy (15.9%), and chronic kidney disease (14.4%). A total of 144 (44.2%) patients had severe illness and 128 (40.1%) had $PaO_2/FiO_2 \leq 300\%$ on admission. A total of 304 patients who were administered MP therapy were enrolled. The median number of days from onset to initial steroid use was 8 (IQR, 6–10) and the number of days of MP use (≥ 20 mg per days) was 11 (IQR 7.16).

Finally, 105 patients with aggressive lung lesions were enrolled; 79 patients received MP dose increments and 26 received an unchanged dose of MP. Table 1 lists the clinical features of the two groups. No significant differences were observed between the groups in terms of age, sex, or comorbidities. The median daily dose of MP before MP adjustment was 40 mg (40, 60) in the dose-increment group and 58 mg (51, 92) in the no-change group ($P < 0.001$). The number of days from onset to MP adjustment did not differ between the groups [9 (IQR 7–14) days *vs.* 7 (IQR 7–13) days; $P = 0.343$].

3.1. Laboratory findings

The laboratory findings on admission and before MP adjustment are shown in Table 1. Baseline laboratory test results, such as lymphopenia and C-reactive protein (CRP), lactate dehydrogenase, and D-dimer levels, did not differ between the groups. The median oxygen index on admission in the dose-increment group was lower than that in the other group [28.5% (IQR, 230–371) *vs.* 33.6% (IQR, 275–403); $P = 0.105$]. The CRP level was tested when the radiological results worsened in the dose-increment group, and it was significantly higher than that in no-change group [3.2 (5.3–47.6) *vs.* 8.15 (2.5–19.1); $P = 0.029$].

3.2. Clinical outcomes

The clinical outcomes are shown in Table 1. We found that 87.3% and 96.2% patients had a WHO outcome score of < 6 in the dose-increment and no-change groups, respectively ($P = 0.285$). Notably, 12.6% of the patients in the dose-increment group had a WHO outcome score of 6 (need high flow or noninvasive ventilation), which was higher than that in the no-change group (3.8%). The dynamics of the WHO scores after MP dose adjustment in the two groups are shown in Figure 2.

Six of the seventy-nine patients in the dose-increment group and one of the twenty-six patients in the no-change group showed increasing WHO outcome scores 96 h after MP adjustment ($P = 0.678$). In-hospital death occurred in six (7.6%) patients in the dose-increment group and in one (3.8%) patient in the no-change group ($P = 0.180$). Two (2.5%) of the seventy-nine patients in the dose-increment group received invasive mechanical ventilation, whereas none in the other group received the same. The median time to hospital discharge was 15 days (IQR, 10–24 days) in the dose-increment group and 14 days (IQR, 10–25 days) in the no-change group ($P = 0.994$) (Figure 3).

3.3. Series chest CT assessment results

Eventually, 95 patients underwent follow-up chest CT 7 days after CT radiological progression. Clinical features and chest CT score changes are shown in Table S2 (*https://www.ddtjournal.com/action/getSupplementalData.php?ID=232*). The median CT score on MP dose adjustment was 10.5 (IQR, 7.8–16.0) in the dose-increment group and 10.5 (IQR, 7.8–16.0) in the no-change group ($P = 0.952$).

Chest CT scanning was conducted before and after MP dose adjustment at an interval of 4 (IQR, 3–5) days in the dose-increment group and 4.5 (IQR: 4–5) days in the no-change group ($P = 0.03$). The CT score changes in the two groups are shown in Figures 4A-4C. We found that 52/69 (75.3%) patients in the dose-increment group and 14/26 (53.8%) patients in the no-change group showed CT score reductions ($P = 0.042$). Meanwhile, 55/69 (79.7%) patients in the dose-increment group and 14/26 (53.8%) in the no-change group showed CT lesion area reductions ($P = 0.012$).

The univariate analysis showed that the time between CT scans and MP dose increment significantly correlated with CT lesion reduction after MP dose adjustment (Table S3, *https://www.ddtjournal.com/action/getSupplementalData.php?ID=232*). The multivariate logistic regression analysis was performed using the CT area reduction and variables including severe illness, immunosuppression, CT scores at MP dose adjustment, time between CT scans, and MP dose increment. The results showed that patients who received increasing MP doses had a proportional benefit in lung involvement reduction compared with patients in the no-change group (odds ratio, 4.235; 95% confidence interval, 1.141–15.718; $P = 0.031$) (Figure 5).

4. Discussion

Treatment with higher doses of steroids decreases clinical worsening, and it may be associated with a significant reduction in mortality (*16,25,26*). However, the efficacy of current steroid dose modulation methods is yet to be demonstrated in patients with lung imaging deterioration who have already received corticosteroids. In this retrospective cohort study involving 105 patients

Table 1. Comparison of clinical characteristics and primary outcomes between groups

	No. total (n = 105)	MP increasing group (n = 79)	MP no-change group (n = 26)	P value
Age (years)	74 (67, 81)	72 (67, 81)	76 (69, 83)	0.286
Sex (male)	68 (64.8)	51 (64.5)	17 (65.4)	0.939
Days from onset to MP dose adjustment (> 14 days)	46 (43.8)	34 (43.0)	12 (46.2)	0.822
Severity on admission				0.823
Moderate	47 (44.8)	36 (45.6)	11 (42.3)	
Severe	58 (55.2)	43 (54.4)	15 (57.7)	
WHO outcome score on MP adjustment				0.285
< 6	94 (89.5)	69 (87.3)	25 (96.2)	
≥ 6	11 (10.5)	10 (12.7)	1 (3.8)	
Diabetes mellitus	39 (37.1)	30 (38.0)	9 (34.6)	0.758
Hypertension	26 (24.8)	20 (25.3)	6 (23.1)	0.818
Malignancy	69 (65.7)	54 (68.4)	15 (57.7)	0.32
Cardiovascular disease	30 (28.6)	21 (26.6)	9 (34.6)	0.432
Chronic kidney disease	13 (12.4)	9 (11.4)	4 (15.4)	0.732
Chronic lung disease	12 (11.4)	7 (8.9)	5 (19.2)	0.149
Immunosuppression	10 (9.5)	7 (8.9)	3 (11.5)	0.706
Mean dose of daily MP before adjustment (mg)	49 (40, 64)	40 (40,60)	58 (51,92)	0.001
Days from onset to MP dose adjustment	13 (10, 17)	13 (10,17)	11.5 (9.8,17.5)	0.964
Days from onset to admission	8 (7, 14)	9 (7,14)	7 (6.5,12.5)	0.343
Oxygen index on admission	295 (241, 379)	285 (230,371)	336 (275,403)	0.105
CT score at adjustment	11 (7, 16)	11 (7,17)	10.5 (7.8,16.0)	0.952
Laboratory data on admission				
lymphocyte count ($\times 10^9$/L)	0.7 (0.4, 1.0)	0.7 (0.5,1)	0.7 (0.4,0.9)	0.472
< 1 × 10^9/L	77 (73.3)	57 (72.2)	20 (76.9)	0.633
≥ 1 × 10^9/L	28 (26.7)	22 (27.8)	6 (23.1)	
Platelet count ($\times 10^9$/L)	163 (117.5, 222.5)	167 (122,228)	157 (109,208)	0.598
CD4 count (cell/μL)	209 (131, 313.5)	221 (131,350)	205 (105,252)	0.266
< 400 (cell/μL)	73 (79.3)	55 (77.5)	18 (85.7)	0.547
≥ 400 (cell/μL)	19 (20.7)	16 (22.5)	3 (14.3)	
D-dimer (mg/L)	0.7 (0.4, 1.7)	0.7 (0.4,1.6)	0.8 (0.4,2.5)	0.456
< 1 mg/L	70 (66.7)	54 (68.4)	16 (61.5)	0.522
≥ 1 mg/L	35 (33.3)	25 (31.6)	10 (38.5)	
Procalcitonin (ng/mL)	0.1 (0.06, 0.16)	0.09 (0.06,0.15)	0.13 (0.08,0.345)	0.056
Serum lactate dehydrogenase (U/L)	289 (227, 344)	286 (223,345)	297 (256,354)	0.173
< 245	30 (29.7)	24 (31.6)	6 (24.0)	0.472
≥ 245	71 (70.3)	52 (68.4)	19 (76.0)	
Serum albumin (gL)	36 (33, 40)	37 (33,40)	36 (33.5,40)	0.849
< 30 (g/L)	8 (7.8)	7 (9.0)	1 (4.0)	0.676
≥ 30 (g/L)	95 (92.2)	71 (91.0)	24 (94.0)	
C-reaction protein (mg/L)				
< 40 (mg/L)	39 (37.5)	28 (35.9)	11 (42.3)	0.559
≥ 40 (mg/L)	65 (62.5)	50 (64.1)	15 (57.7)	
Clycosylated hemoglobin (%)	6.3 (5.9, 7.1)	6.3 (5.9,6.9)	6.2 (5.9,7.35)	0.97
Interleukin 1β (pg/mL)	5 (5, 5)	5 (5,5)	5 (5,5)	0.512
Interleukin 2 (pg/mL)	721 (525, 1007)	735 (545,1023.5)	707 (497,928)	0.507
Interleukin 6 (pg/mL)	7.6 (3.6, 21.6)	7.3 (3.8,16.1)	8.33 (3,33.3)	0.528
Interleukin 8 (pg/mL)	21 (10, 46)	21 (11,44)	21 (8,55)	0.561
Interleukin 10 (pg/mL)	6 (5, 11)	5.4 (5,10.7)	7 (5,17.2)	0.343
Laboratory data before MP adjustment				
lymphocyte count ($\times 10^9$/L)	0.7 (0.5, 0.9)	0.7 (0.5,1.0)	0.6 (0.4,0.8)	0.105
< 1 × 10^9/L	72 (76.6)	50 (73.5)	22 (84.6)	0.292
≥ 1 × 10^9/L	22 (23.4)	18 (26.5)	4 (15.4)	
D-dimer (mg/L)	0.86 (0.45, 1.705)	0.91 (0.43,1.73)	0.81 (0.485,1.485)	0.806
< 1 mg/L	49 (53.3)	35 (52.2)	14 (56.0)	0.748
≥ 1 mg/L	43 (46.7)	32 (47.8)	11 (44.0)	
Serum lactate dehydrogenase (U/L)	290 (230, 359)	287 (220,362)	304 (242.75,339.75)	0.738
Procalcitonin (ng/mL)	0.07 (0.05, 0.1)	0.07 (0.05,0.1)	0.07 (0.04,0.1)	0.628
C-reaction protein (mg/L)	13.6 (4.5, 38.6)	23.2 (5.3,47.6)	8.15 (2.5,19.1)	**0.029**
< 40 (mg/L)	72 (75.5)	47 (69.1)	25 (96.2)	**0.005**
≥ 40 (mg/L)	22 (23.4)	21 (30.9)	1 (3.8)	
Interleukin 1β (pg/mL)	5 (5, 5)	5 (5,5)	5 (5,5)	0.182
Interleukin 2 (pg/mL)	737.5 (514.8, 1060.8)	738 (512.5,1064.5)	618 (439.5,803.5)	0.308
Interleukin 6 (pg/mL)	3.7 (2, 7.7)	3.8 (2.1,10.1)	3.2 (2,5.45)	0.299
Interleukin 8 (pg/mL)	21.0 (12.5, 49.5)	22 (12,39.5)	19 (13,91.5)	0.935
Interleukin 10 (pg/mL)	5.0 (5.0, 6.7)	15 (10,24)	5 (5,8.05)	0.797
Noninvasive ventilation or high flow treatment	14 (13.3)	5 (5,6.75)	1 (3.8)	0.18

Table 1. Comparison of clinical characteristics and primary outcomes between groups (continued)

	No. total (n = 105)	MP increasing group (n = 79)	MP no-change group (n = 26)	P value
Mechanical ventilation requirement	2 (1.9)	2 (2.5)	0	1
Admission to ICU	2 (1.9)	2 (2.5)	0	
Length of stay	15 (10, 24)	15 (10,24)	14 (10,25)	0.994
In-hospital death	7 (6.7)	6 (7.6)	1 (3.8)	0.678
WHO score increment 96 h after adjustment	7 (6.7)	6 (7.6)	1 (3.8)	0.678

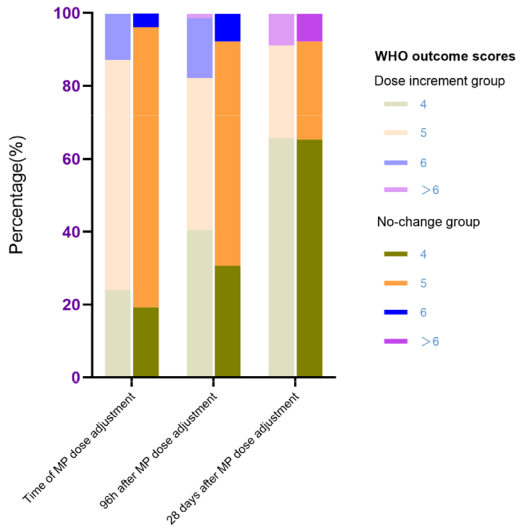

Figure 2. WHO outcome score proportion and dynamics between the groups. Light bar represents the MP dose-increment group; dark bar represents the no-change group. The three sets of bars show the dynamics of WHO outcome score components before and after MP dose adjustment.

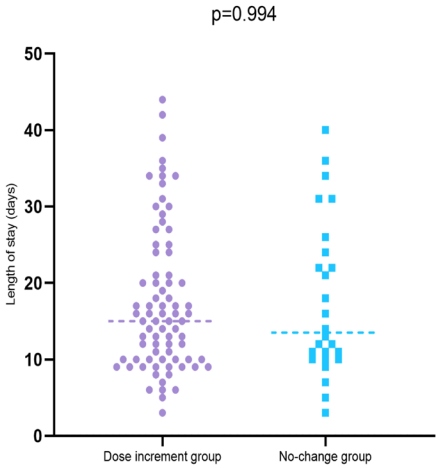

Figure 3. Length of stay in the MP dose-increment and no-change groups.

with COVID-19 with aggressive chest imaging when using steroids, increasing the MP dose was an efficient method for improving lung involvement compared with an unchanged MP dose. Our study provides evidence that MP dose increments prevent radiological progression in patients with deteriorated lung lesions. In our hospital, most participants were older individuals with complications and were at a high risk of progressing to more severe or critical illness. Thus, steroids were the routine therapeutic agents for high-risk patients with moderate-to-severe COVID-19 pneumonia.

We selected MP as the corticosteroid for this study because it has a faster effect and a better penetration in the lung tissue than dexamethasone (*27*). The initial MP dosage in the present study was 40–80 mg per day, depending on the illness severity and severe disease risk. One-third of the patients showed lung lesion deterioration during MP treatment and may have been resistant to steroids (defined as refractory disease) (*28*). This may be due to the low expression of glucocorticoid receptors in these patients. A previous study showed that patients with COVID-19 with high *NR3C1* expression showed a clinical response to corticosteroids (*29*).

Apparently, the beneficial effect of steroid therapy in patients with COVID-19 depends on the selection of the appropriate dose in patients with illness at different levels of severity. A previous study reported that intravenous MP pulse therapy might be beneficial in critically ill patients with acute COVID-19 (*30*). In patients with severe disease, pulsed MP treatment failed to decrease the mortality or intubation rate (*18*). These pulsed-dose therapies have unclear benefits and may slow the clearance of viral RNA and promote further infections (*31,32*). Herein, we propose a steroid treatment strategy in which MP dose is specifically adjusted according to lung involvement to deliver the drug at the right dose to optimize patient benefits. Increasing the MP dose by 20–40 mg per day in patients with COVID-19 with lung lesion deterioration was found to be an effective approach for preventing severe lung lesions.

The rate of CT score reduction before and after the MP dose increment was considerable higher than that in the no-change group. Notably, the sensitivity of CT lesion improvement after MP dose adjustment, as determined by physicians, was higher than that among the CT scoring systems. The reason of this discrepancy may be the area reduction ranging from 1% to 44% for every increase in score of 1 according to the chest CT scoring system. Finally, we selected the lung lesion area reduction as determined by physicians as the secondary outcome and investigated the factors related to this outcome.

Although an increase in the MP dose improved lung involvement in patients, it failed to decrease the

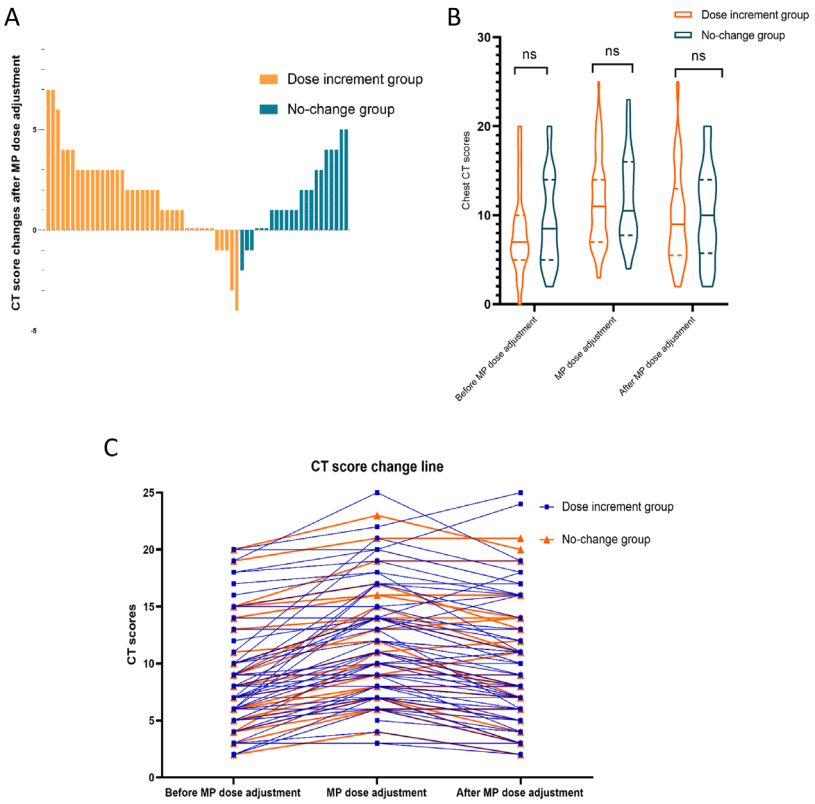

Figure 4. CT score dynamics during MP therapy. A. Chest CT score changes after MP dose adjustment. CT score reduction percentage in the dose-increment group was higher than that in the no-change group. Orange and purple bars represent CT score changes in the dose-increment and no-change groups, respectively. CT score changes showed no significant differences between the groups. **B**. Violin plot showing chest scores between the groups at pre-MP dose adjustment, increasing dose, and post-MP dose adjustment time points. ns, no significant difference between groups. **C**. Spaghetti plot showing CT scores at three time points for 95 patients with available data. Lines connect measurements for individual patients.

	Adjusted OR(95%CI)	p value
Clinical features		
Age(>70y)	1.454(0.445-4.755)	0.535
Sex(male)	1.338(0.364-4.92)	0.662
Days from onset to MP adjustment	0.974(0.888-1.068)	0.57
WHO outcome scores(≥6)	7.105(0.371-136.242)	0.193
Diabetes mellitus	3.616(0.982-13.307)	0.053
Hypertension	1.213(0.254-5.795)	0.808
Malignancy	0.352(0.089-1.391)	0.136
Cardiovascular disease	0.791(0.206-3.039)	0.733
Chronic kidney disease	0.649(0.121-3.487)	0.615
Chronic lung disease	0.424(0.077-2.319)	0.322
Illness Severity(moderate)*	0.539(0.131-2.222)	0.393
Immunosuppression*	0.402(0.069-2.351)	0.312
Mean dose of every MP before adjustment	1.01(0.987-1.033)	0.397
MP dose increasing*	4.235(1.141-15.718)	**0.031**
Chest CT lesion evaluation		
CT score at PM dose adjustment*	0.882(0.751-1.035)	0.123
Time between CT scans conducted*	0.767(0.503-1.169)	0.217

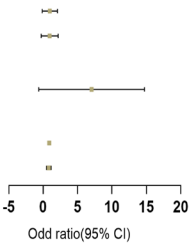

Figure 5. Factors related to CT lesion reduction after MP dose adjustment in patients with COVID-19 with radiological progression. Univariate and multivariate logistic analyses of clinical and CT features of improved lung lesions in non-ICU patients with pneumonia. *factors with $P < 0.2$ in the univariate analysis. Odds ratios are plotted as squares, and the size of each square is proportional to the amount of statistical information available. The horizontal lines represent the 95% confidence intervals.

mortality rate in the current study, which is consistent with the findings of a previous study (*33*). However, unlike previous studies, we investigated the effect of MP dose increment in patients with steroid refractory disease. We hypothesized that the mortality rate in the group that received MP dose adjustment will be low. However, our results contradicted this hypothesis. The main reason for this similar mortality rate may be the

larger proportion of patients with WHO outcome score ≥ 6 in the dose-increment group. The WHO outcome score and serum CRP level at the adjustment stage in the dose-increment group were considerably higher than those in the no-change group. These parameters are associated with increased mortality and exacerbation of COVID-19 (*34,35*).

Even though patients in the dose-increment group did not show significantly lower mortality rates than those in the no-change group, treatment with a higher dose of steroids for at least 10 days significantly reduced mortality in patients with COVID-19, as reported by Taboada *et al.* (*16*) . Further studies should directly investigate the outcomes in a large number of patients with COVID-19 controlled for the same risk factors.

This study had a few limitations. First, because of the small number of aggressive CT patients and the low mortality rate, the mortality rate among the groups was not significantly different. Therefore, we did not conduct Cox regression analysis. Studies with larger cohorts are required. Furthermore, this was an observational study influenced by factors such as the various times of initial MP dosing from onset and loss to CT follow-up. Such factors may have had confounding effects on the outcomes. Finally, we did not follow-up for the effect after discharge among the survivors. Despite these limitations, our study provides a feasible strategy for optimizing steroid therapy in patients with COVID-19 who are not in the ICU.

In conclusion, we demonstrated a strategy for preventing the progression of lung lesions by increasing steroid doses in patients with COVID-19 with refractory pneumonia. We reported the performance of patients with deterioration of lung involvement to demonstrate that our approach may be a remedial measure in refractory patients already using steroids. Treatment may not have been associated with mortality in our patient cohort. This study presents real-life data on the personalized adjustment of steroid doses in patients with COVID-19. A more precise dose adjustment of steroids should be considered in future prospective and larger studies in patients with high risk of illness worsening.

Acknowledgements

We thank all members from the infectious diseases group for thoughtful discussions.

Funding: This project was supported by Shanghai Municipal Commission of Health (No.20204Y0336).

Conflict of Interest: The authors declare that the research was conducted in the absence of any commercial or financial relationships that could be construed as a potential conflict of interest.

References

1. WHO Coronavirus (COVID-19) Dashboard, 2023. *https://covid19.who.int/* (accessed September 3, 2023).
2. Najjar-Debbiny R, Gronich N, Weber G, Khoury J, Amar M, Stein N, Goldstein LH, Saliba W. Effectiveness of paxlovid in reducing severe coronavirus disease 2019 and mortality in high-risk patients. Clin Infect Dis. 2023; 76:e342-9.
3. Guimarães PO, Quirk D, Furtado RH, *et al.* Tofacitinib in patients hospitalized with Covid-19 pneumonia. N Engl J Med. 2021; 385:406-415.
4. Ely EW, Ramanan AV, Kartman CE, de Bono S, Liao R, Piruzeli MLB, Goldman JD, Saraiva JFK, Chakladar S, Marconi VC, COV-BARRIER Study Group. Efficacy and safety of baricitinib plus standard of care for the treatment of critically ill hospitalised adults with COVID-19 on invasive mechanical ventilation or extracorporeal membrane oxygenation: an exploratory, randomised, placebo-controlled trial. Lancet Respir Med. 2022; 10:327-336.
5. Sholzberg M, Tang GH, Rahhal H, *et al*. Effectiveness of therapeutic heparin versus prophylactic heparin on death, mechanical ventilation, or intensive care unit admission in moderately ill patients with covid-19 admitted to hospital: RAPID randomised clinical trial. BMJ. 2021; 375:n2400.
6. Baumann KL, Sholzberg M, Cushman M. Anticoagulation in hospitalized patients with COVID-19. Blood. 2022; 140:809-814.
7. National Institutes of Health, 2021. Coronavirus Disease 2019 (COVID-19) Treatment Guidelines. *https://www.covid19treatmentguidelines.nih.gov/.* (accessed September 3, 2023).
8. RECOVERY Collaborative Group; Horby P, Lim WS, *et al*. Dexamethasone in hospitalized patients with Covid-19. N Engl J Med. 2021; 384:693-704.
9. Bartoletti M, Azap O, Barac A, Bussini L, Ergonul O, Krause R, Paño-Pardo JR, Power NR, Sibani M, Szabo BG, Tsiodras S, Verweij PE, Zollner-Schwetz I, Rodríguez-Baño J. ESCMID COVID-19 living guidelines: drug treatment and clinical management. Clin Microbiol Infect. 2022; 28:222-238.
10. National Institute for Health and Care Excellence, 2019. Chronic obstructive pulmonary 499 disease in over 16s: diagnosis and management. *https://www.nice.org.uk/guidance/ng115/chapter/Recommendations#systemic-corticosteroids* (accessed June 11 2023).
11. National Institute for Health and Care Excellence, 2022. Oral corticosteroids for asthma. *https://cks.nice.org.uk/topics/asthma/prescribing-information/oral-corticosteroids/* (accessed June 11 2023).
12. Li K, Wu J, Wu F, Guo D, Chen L, Fang Z, Li C. The clinical and chest CT features associated with severe and critical COVID-19 pneumonia. Invest Radiol. 2020; 55:327-331.
13. Rahimi E, Shahisavandi M, Royo AC, Azizi M, El Bouhaddani S, Sigari N, Sturkenboom M, Ahmadizar F. The risk profile of patients with COVID-19 as predictors of lung lesions severity and mortality-Development and validation of a prediction model. Front Microbiol. 2022; 13:893750.
14. Ruch Y, Kaeuffer C, Ohana M, Labani A, Fabacher T, Bilbault P, Kepka S, Solis M, Greigert V, Lefebvre N, Hansmann Y, Danion F. CT lung lesions as predictors of

early death or ICU admission in COVID-19 patients. Clin Microbiol Infect. 2020; 26:1417.e5-8.
15. Granholm A, Munch MW, Myatra SN, *et al*. Higher *vs* lower doses of dexamethasone in patients with COVID-19 and severe hypoxia (COVID STEROID 2) trial: Protocol for a secondary Bayesian analysis. Acta Anaesthesiol Scand. 2021; 65:702-710.
16. Taboada M, Rodríguez N, Varela PM, *et al*. Effect of high versus low dose of dexamethasone on clinical worsening in patients hospitalised with moderate or severe COVID-19 pneumonia: an open-label, randomised clinical trial. Eur Respir J. 2022; 60:2102518.
17. WHO Working Group on the Clinical Characterisation and Management of COVID-19 infection. A minimal common outcome measure set for COVID-19 clinical research. Lancet Infect Dis. 2020; 20:e192-197.
18. Corral-Gudino L, Cusacovich I, Martín-González JI, *et al*. Effect of intravenous pulses of methylprednisolone 250 mg versus dexamethasone 6 mg in hospitalised adults with severe COVID-19 pneumonia: An open-label randomised trial. Eur J Clin Invest. 2023; 53:e13881.
19. Adams HJA, Kwee TC, Yakar D, Hope MD, Kwee RM. Chest CT imaging signature of coronavirus disease 2019 infection: In pursuit of the scientific evidence. Chest. 2020; 158:1885-1895.
20. Elmokadem AH, Mounir AM, Ramadan ZA, Elsedeiq M, Saleh GA. Comparison of chest CT severity scoring systems for COVID-19. Eur Radiol. 2022; 32:3501-3512.
21. Hajiahmadi S, Shayganfar A, Janghorbani M, Esfahani MM, Mahnam M, Bakhtiarvand N, Sami R, Khademi N, Dehghani M. Chest computed tomography severity score to predict adverse outcomes of patients with COVID-19. Infect Chemother. 2021; 53:308-318.
22. Jayachandran AK, Nelson V, Shajahan ME. Chest CT severity score as a predictor of mortality and short-term prognosis in COVID-19. J Family Med Prim Care. 2022; 11:4363-4367.
23. Ye Z, Zhang Y, Wang Y, Huang Z, Song B. Chest CT manifestations of new coronavirus disease 2019 (COVID-19): a pictorial review. Eur Radiol. 2020; 30:4381-4389.
24. Chang YC, Yu CJ, Chang SC, Galvin JR, Liu HM, Hsiao CH, Kuo PH, Chen KY, Franks TJ, Huang KM, Yang PC. Pulmonary sequelae in convalescent patients after severe acute respiratory syndrome: evaluation with thin-section CT. Radiology. 2005; 236:1067-1075.
25. Russo A, Davoli C, Borrazzo C, *et al*. Clinical characteristics and outcome of hospitalized COVID-19 patients treated with standard dose of dexamethasone or high dose of methylprednisolone. Biomedicines. 2022; 10:1548.
26. Toroghi N, Abbasian L, Nourian A, Davoudi-Monfared E, Khalili H, Hasannezhad M, Ghiasvand F, Jafari S, Emadi-Kouchak H, Yekaninejad MS. Comparing efficacy and safety of different doses of dexamethasone in the treatment of COVID-19: a three-arm randomized clinical trial. Pharmacol Rep. 2022; 74:229-240.
27. Torres A, Sibila O, Ferrer M, Polverino E, Menendez R, Mensa J, Gabarrús A, Sellarés J, Restrepo MI, Anzueto A, Niederman MS, Agustí C. Effect of corticosteroids on treatment failure among hospitalized patients with severe community-acquired pneumonia and high inflammatory response: a randomized clinical trial. JAMA. 2015; 313:677-686.
28. Imai R, Ro S, Tomishima Y, Nishimura N. Steroid resistance and rebound phenomena in patients with COVID-19. Respir Investig. 2021; 59:608-613.
29. Aliska G, Nafrialdi N, Lie KC, Setiabudy R, Putra AE, Widyahening IS, Harahap AR. The role of the glucocorticoid receptor and its impact on steroid response in moderate-severe COVID-19 patients. Eur J Pharmacol. 2023; 943:175555.
30. Moromizato T, Sakaniwa R, Tokuda Y, Taniguchi K, Shibuya K. Intravenous methylprednisolone pulse therapy and the risk of in-hospital mortality among acute COVID-19 patients: Nationwide clinical cohort study. Crit Care. 2023; 27:53.
31. Li J, Liao X, Zhou Y, Wang L, Yang H, Zhang W, Zhang Z, Kang Y. Association between glucocorticoids treatment and viral clearance delay in patients with COVID-19: Asystematic review and meta-analysis. BMC Infect Dis. 2021; 21:1063.
32. Pantazopoulos I, Mavrovounis G, Kyritsis A, Perlepe G, Miziou A, Gourgoulianis K. Early corticosteroid initiation delays viral RNA clearance in respiratory secretions of COVID-19 patients. Adv Respir. 2021; 89:624-635.
33. COVID STEROID 2 Trial Group, Munch MW, Myatra SN, *et al*. Effect of 12 mg *vs* 6 mg of dexamethasone on the number of days alive without life support in adults with COVID-19 and severe hypoxemia: The COVID STEROID 2 randomized trial. JAMA. 2021; 326:1807-1817.
34. Ayanian S, Reyes J, Lynn L, Teufel K. The association between biomarkers and clinical outcomes in novel coronavirus pneumonia in a US cohort. Biomark Med. 2020; 14:1091-1097.
35. Miyata Y, Inoue H, Hirai K, *et al*. Serum cystatin C and CRP are early predictive biomarkers for emergence of hypoxia in COVID-19. Am J Med Sci. 2022; 364:706-713.

Received September 25, 2024; Revised December 15, 2024; Accepted December 18, 2024.

**Address correspondence to:*
Bijie Hu, Department of Infectious Diseases, Zhongshan Hospital, Fudan University, China.
E-mail: hu.bijie@zs-hospital.sh.cn

Released online in J-STAGE as advance publication December 24, 2024.

Original Article

DOI: 10.5582/ddt.2024.01079

Acupuncture and Bushen Quyu decoction improved endometrial receptivity, hormone secretion, and uterine artery blood flow for repeated implantation failure patients undergoing *in vitro* fertilization and embryo transfer

Qi Zhou[1], Lina Song[1], Jiahui Ma[2], Danyi Tang[1], Qing Qi[3], Hongmei Sun[4], Yan Du[2,*], Ling Wang[5,6,*]

[1] Department of Gynecology, Yangpu District Hospital of Traditional Chinese Medicine, Shanghai, China;
[2] Clinical Research Unit, Obstetrics and Gynecology Hospital of Fudan University, Shanghai, China;
[3] School of Physical Education and National Equestrian Academy, Wuhan Business University, Wuhan, Hubei, China;
[4] Hexi University, Zhangye, Gansu, China;
[5] Department of Obstetrics and Reproductive Immunology, Shanghai East Hospital of Tongji University, Shanghai, China;
[6] Guizhou University of Traditional Chinese Medicine (TCM), Guiyang, Guizhou, China.

SUMMARY Acupuncture and traditional Chinese medicine (TCM) have shown certain benefits in assisted *in vitro* fertilization and embryo transfer (IVF-ET). In this study, we evaluated the efficacy and safety of the combination of acupuncture combined with the Bushen Quyu decoction in patients with failures of IVF-ET. This study was conducted at Shanghai Yangpu District Hospital of TCM from May to November of 2021. Patients with failed IVF-ET received either combined therapy or the routine procedure (control group). The main outcomes were implantation rate and clinical pregnancy rate. Radioimmunoassay was used to detect serum levels of estradiol (E2) and progesterone on the day of injection of human chorionic gonadotropin (hCG). The endometrial thickness, resistance index (RI), and pulsatility index (PI) of bilateral uterine arteries were measured by color Doppler ultrasound. Safety was assessed in all participants. After 3 months of treatment, the implantation rate (61.9% *vs*. 47.7%, $P = 0.187$) and clinical pregnancy rate (52.4% *vs.* 36.4%, $P = 0.135$) of patients with IVF-ET failure receiving acupuncture therapy combined with Bushen Quyu decoction appeared to be higher than those of the routine procedure group, although the increase was not statistically significant. However, the serum E2 level and endometrial thickness of patients in the combined therapy group increased significantly than those of the control group after hCG injection. The RI and PI values of bilateral uterine arteries in the combined therapy group were significantly lower than those in the control group after hCG injection. No difference of adverse events was observed between combined therapy group and control group (11.9% *vs.* 11.36%, $P = 0.962$). Acupuncture therapy combined with TCM treatment may improve endometrial receptivity and hormone secretion, and increase uterine artery blood flow.

Keywords endometrial receptivity, *in vitro* fertilization embryo transfer, acupuncture, Bushen Quyu decoction, pregnancy rate

1. Introduction

Infertility has become a global social and health problem. According to statistics, infertility accounts for 10-15% of married couples of childbearing age in China (*1*). The rapid development of *in vitro* fertilization and embryo transfer (IVF-ET) technology has brought hope to infertile patients and improved the success rate of infertility treatment (*2*). After decades of development, IVF and its derivative technologies have made great progress through improving the ovulation promotion program and developing the laboratory culture system. However, the implantation rate and clinical pregnancy rate of embryos have not been satisfactory (*3*).

Endometrial receptivity is the ability of endometrium to accept embryos during a specific time period, and is a key factor affecting the outcome of IVF-ET. It is estimated that embryo factors account for about one third

of implantation failures, and the remaining two thirds of implantation failures are caused by poor endometrial receptivity or abnormal interaction between embryo and endometrium (*4*). How to improve the pregnancy outcome of patients with repeated IVF-ET transplantation failure by regulating endometrial receptivity is an urgent clinical problem.

An increasing number of infertile couples have chosen acupuncture, traditional Chinese medicine (TCM) and other auxiliary methods to improve the success rate of IVF-ET. Studies have found that acupuncture was helpful to increase the pregnancy rate (*5*). Compared to those without acupuncture or TCM treatment, acupuncture can help reduce the rate of miscarriage. In addition, TCM has certain feasibility in improving endometrial receptivity and the blastocyst on endometrium (*6*). Worldwide, there is an increasing trend of implementing acupuncture as a complementary therapy during IVF. Acupuncture has been applied for regulating hormone secretion, increasing uterine blood flow and stimulating secretion of endogenous opioids (*7*). Bushen Quyu decoction is commonly prescribed in our hospital, and retrospective data have shown that the majority of cases who have been treated with combined acupuncture and TCM have had more success in pregnancy than cases with no TCM or acupuncture treatment. However, its clinical efficacy lacks the support of evidence-based medicine. Therefore, we conducted a single center observational study to evaluate the clinical efficacy and safety of acupuncture combined with TCM in patients with IVF-ET failure of the kidney deficiency and blood stasis type.

2. Methods

2.1. Study design and participants

This study is a single center observational study. Women who underwent IVF-ET from May to November of 2021 at the gynecology clinic of Shanghai Yangpu District Hospital of TCM were recruited. The diagnostic criteria of infertility is that the couples have normal sexual life after marriage, and have not been pregnant for more than one year without contraception (*8*). The syndrome diagnostic criteria of kidney deficiency and blood stasis syndrome in infertility and blood stasis syndrome in hypomenorrhea were formulated according to the Criteria for the Diagnostic Efficacy of TCM Diseases and Syndromes issued by the Chinese Medicine Administration in 2012 (*9*), and the TCM Gynecology edited by Ma Baozhang (*10*). All patients experienced one or more IVF-ET transplant failures.

Inclusion criteria were: (*i*) meeting the diagnostic criteria of infertility; (*ii*) conforming to kidney deficiency and blood stasis syndrome; (*iii*) patient's age was 23-42 years old; (*iv*) embryos to be transferred were of high quality, and frozen thawed embryo transfer was planned; (*v*) given informed consent. Exclusion criteria were: (*i*) confirmed obvious and serious other organic diseases in the reproductive organs, which cannot bear pregnancy; (*ii*) infertility caused by genetic factors; (*iii*) women suffering from serious mental illness, acute infection of urogenital system, and sexually transmitted diseases; (*iv*) women with a history of habitual abortion.

2.2. Ethics

This study has been approved by the Ethics Committee of Yangpu District Hospital of TCM (Ethics No.: YPZY-2018-LC-02), and each patient has provided written informed consent. This study was conducted in accordance with the principles of the 2000 Declaration of Helsinki.

2.3. Procedures

Natural cycle or semi natural cycle were used to prepare endometrium for frozen embryo transfer for both groups. Natural cycle is suitable for those with regular menstrual cycle and ovulation; semi natural cycle is suitable for those with irregular or no ovulation. Oral letrozole 2.5-5 mg/d was administrated for 3-5 days after menstruation. The hCG injection day of the two schemes is the date of maximum diameter of the main follicle reaching 18 mm.

The control group was operated according to the routine procedure of frozen thawed embryo transfer, and the combined therapy group was treated with acupuncture combined with the Bushen Quyu decoction before transplantation on the basis of the routine procedure of frozen thawed embryo transfer.

Acupuncture scheme: point positioning were chosen based on the 7th edition of Meridian Acupuncture (*11*). Select the following acupoints: CV4 (Guanyuan), CV6 (Qihai), CV3 (Zhongji), EX-CA1 (Zigong), SP6 (Sanyinjiao), LI4 (Hegu, both sides), BL23 (Shenshu), DU4 (Mingmen), BL32 (Ciliao) and SP10 (Xuehai, both sides). Needles: according to the regulations of the special clinical research team of the "Acupoint Code", 30 # 1.5 inch disposable sterile needle (Huatuo brand, Suzhou, China) was selected, with a specification of 0.25 × 40 mm. Operation: refer to the operation method of "Meridians and Acupoints" compiled by Shen Xueyong, the textbook of the national planning of Chinese medicine colleges and universities in the new century. The patient first emptied the urine and then took the supine position, fully exposed the site of the operation, after local routine disinfection at selected acupoints, quickly pierced the needle at a 90-degree angle into 0.8-1.2 inches, and the above acupoints were repeatedly inserted and twisted using the flat supplement and diarrhea technique until the patient felt local numbness and heaviness, then the needle was left for 30 minutes after obtaining the gas. The above acupuncture treatment was performed 2-3 times/week except during

menstruation, and was stopped after transplantation. The patients were treated with medicine and acupuncture for 3 menstrual cycles, and the patients who received frozen embryo transfer during the treatment period or within 2 months after the treatment were eligible to be included in the group.

The Bushen Quyu decoction was prepared by the TCM pharmacy of Yangpu District Hospital of TCM. The basic herbs and dosage were as follows: Dangshen (tangshen) 15g, Baizhu (Largehead Atractylodes Rhizome) 15g, Tusizi (Chinese Dodder seed) 15-30g, Nvzhenzi (Glossy privet fruit) 10g, Danggui (Chinese Angelica) 15g, Sanqi (*Sanchi*) 3-5g and Danshen (Dan-Shen Root) 9g. Patients received one full dose (taking at two half-doses: morning and evening) per day orally. Each dose was decocted with water, and taken after warming. The administration was stopped during menstruation, or immediately after detection of pregnancy.

Human chorionic gonadotropin (hCG) injection was performed when the maximum diameter of the main follicle grew to 18 mm. On the day of hCG injection, the peripheral blood of patients was drawn. The levels of estradiol (E2) and progesterone in the peripheral serum of patients were detected by radioimmunoassay. The endometrial thickness, resistance index (RI), and pulsatility index (PI) of bilateral uterine arteries were measured on the day of hCG injection by ultrasound using the GE Volkswagen E8 color Doppler, RM6C7.5MHz transvaginal probe model (General Electric Medical Systems, Milwaukee, WI, USA). Adverse events including breast pain, nausea, rash, headache and other symptoms were recorded.

2.4. Outcomes

The main outcomes of this study were implantation rate and clinical pregnancy rate. Blood test β-hCG positive patients 14 days after transplantation were regarded as biochemical pregnancy, which indicated successful implantation. The implantation rate was calculated as: number of successful implantation/number of patients ×100%. Four weeks after transplantation, ultrasound monitoring was performed. Those who detected with gestational sac, embryo bud and fetal heart beat were regarded as clinical pregnancy. The clinical pregnancy rate was calculated as: number of clinical pregnancies/ number of patients ×100%.

In addition, serum levels of E2 and progesterone, endometrial thickness, RI and PI of bilateral uterine arteries were compared between the two groups on the day of hCG injection.

2.5. Statistical analysis

Categorical variables were expressed by rate (%), and compared using the Chi-square test or Fisher's exact test. The continuous data that conform to the normal distribution were expressed by mean ± SD, and compared using Student's *t*-test. Continuous variables that do not conform to the normal distribution were expressed as median (interquartile range) [M (IQR)], and compared using Mann-Whitney *U* test. All statistical analyses were conducted using SPSS 24.0 statistical software. A two-sided $P < 0.05$ denoted as statistical significance.

3. Results

3.1. Patient characteristics

A total of 86 participants were recruited, including 42 women received combined therapy, and 44 women received routine treatment (the control group). Before treatment, there was no significant difference between the two groups in terms of age, infertility years, IVF-ET times and body mass index (BMI) ($P > 0.05$ for all). In addition, there was no significant difference between the two groups in terms of the causes of assisted pregnancy ($P = 0.991$) (Table 1).

3.2. Pregnancy rate of patients with IVF-ET failure

As shown in Table 2, the implantation rate of patients with IVF-ET failure receiving combined treatment appeared to be higher than those of the routine procedure group, although the increase was not statistically significant (61.9% *vs.* 47.7%, $P = 0.187$). In addition, although not reaching statistical significance, the clinical pregnancy rate appeared to be higher of the combined therapy group than the control group (52.4% *vs.* 36.4%, $P = 0.135$).

3.3. Hormone levels and endometrium thickness after hCG injection

As shown in Table 3, there was no difference of the E2 level between the two groups before hCG injection. After

Table 1. Population characteristics

	Combined therapy group ($n = 42$)	Control group ($n = 44$)	*P*
Age	31.88 ± 4.27	30.84 ± 3.46	0.22
Infertility years	3 (3-4)	3 (3-4)	0.84
IVF-ET times	2 (2-3)	3 (2-4)	0.28
BMI	22.62 ± 1.48	22.32 ± 2.22	0.46
Cause of assisted pregnancy			0.991*
Fallopian tube	21	24	
Ovulation disorder	5	5	
Endometriosis	3	3	
Spouse factor	12	11	
Unknown cause	1	1	

BMI, body mass index; IVF-ET, *in vitro* fertilization and embryo transfer. *Fisher's exact test.

Table 2. Comparison of pregnancy rate between the two groups

	Combined therapy group (n = 42)	Control group (n = 44)	P
Implantation			0.187
Yes	26 (61.9%)	21 (47.7%)	
No	16 (38.1%)	23 (52.3%)	
Clinical pregnancy			0.135
Yes	22 (52.4%)	16 (36.4%)	
No	20 (47.6%)	28 (63.6%)	

Table 3. Comparison of serum hormone levels and endometrial thickness before and after hCG injection between the two groups (mean ± SD)

	Combined therapy group (n = 42)	Control group (n = 44)	P
Estradiol (pmol/L)			
Before treatment	833.5 ± 110.8	805.6 ± 123.8	0.28
After treatment	916.2 ± 100.6	781.6 ± 186.0	< 0.001
Progesterone (nmol/L)			
Before treatment	1.2 ± 0.4	1.3 ± 0.3	0.07
After treatment	1.3 ± 0.3	1.3 ± 0.3	0.81
Endometrial thickness (mm)			
Before treatment	7.8 ± 0.9	8.1 ± 0.9	0.14
After treatment	8.8 ± 0.8	8.4 ± 1.1	0.048

hCG injection, the E2 level in the combined therapy group was significantly higher compared with that in the control group (P < 0.001). There was no statistically significant difference of the progesterone level between the two groups both before and after hCG injection.

As for the average endometrial thickness, there was no difference between the two groups before hCG injection. After hCG injection, the endometrial thickness in the combined therapy group was significantly higher compared with the control group (Table 3, P = 0.048).

3.4. Uterine artery blood flow

As shown in Table 4, before hCG injection, all variables of uterine artery blood flow were comparable between the two groups. However, after hCG injection, bilateral uterine artery resistance index (RI) and pulsation index (PI) of patients in the combined therapy group were significantly lower than those in the control group (P < 0.001 for all).

3.5. Adverse events

As shown in Table 5, the recorded adverse events included breast swelling and pain, nausea, rash, and headache in both groups. There was no significant difference of adverse events between the combined therapy group and the control group (P = 0.962).

Table 4. Changes of uterine artery blood flow before and after hCG injection between the two groups (mean ± SD)

	Combined therapy group (n = 42)	Control group (n = 44)	P
Right RI			
Before treatment	0.77 ± 0.15	0.78 ± 0.15	0.71
After treatment	0.58 ± 0.13	0.78 ± 0.17	< 0.001
Right PI			
Before treatment	2.83 ± 0.53	2.90 ± 0.52	0.58
After treatment	2.24 ± 0.25	2.78 ± 0.53	< 0.001
Left RI			
Before treatment	0.77 ± 0.17	0.76 ± 0.16	0.87
After treatment	0.55 ± 0.18	0.79 ± 0.15	< 0.001
Left PI			
Before treatment	2.77 ± 0.61	2.84 ± 0.48	0.58
After treatment	2.37 ± 0.26	2.88 ± 0.47	< 0.001

RI, resistance index; PI, pulsatility index.

Table 5. Comparison of adverse events (n/%)

	Combined therapy group (n = 42)	Control group (n = 44)	P
Total	5 (11.9%)	5 (11.36%)	0.962*
Breast swelling and pain	1 (2.38%)	2 (4.54%)	
Nausea	2 (4.76%)	1 (2.27%)	
Rash	1 (2.38%)	1 (2.27%)	
Headache	1 (2.38%)	1 (2.27%)	

*Fisher's exact.

4. Discussion

This study indicated that the implantation rate and clinical pregnancy rate of patients with IVF-ET failure receiving acupuncture therapy combined with Bushen Quyu decoction treatment appeared to be higher than those of the routine procedure group, although the increase was not statistically significant. After hCG injection, the endometrial thickness in the combined therapy group was higher than that in the control group, while PI and RI were lower than those in the control group. Our results suggested that the combined therapy increased the level of estradiol in IVF-ET patients and improved endometrial receptivity, possibly because the TCM decoction can reduce the blood flow resistance of uterine artery to promote the development of endometrium and help embryo implantation.

The endometrial thickness refers to the total length of the endometrium of the anterior and posterior walls of the uterus and the uterine space, and changes periodically with the menstrual cycle. A moderate endometrial thickness is easy for embryo implantation, while a thin endometrium can significantly reduce the rate of embryo implantation (*12*). Estrogen and progesterone are hormones that play a leading role in the periodic development and transformation of endometrium. Estrogen is essential to maintain the proliferation of endometrium in follicular stage, and can

promote the proliferation and growth of endometrium, as well as repair and restore the damaged endometrium. Meanwhile, estrogen and progesterone also regulate uterine artery blood flow. A high level of estrogen can expand uterine artery blood vessels, increase compliance of uterine artery wall, reduce arterial blood flow resistance, and accelerate uterine artery blood flow speed (*13-14*). Previous studies have reported that for patients who failed IVF-ET receiving treatment of warm acupuncture at abdominal and lumbosacral points for 3 menstrual cycles, the endometrial thickness and uterine blood perfusion increased significantly, while bilateral PI values decreased. Warm acupuncture can improve the clinical pregnancy rate of patients who failed high-quality frozen thawed embryo transfer after re-transplantation (*15*).

With the development of ultrasound diagnostic technology, it is possible to study and evaluate endometrial receptivity by measuring uterine hemodynamic parameters with transvaginal color Doppler ultrasound, a non-invasive method (*16*). In assisted reproductive technology, Doppler ultrasound has been applied to monitor parameters such as endometrial thickness, morphology, arterial blood flow, and endometrial blood flow perfusion, which are reliable indexes of endometrial receptivity and pregnancy outcome. Endometrial blood flow is the main nutrient vessel of the endometrium. Rich blood flow indicates favorable internal environment of the endometrium during the transplantation window, which is associated with a better outcome of embryo pregnancy. It was found that more blood flow branches in the endometrium and under endometrium were associated with higher success rate of embryo implantation (*17*). For patients with poor endometrial blood flow, TCM can be applied to improve the uterine artery and endometrial blood flow, increase the clinical pregnancy rate of FET, and reduce the waste of embryos. Of the Bushen Quyu decoction, Nvzhenzi (Glossy privet fruit) and Tusizi (Chinese Dodder seed) are the principal medicines dedicating to nourish kidney energy. Baizhu (Largehead Atractylodes Rhizome) and Dangshen (tangshen) are adjuvant drugs with the effect of strengthening the spleen. When the spleen is healthy, the Qi and Blood are active. The addition of Danggui (Chinese Angelica), Sanqi (Sanchi) and Danshen (Dan-Shen Root) have the effect of activating blood and eliminating stasis.

The acupoints selected in this study, including CV4 (Guanyuan), CV6 (Qihai), CV3 (Zhongji), EX-CA1 (Zigong), SP6 (Sanyinjiao), LI4 (Hegu), BL23 (Shenshu), DU4 (Mingmen), BL32 (Ciliao), SP10 (Xuehai) and other acupuncture points can play the roles of warming the womb, recuperating Chong Ren, and cultivating Yuan Qi. The acupuncture treatment can enhance the blood supply of the ovary and uterus, enhance the contraction of smooth muscle, accelerate blood circulation, stimulate the formation of ovarian capsule, promote the rupture of follicle wall, help mature follicles to discharge, and regulate the autonomic nervous system to enhance endometrial receptivity. Previous studies have shown that warming needle can improve the local temperature of the lower abdomen, accelerate the blood circulation around the uterus and accessories, promote the absorption of endometrial effusion, improve the uterine environment and endometrial receptivity, and increase the clinical pregnancy rate (*18*). It is also worth noting that the adverse events of the combined therapy were relatively mild, since the herbs used in the Bushen Quyu decoction in general have no obvious toxic and side effects.

This study has a few limitations. First, the retrospective nature of the study may introduce certain biases, although comparison of baseline characteristics showed there were no significant differences between the two groups. Second, our sample size is limited, which may explain why we did not detect a significant increase of the implantation rate and clinical pregnancy rate of patients with IVF-ET failure. However, we did detect improvements of endometrial receptivity and hormone secretion, as well as uterine artery blood flow, which are consistent with previous studies. In the future, a well-designed randomized clinical trial with sufficient sample size is needed to fully evaluate the efficacy of the combined treatment.

In summary, the combined therapy of Bushen Quyu decoction and acupuncture can improve endometrial receptivity and hormone secretion, and increase uterine artery blood flow of patients receiving IVF-ET, although the combined treatment did not significantly improve implantation rate and clinical pregnancy rate. In addition, this combination treatment is safe and does not increase adverse reactions.

Funding: This work was supported by grants from a project of Shanghai Municipal Health and Family Planning Commission Traditional Chinese Medicine (grant no. 2018LQ021 to Q Zhou), a project of National Natural Science Foundation of China (grant no. 82374243 to Wang L), National Administration of Traditional Chinese Medicine "Huang Suying National Famous Traditional Chinese Medicine Expert Heritage Studio" (Document Number: [National Traditional Chinese Medicine Personnel Education Letter] 2022 No. 75), and Shanghai Municipal Health Commission "Huang Suying Shanghai Famous Traditional Chinese Medicine Academic Experience Research Studio" (grant no. SHGZS-202247).

Conflict of Interest: The authors have no conflicts of interest to disclose.

References

1. Feng YJ. Obstetrics and Gynecology. People's Medical Publishing House, Beijing, 2010; *pp*. 408-409. (in

Chinese)
2. Chiware TM, Vermeulen N, Blondeel K, Farquharson R, Kiarie J, Lundin K, Matsaseng TC, Ombelet W, Toskin I. IVF and other ART in low- and middle-income countries: A systematic landscape analysis. Hum Reprod Update. 2021; 27:213-228.
3. Katler QS, Kawwass JF, Hurst BS, Sparks AE, McCulloh DH, Wantman E, Toner JP. Vanquishing multiple pregnancy in *in vitro* fertilization in the United States-a 25-year endeavor. Am J Obstet Gynecol. 2022; 227:129-135.
4. Vuong LN. Alteration of final maturation and laboratory techniques in low responders. Fertil Steril. 2022; 117:675-681.
5. Qi Y, Wang X, Hou S, Wu Z, Xu X, Pang C. Intracavitary physiotherapy combined with acupuncture mediated AMPK/mTOR signalling to improve endometrial receptivity in patients with thin endometrium. Eur J Obstet Gynecol Reprod Biol. 2022; 277:32-41.
6. Maharajan K, Xia Q, Duan X, Tu P, Zhang Y, Liu K. Therapeutic importance of Zishen Yutai Pill on the female reproductive health: A review. J Ethnopharmacol. 2021; 281:114523.
7. Xue HM, Li YM, Chen YT, Li C, Zhang Y, Jin P, Li ML, Lin Y. Effect of staging treatment of Tongyuan acupuncture on pregnancy outcome in patients with recurrent implantation failure of thin endometrium type. Zhongguo Zhen Jiu. 2021; 41:1338-1342. (in Chinese)
8. Gnoth C, Godehardt E, Frank-Herrmann P, Friol K, Tigges J, Freundl G. Definition and prevalence of subfertility and infertility. Hum Reprod. 2005; 20:1144-1147.
9. Diagnostic efficacy criteria of TCM disease. Nanjing University Press, Nanjing, 2012; *pp.* 60-72. (in Chinese)
10. Ma Baozhang. Gynecology of traditional Chinese medicine. China Press of Chinese Medicine, Beijing, 2012; *pp.* 94-95. (in Chinese)
11. Shen X. Meridian acupuncture. China Press of Chinese Medicine, 2007; *pp.* 38-40; 198; 234. (in Chinese)
12. Lv H, Li X, Du J, *et al.* Effect of endometrial thickness and embryo quality on live-birth rate of fresh IVF/ICSI cycles: A retrospective cohort study. Reprod Biol Endocrinol. 2020; 18:89.
13. Habara T, Nakatsuka M, Konishi H, Asagiri K, Noguchi S, Kudo T. Elevated blood flow resistance in uterine arteries of women with unexplained recurrent pregnancy loss. Hum Reprod. 2002; 17:190-194.
14. Chang K, Lubo Zhang. Review article: Steroid hormones and uterine vascular adaptation to pregnancy. Reprod Sci. 2008; 15:336-48.
15. Su WW, Tian JS, Gao XA. Effect of warming acupuncture on uterine blood perfusion in patients with failed high-quality freeze-thawed embryo transfer. Zhongguo Zhen Jiu. 2020; 40:498-502. (in Chinese)
16. Kupesic S, Bekavac I, Bjelos D, Kurjak A. Assessment of endometrial receptivity by transvaginal color Doppler and three-dimensional power Doppler ultrasonography in patients undergoing *in vitro* fertilization procedures. J Ultrasound Med. 2001; 20:125-134.
17. Wu HB, Li LM, Yuan H, Li MJ. Assessment of pregnancy outcomes during in IVF-ET by endometrial and subendometrial blood flows measured by vaginal color Doppler ultrasound on the day of HCG injection. China Journal of Modern Medicine. 2009; 19:2364-2368. (in Chinese)
18. Su WW, Gao XA, Gao ZY, Pan JL, Deng F, He WT. Clinical observation on the therapeutic effect of warm acupuncture on endometrial cavity fluid from *in vitro* fertilization-embryo transfer. Zhongguo Zhen Jiu. 2019; 39:923-926. (in Chinese)

Received October 18, 2024; Revised December 9, 2024; Accepted December 14, 2024.

**Address correspondence to:*
Ling Wang, Department of Obstetrics and reproductive Immunology, Shanghai East Hospital, Tongji University School of Medicine, No. 1800 Yuntai Road, Shanghai 200100, China.
E-mail: dr.wangling@vip.163.com

Yan Du, Clinical Research Unit, Obstetrics and Gynecology Hospital of Fudan University, No. 128 Shenyang Road, Shanghai, China 200090.
E-mail: sophiedu_61@163.com

Released online in J-STAGE as advance publication December 21, 2024

Original Article

DOI: 10.5582/ddt.2024.01080

Baricitinib-loaded EVs promote alopecia areata mouse hair regrowth by reducing JAK-STAT-mediated inflammation and promoting hair follicle regeneration

Haowen Tang[1,§], Fangfang Wang[2,§], Rui Yang[3], Ziqi Zhao[4], Ying Zhang[5], Li Yang[1,*], Bingmin Li[5,*]

[1] Faculty of Hepato-Pancreato-Biliary Surgery, First Medical Center of Chinese PLA General Hospital, Beijing, China;
[2] The 55th retirement of Haidian district affiliated to Beijing Garrison, Beijing, China;
[3] School of Medicine, Nankai University, Tianjin, China;
[4] School of clinical medicine, China Medical University, Shenyang, Liaoning, China;
[5] Department of Dermatology, Fourth Medical Center of Chinese PLA General Hospital, Beijing, China.

SUMMARY Alopecia areata (AA) is a common and recurrent type of hair loss. Despite oral administration of baricitinib exerts a good effect on refractory AA, the long-term administration of baricitinib carries significant side effects, poor compliance, and the efficacy is difficult to maintain after drug withdrawal. Therefore, the exploration of a safe and effective local administration of baricitinib to treat AA is of great clinical importance. However, baricitinib has a large molecular weight and is barely soluble in water, while the hair follicle lies deep, thus conventional topical dosage forms are ineffective. This study investigated the efficacy of local injection of baricitinib-loaded mesenchymal stem cell exosomes (EVs) in the treatment of AA. First, we constructed baricitinib loaded EVs (EV-B) and established AA mouse model by intravenously injection with murine INF-γ according to previous literature reports. The therapeutic effects of EV-B on hair regrowth were recorded and the underlying mechanism was also analyzed by Luminex protein biochip test and western-blot. Compared to control group, the baricitinib, EV and EV-B groups exhibited improved hair coverage in the AA mouse model. Besides, EV-B group achieved the optimal effect. The underlying mechanism might be attributed to the improvement of drug delivery efficiency as well as the synergistic effect of EVs, leading to better inhibition of JAK-STAT pathway and upregulation of the Wnt/β-catenin pathway. Our findings proved the effectiveness of EV-B on the treatment of AA, and might provide a new therapeutic approach for AA in future clinical application.

Keywords Alopecia areata, baricitinib, mesenchymal stem cell, exosomes

1. Introduction

Alopecia areata (AA) is a common inflammatory non-scarring type of hair loss that affects approximately 2% of the global population (*1,2*). The initial cause of AA remains elusive, while current research has shown that the loss of immune privilege in the hair follicle (HF) and the subsequent autoimmune response is a major precondition for the development of AA (*3,4*).

HFs are normally immune privileged sites under physiological conditions. However, in AA, this immune privilege is disrupted, leading to increased expression of major histocompatibility complex (MHC) I and II, along with the up-regulation of adhesion molecules and chemokines in anagen hair bulbs. This disruption exposes autoantigens and allows the infiltration of $CD8^+$ T cells (*1,3*). These $CD8^+$ T cells produce interferon-gamma (IFN-γ) and enhance the production of interleukin-15 (IL-15) *via* Janus kinases 1 (JAK1) and 2 (JAK2) signaling pathway. IL-15, in turn, binds to the surface of $CD8^+$ T cells and activate JAK1 and JAK3 to enhance the production of IFN-γ (*3*). The inflammation disrupts the hair cycle, inducing dystrophic anagen and premature catagen phases, ultimately leading to hair loss in AA (*3,5*).

Given the predominant role of the JAK-STAT signaling pathway in the initiation and progression of AA, Janus kinase inhibitors (JAKi) have emerged as promising drugs for the treatment of AA (*6,7*). As an effective JAK1 and JAK2 inhibitor, baricitinib is the first JAKi approved for the treatment of severe AA in

the USA and the EU (*4,8*). Despite oral baricitinib shows ideal therapeutic effects on severe AA, there are still concerns about long-term side effects such as increased infection or cancer risk (*9,10*). Besides, AA frequently recurs after the treatment cessation. Therefore, a topical formulation of baricitinib may be an ideal option for maintenance therapy (*11*). However, there is no such topical formulation of JAKi has yet been developed (*5*). Therefore, exploring an effective way for topical baricitinib administration is crucial for clinical practice.

Extracellular vesicles (EVs) are natural nanosized membrane vesicles derived from most cell types. As carriers, EVs carry and deliver various biomolecules and play an important role in cell-to-cell communication (*12*). EVs are valued for their stability, low immunogenicity, safety, and cell targeting capabilities, making them a promising drug delivery system (*13*). The approaches for EVs' loading can be divided into exogenous and endogenous loading. The endogenous loading methods include electroporation, simple incubation, sonication, extrusion and freeze-thawing (*14*). It's worth noting that EVs have been employed to deliver a variety of "cargos" such as nucleic acids, protein, metal nanoparticles as well as chemotherapeutic drugs, achieving ideal therapeutic effect (*15-18*).

In this study, we loaded the mesenchymal stem cells (MSCs)-derived EVs with baricitinib and evaluated its therapeutic effect on alopecia areata *in vivo*. The underlying mechanism was also explored. Our study may provide a theoretical basis for the topical administration of baricitinib in treating AA.

2. Materials and Methods

2.1. Cell culture

Human placentas-derived mesenchymal stem cells (dMSCs) were obtained from Shenyang Cell Center (Shenyang, China). These cells were cultured in Human Mesenchymal Cells Serum-free Culture Medium (NC0106, yocon, China). The supernatant of MSCs (passage 1-6) was collected for the subsequent experiments. Dermal papillary cells were purchased from Meissen CTCC (Hangzhou, China) and cultured in Dulbecco's Modified Eagle's Medium (DMEM) (12100, solarbio, China) supplemented with 10% fetal bovine serum (S9000, solarbio, China).

2.2. Isolation and characteristics of EVs

EVs were isolated from supernatant using a series of ultra-high-speed centrifugation procedures according to the published literatures. The morphology of EVs was observed by transmission electron microscope (TEM) (Hitachi, Japan), and the particle size was determined by nanoparticle tracking analyzer (Particle Metrix GmbH, Germany). The expression of EV positive markers CD63 (ab68418, abcam, USA), TSG101 (ab133586, abcam, USA), CD81 (ab232390, abcam, USA) and negative marker calnexin (ab133615, abcam, USA), were analyzed by Western blot.

2.3. Preparation of baricitinib-loaded EVs

Baricitinib was loaded into exosomes with electroporation. Briefly, 2E+11 particles of exosomes were co-incubated with 2 mL Gene Pulser Electroporation buffer and 1400 μg baricitinib (MedChemExpress, HY-15315) at 37℃ for 30 min. The mixture was then transferred to a cuvette and electroporated under the following conditions: 125 μF, 250 V, Max capacitance, 10 pulses with a 2 s interval. The electroporated exosomes were washed with PBS for 3 times in 100 kDa ultrafiltration tube, and then concentrated to 150 μL. This process was repeated until a sufficient amount of baricitinib-loaded EVs was collected. Baricitinib-loaded EVs were lysed with 1% Tween-20 and subjected to high-performance liquid chromatography (HPLC) testing. The procedure of HPLC are as follows. Baricitinib was dissolved to 10 mg/mL in DMSO and diluted to 1,000, 500, 250, 125, 62.5, 31.25, 15.6 μg/mL. 10 μL aliquots of each sample was injected into the HPLC system (Agilent 1260, USA). All data were acquired using a C18 column with the mobile phase H_2O: ACN (50:50, v/v) at a flow rate of 1 mL/min at 45℃. The elution of baricitinib was monitored by measuring absorbance at 254 nm, the standard curve was obtained by linear fitting with baritinib concentration as X axis and peak area as Y axis. The EV-B were transferred to 1% Tween and incubated at 4℃ for 2 hours and baricitinib was released. The solution was detected by HPLC and the concentration of baricitinib in EV-B was calculated according to the standard curve.

2.4. Uptake assay

The uptake assay was conducted to verify whether the baricitinib-loaded EVs could be endocytosed by dermal papillary cells (DPs). EVs was labeled with actin (cytoskeleton, red), and DP cells were counterstained by PKH67 (membrane, green) and DAPI (cell nucleus, blue). The internalization process was observed under confocal microscope (Leica, Germany).

2.5. Animal study

This study was approved by the Ethics Committees of the PLA General Hospital. Twenty 6-week-old female C57BL/6 mice purchased from the SPF Biotechnology (Beijing, China) were employed in this study. They were intravenously injected with murine INF-γ at a dose of 2×10^4 U (P00215, solarbio) for three consecutive days, followed by injections every 7 days (*19, 20*).

At 8.5 weeks after birth, the mice were shaved and randomly assigned into four groups. The control group was injected with 1 mL saline, the baricitinib group was injected with 1 mL of an 86.37 μg/mL baricitinib solution, the EV group was injected with 1 mL of a 2.48 × 10^{11} particles/mL EV solution, and the baricitinib + EV group was injected with 1 mL baricitinib-loaded EVs, which contained 86.37 μg baricitinib and 2.48 × 10^{11} EV particles in average. The solution was injected at 16 sites evenly within the shaved area in each group. The mice received those treatments above every day for two weeks. Photographs were taken at day 5, 10, 15, and day 20 after shaving to document the hair growth. At day 20, the mice were euthanized, and the entire dorsal skin was obtained for further histological analysis.

2.6. Western blot analysis

The skin tissue in each group was lysed by RIPA buffer (Invitrogen). Protein concentrations were measured by BCA Protein Assay Kit (PC0020, Solarbio, China). Equal amounts of heat-denatured protein samples were separated by BeyoGel™ TBE Precast PAGE Gel (D0171S, Beyotime, China) and then transferred onto PVDF membrane and blocked with 5% non-fat dried milk for 1 hour, followed by incubation with specific primary antibodies (4°C overnight), and secondary antibodies for 2 h. The specific antibodies include IFN-γ (# 8455S, Cell Signaling Technology, USA), Jak-2 (ab108596, abcam, USA), Stat-1 (ab109457, abcam, USA), IL-15 (ab52816, abcam, USA), β-catenin (ab32572, abcam, USA). The blots were finally detected by chemiluminescence.

2.7. Detection of inflammatory cytokines

Skin tissues from each group were collected, and proteins were extracted using RIPA buffer (Invitrogen). Inflammatory cytokines were detected by Luminex protein biochip testing system (Bio-Plex MAGPIX System, Bio-Rad) and a test kit (Bio-Plex Pro Mouse Cytokine Grp, #M60009RDPD), following the manufacturer's instructions.

2.8. Statistical analysis

Data are presented as the mean ± SD, and all the experiments were conducted at least three times. Statistical analysis was performed using one-way analysis of variance (ANOVA) for comparison of group means. Two-way ANOVA was employed for comparison among groups at different time points. $P < 0.05$ was considered statistically significant.

3. Results

3.1. Characteristics of EVs

The characteristics of EVs were determined by TEM, nanoparticle tracking analyzer (NTA) and Western blotting. The ultrastructure of EVs was presented in Figure 1A, which exhibited a typical cup shape and a smooth double-layer structure. Particle diameters were measured by NTA (Figure 1A). The average diameter of particles was 109.7 nm for the EV group and 120.6 nm for the EV-B group. The morphological characteristics in both groups were consistent with those described for EVs in previous studies. The positive markers of EVs including CD63, TSG101 and CD81 were detected by western blot, but the negative marker calnexin was undetectable in both groups (Figure 1B). The concentration of baricitinib was detected by HPLC. The result showed that the concentration of baricitinib is 86.37 μg/mL in the supernatant from sample of EV-B group (Figure 1C). The concentration of EV is 2.48 × 10^{11} particles/mL (Figure 1D). Uptake assay revealed that after 12 hours, the EVs in EV-B group (labeled with Phalloidin, red fluorescence) could be internalized by dermal papillary (DP) cells (the nucleus was labeled with DAPI, blue fluorescence, and cytoskeleton was labeled with PKH-67, green fluorescence) (Figure 2).

3.2. EV-B promote hair regrowth in mice

To assess hair growth in C57BL/6 mice, photographic images were captured at intervals of 5, 10, 15 and 20 days. 10 days after the treatment, the skin color of baricitinib, EV and EV-B groups shifted from pink to light gray. Besides, the EV-B group began to show some hair growth. By day 15, the baricitinib, EV and EV-B groups exhibited improved hair coverage compared to the control group. In addition, the EV-B group achieved most significant improvement among groups. By day 20, the entire depilated area on the backs of the mice in the EV-B group was covered with new hair (Figure 3). The above results showed that both baricitinib solution and EV could promote hair growth in AA mouse model, while EV-B had a more significant effect. Compared to baricitinib group, the better efficacy of EV-B may be attributed to the improvement of drug delivery efficiency as well as the synergistic effect of EVs.

3.3. EV-B exerts its role by inhibiting JAK-STAT pathway and activating Wnt/β-catenin pathway

Luminex protein biochip testing system and Western-blot were employed to illustrate the regulatory mechanism by which EV-B promotes hair regrowth. As is shown in Figure 4, compared to control group, EV-B significantly down-regulated the expression of IFN-γ and IL-2 in mice tissue. In addition, the expression levels of IFN-γ, Jak-2, Stat-1, IL-15 and β-catenin in mice tissue were also detected by Western-blot. The results indicated that EV-B down-regulated the expression of IFN-γ, Jak-2, Stat-1 and IL-15, and up-regulated the expression of β-catenin

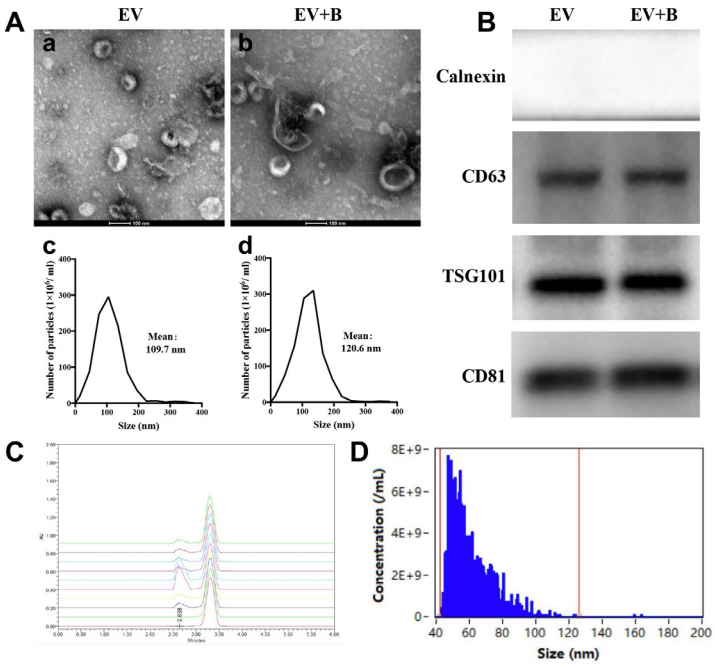

Figure 1. Characteristics of EVs. (**A**) (a-b) Ultrastructure of EVs, scale bar = 100 nm. (c-d) particle size distribution measured by nanoparticle tracking analyzer. (**B**) The expression level of exosome negative marker Calnexin and positive maker CD63, TSG101 and CD81 measured by western-blot. (**C**) The solution of EV-B was detected by HPLC, the average peak area was 466823 and the concentration of baricitinib in EV-B was 86.37 μg/mL. (**D**) The number of EV-B particles was measured by nanoflow, there is 2.48×10^{11} particles/mL in EV-B solution. These results provide the standard concentration of baricitinib and EVs in control group in the following experiments (EVs: extracellular vesicles, EV-B: baricitinib loaded EVs; HPLC: high-performance liquid chromatography).

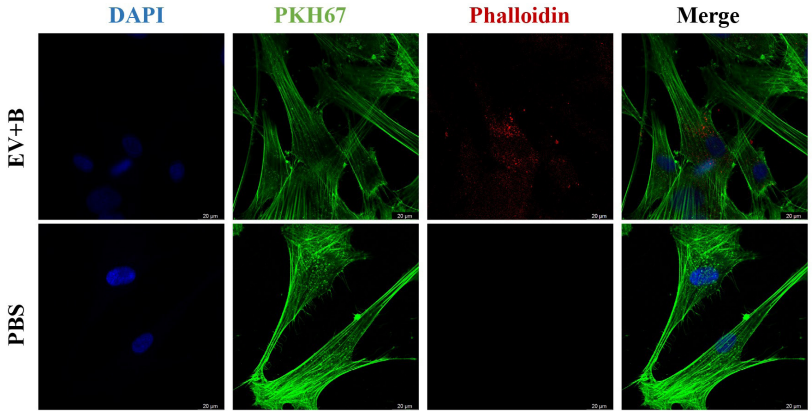

Figure 2. Uptake assay. The membrane of EVs were labeled with phalloidin (red). DPs cytoskeleton was counterstained by PKH67 (green) and nucleus was labeled by DAPI (blue). (EVs: extracellular vesicles, DPs: dermal papillary cells, PKH67: a kind of green fluorescent cell membrane dye, DAPI: a kind of blue fluorescent cell nucleus dye).

(Figure 5). Compared to baricitinib group, the expression of Jak-2, Stat-1, IL-15 in EV-B group were significantly down-regulated ($P < 0.05$), which achieved a better effect of inhibiting the inflammation. As is known, IFN-γ, Jak-2, Stat-1, IL-15, β-catenin and IL-2 are key elements of JAK-STAT pathway. β-catenin is also one of the important effector molecules of the Wnt/β-catenin pathway as well as a common marker for anagen hair follicles. These results indicate that EV-B promotes hair growth by inhibiting inflammation and promoting hair follicle regeneration (Figure 6).

4. Discussion

Alopecia areata (AA) is a common chronic autoimmune disease characterized by the loss of the immune privilege of hair follicle (*1*). Although the exact pathobiology remains elusive, the JAK-STAT signaling pathway plays a pivotal role in the initiation and development of AA (*5*). Baricitinib is a small molecule (371.41 Da) adenosine

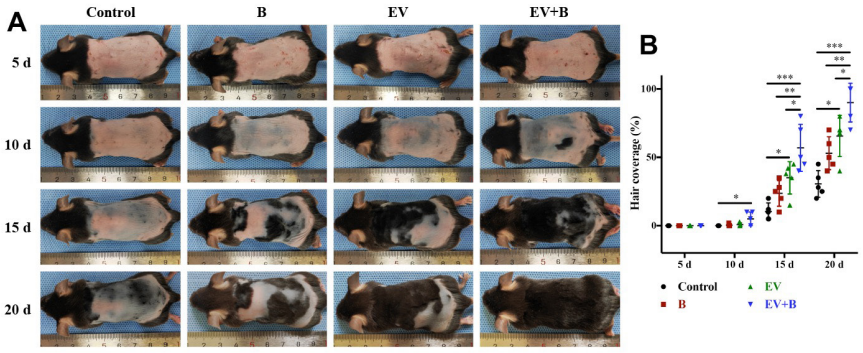

Figure 3. EV-B promotes hair regrowth *in vivo*. (**A**) Hair regrowth progression from day 5 to day 20. (**B**) The statistical analysis of hair coverage rate in each group ($n = 5$). *$P < 0.05$; **$P < 0.01$; ***$P < 0.001$.

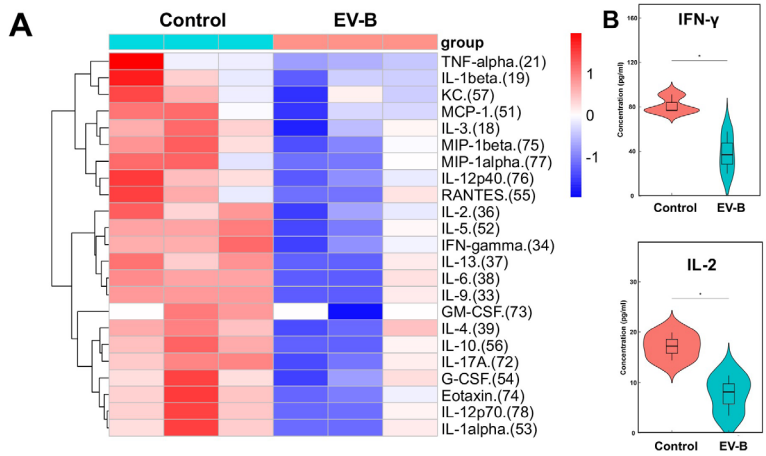

Figure 4. EV-B reduces the inflammation response. (**A**) Luminex protein biochip test between control group and EV-B group ($n = 3$). (**B**) The concentration of IFN-γ and IL-2 between control group and EV-B group ($n = 3$) *$P < 0.05$; (EV-B: baricitinib loaded EVs, IFN-γ: interferon-γ, IL-2: interleukin-2).

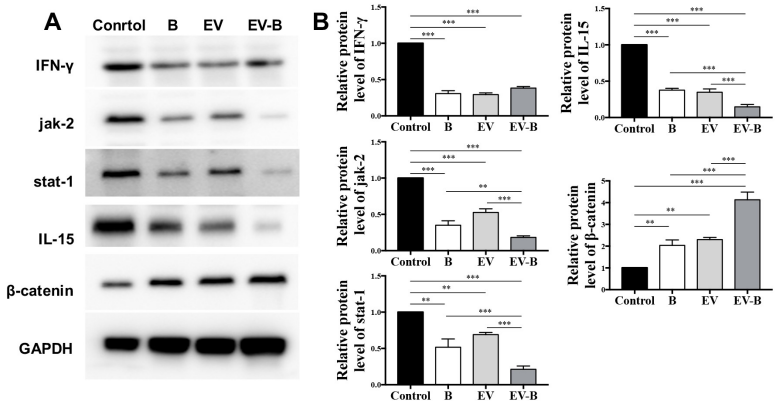

Figure 5. EV-B exert its role by up-regulating Wnt/β-catenin pathway and down-regulating JAK-STAT pathway. (**A**) The expression level of IFN-γ, jak-2, stat-1, IL-15, β-catenin in each group. (**B**) The relative protein level in each group. The result was normalized to GAPDH expression. *$P < 0.05$; **$P < 0.01$; ***$P < 0.001$. (EV-B: baricitinib loaded EVs, IFN-γ: interferon-γ, jak-2: Janus Kinase 2, stat-1: signal transducer and activator of transcription 1, IL-15: interleukin-15).

triphosphate competitive inhibitor that selectively inhibits the JAK1 and JAK2 enzymes. The *in-vitro* half maximal inhibitory concentrations (IC_{50}) for JAK1 and JAK2 are 5.9 nM and 5.7 nM, respectively (*6*). Oral baricitinib has demonstrated high efficacy in patients with moderate to severe alopecia areata and is approved for the treatment of severe AA in many countries. While systemic treatments can lead to unwanted long-term

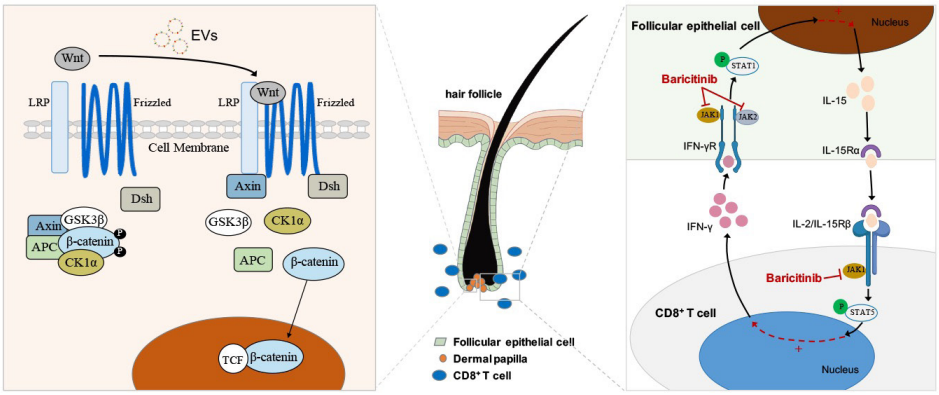

Figure 6. The therapeutic mechanism of EV-B in the treatment of AA. The therapeutic mechanism of EV-B in the treatment of AA may be the inhibition of JAK-STAT pathway and the upregulation of the Wnt/β-catenin pathway. (EV-B: baricitinib loaded EVs, AA: alopecia areata).

side effects, making topical application of baricitinib a potentially desirable treatment option for AA (*5*). Despite this, baricitinib has high molecular weight and very poorly water solubility (0.357 mg/mL to 0.46 mg/mL at 25°C) present challenges for its effective delivery as a topical treatment (*21*). Therefore, it is important to explore a proper drug carrier to improve the efficacy of topical baricitinib.

Exosomes have been investigated as delivery vesicles for various drugs. The exosome delivery system has specific advantages such as stability, a long-circulating half-life, specificity for targeting tissues, low immunogenicity and satisfactory biocompatibility. For example, Kim *et al*. (*17*) used exosome to deliver a RAGE-binding peptide for the treatment of acute lung injury. Wang *et al*. (*22*) used HEK-293T-derived exosomes loaded with adriamycin to improve the efficacy of tumor radiotherapy and chemotherapy. Zhu *et al*. (*16*) used ESC-exos as a therapeutic carrier to deliver paclitaxel and treat brain glioma.

MSCs are cell populations known for their self-renewal activity, which has broad prospects in tissue repair and regeneration. Lee *et al*. (*23*) reported that MSCs not only up-regulated the Wnt/β-catenin pathway to promote hair follicle growth, but also antagonized IFN-γ-induced hair follicle inflammation by down-regulating the JAK-STAT pathway in outer hair root sheath cells. While the safety of cell therapy remains controversial, exosome provides a major breakthrough to overcome the therapeutic limitations of MSCs. Therefore, MSC-derived EVs can promote the growth phase of hair follicles as well as inhibit inflammation. Their unique structure and properties make them an ideal drug carrier to load baricitinib.

In conclusion, we built baricitinib-loaded EVs and demonstrated that they can effectively promote hair growth in mice. The underlying mechanism may be the inhibition of JAK-STAT pathway and the upregulation of the Wnt/β-catenin pathway. Compared to baricitinib group, the better efficacy of EV-B may be attributed to the improvement of drug delivery efficiency as well as the synergistic effect of EVs. Our findings proved the effectiveness of EV-B, which could possibly be of practical use in the field of AA treatment.

Funding: This work was supported by grants from the Beijing Natural Science Foundation (L244027), Beijing Natural Science Foundation (7234388) and Youth Independent Innovation Science Fund of PLAGH (22QNFC013).

Conflict of Interest: The authors have no conflicts of interest to disclose.

References

1. Zhou C, Li X, Wang C, Zhang J. Alopecia areata: an update on etiopathogenesis, diagnosis, and management. Clin Rev Allergy Immunol. 2021; 61:403-423.
2. Vano-Galvan S, Figueras-Nart I, Artime E, Diaz-Cerezo S, Nunez M, Iglesias C, Artes M, Huete T. Epidemiological, clinical and economic burden of alopecia areata in Spain: a real-world retrospective study. The PETALO study. Eur J Dermatol. 2024; 34:163-175.
3. Strazzulla LC, Wang EHC, Avila L, Lo Sicco K, Brinster N, Christiano AM, Shapiro J. Alopecia areata: Disease characteristics, clinical evaluation, and new perspectives on pathogenesis. J Am Acad Dermatol. 2018; 78:1-12.
4. Fung S, Shirley M. Baricitinib: A review in severe alopecia areata. Am J Clin Dermatol. 2023; 24:661-668.
5. Wang EHC, Sallee BN, Tejeda CI, Christiano AM. JAK inhibitors for treatment of alopecia areata. J Invest Dermatol. 2018; 138:1911-1916.
6. Kincaid CM, Arnold JD, Mesinkovska NA. Baricitinib as the first systemic treatment for severe alopecia areata. Expert Rev Clin Immunol. 2023, 19:565-573.
7. Guan R, Lin Y, Zhang C, Wang Z, Wu Z, Liu X, Chen X, Piao Y. Comparative efficacy and safety of systemic steroids, oral JAK inhibitors and contact immunotherapy in the treatment of severe alopecia areata: a systematic review and network meta-analysis. Arch Dermatol Res. 2024; 316:483.
8. Zhang Y, Wang F, Li X, Zhao Y, Zhang J, Zhao W, Zhou C.

Oral abrocitinib for treatment of refractory alopecia areata: A retrospective study. J Am Acad Dermatol. 2024:S0190-9622(24)02876-7.
9. King B, Ohyama M, Kwon O, *et al*. Two phase 3 trials of baricitinib for alopecia areata. N Engl J Med. 2022; 386:1687-1699.
10. King B, Ko J, Kwon O, Vano-Galvan S, Piraccini BM, Dutronc Y, Yu G, Liu C, Somani N, Ball S, Mesinkovska NA. Baricitinib withdrawal and retreatment in patients with severe alopecia areata: The BRAVE-AA1 randomized clinical trial. JAMA Dermatol. 2024, 160:1075-1081.
11. Guo HW, Ye ZM, Chen SQ, McElwee KJ. Innovative strategies for the discovery of new drugs against alopecia areata: taking aim at the immune system. Expert Opin Drug Discov. 2024; 19:1321-1338.
12. Bian X, Li B, Tang H, Li Q, Hu W, Wei Q, Ma K, Yang Y, Li H, Fu X, Zhang C. Extracellular vesicles derived from fibroblasts induced with or without high glucose exert opposite effects on wound healing and angiogenesis. Front Surg. 2022; 9:1065172.
13. Golchin A, Shams F, Basiri A, Ranjbarvan P, Kiani S, Sarkhosh-Inanlou R, Ardeshirylajimi A, Gholizadeh-Ghaleh Aziz S, Sadigh S, Rasmi Y. Combination therapy of stem cell-derived exosomes and biomaterials in the wound healing. Stem Cell Rev Rep. 2022; 18:1892-1911.
14. Elsharkasy OM, Nordin JZ, Hagey DW, de Jong OG, Schiffelers RM, Andaloussi SE, Vader P. Extracellular vesicles as drug delivery systems: Why and how? Adv Drug Deliv Rev. 2020; 159:332-343.
15. Meng W, He C, Hao Y, Wang L, Li L, Zhu G. Prospects and challenges of extracellular vesicle-based drug delivery system: considering cell source. Drug Deliv. 2020; 27:585-598.
16. Zhu Q, Ling X, Yang Y, Zhang J, Li Q, Niu X, Hu G, Chen B, Li H, Wang Y, Deng Z. Embryonic stem cells-derived exosomes endowed with targeting properties as chemotherapeutics delivery vehicles for glioblastoma therapy. Adv Sci (Weinh). 2019; 6:1801899.
17. Kim G, Lee Y, Ha J, Han S, Lee M. Engineering exosomes for pulmonary delivery of peptides and drugs to inflammatory lung cells by inhalation. J Control Release. 2021; 330:684-695.
18. Cao Y, Lu S, Tang H. miR-141-3p-loaded extracellular vesicles ameliorate intrahepatic bile duct stone disease by decreasing MUC5AC expression *via* the MAPK pathway. Intractable Rare Dis Res. 2024.
19. Gilhar A, Kam Y, Assy B, Kalish RS. Alopecia areata induced in C3H/HeJ mice by interferon-gamma: evidence for loss of immune privilege. J Invest Dermatol. 2005; 124:288-289.
20. Chen L, Fan B, Gu H, Yang L, Li X. Effects of baicalin on alopecia and the associated mechanism. Biomed Res Int. 2022; 2022:3139123.
21. Mohammadi-Meyabadi R, Beirampour N, Garros N, Alvarado HL, Limon D, Silva-Abreu M, Calpena AC, Mallandrich M. Assessing the solubility of baricitinib and drug uptake in different tissues using absorption and fluorescence spectroscopies. Pharmaceutics. 2022; 14:2714.
22. Wang C, Li N, Li Y, Hou S, Zhang W, Meng Z, Wang S, Jia Q, Tan J, Wang R, Zhang R. Engineering a HEK-293T exosome-based delivery platform for efficient tumor-targeting chemotherapy/internal irradiation combination therapy. J Nanobiotechnology. 2022; 20:247.
23. Lee YJ, Park SH, Park HR, Lee Y, Kang H, Kim JE. Mesenchymal stem cells antagonize IFN-induced proinflammatory changes and growth inhibition effects *via* Wnt/beta-catenin and JAK/STAT pathway in human outer root sheath cells and hair follicles. Int J Mol Sci. 2021; 22:4581.

Received November 15, 2024; Revised December 7, 2024; Accepted December 8, 2024.

[§]These authors contributed equally to this work.
**Address correspondence to:*
Bingmin Li, Department of Dermatology, Fourth Medical Center of Chinese PLA General Hospital, Beijing, China.
E-mail: libingmin09@163.com

Li Yang, Faculty of Hepato-Pancreato-Biliary Surgery, First Medical Center of Chinese PLA General Hospital.
E-mail: ylbj1023@163.com

Released online in J-STAGE as advance publication December 11, 2024.

Original Article

DOI: 10.5582/ddt.2024.01085

Agarwood as a potential therapeutic for Alzheimer's disease: Mechanistic insights and target identification

Ya-nan Ma[1], Xiqi Hu[1], Kenji Karako[2], Peipei Song[3,*], Wei Tang[2,3], Ying Xia[1,*]

[1] Department of Neurosurgery, Haikou Affiliated Hospital of Central South University Xiangya School of Medicine, Haikou, China;
[2] Department of Surgery, Graduate School of Medicine, The University of Tokyo, Tokyo, Japan;
[3] National Center for Global Health and Medicine, Tokyo, Japan.

SUMMARY Alzheimer's disease (AD) is a progressive neurodegenerative disorder characterized by cognitive decline, memory loss, and functional impairments. Despite extensive research, its pathogenesis remains incompletely understood, and effective treatments are limited. This study explored the therapeutic potential of agarwood in AD by integrating network pharmacology, protein-protein interaction (PPI) network analysis, and single-cell expression analysis. The results revealed that agarwood compounds may modulate key inflammatory genes such as *NFKB1*, *STAT1*, and *TLR4*, alleviating neuroinflammation; enhance the expression of *HSP90* and regulate KDR signaling to improve blood-brain barrier (BBB) integrity; and promote the activity of PTPN11 and CXCR4 to support oligodendrocyte precursor cell (OPC) repair and remyelination. Single-cell expression analysis highlighted cell-type-specific expression patterns, particularly in OPCs and endothelial cells, underscoring their relevance in AD pathology. Agarwood's multi-dimensional therapeutic potential positions it as a promising candidate for the development of novel AD treatments.

Keywords Alzheimer's disease, agarwood, network pharmacology, neuroinflammation, blood-brain barrier, oligodendrocyte precursor cells

1. Introduction

Alzheimer's disease (AD) is a multifaceted, progressive neurodegenerative disorder and the most prevalent cause of dementia, characterized by cognitive decline, memory loss, and impaired daily functioning (*1*). In 2018, approximately 50 million people worldwide were affected by AD, with projections indicating that this number may rise to 152 million by 2050 (*2*). The increasing incidence of AD imposes significant social and economic burdens, creating immense challenges for both individuals and society (*3*). Current therapeutic approaches, which include traditional pharmacological treatments and immunotherapies, have shown limited efficacy, as no curative treatment targeting AD has been identified (*4*). This underscores the pressing need for further research into the underlying biological mechanisms of AD and the development of more effective therapeutic strategies.

Traditional Chinese medicine (TCM) has garnered attention in clinical practice due to its notable therapeutic effects and minimal side effects. Among these, agarwood, a valuable tropical plant, is rich in terpenoids, such as agarwood oil and agarol, which possess antioxidant, anti-inflammatory, and neuroprotective properties. Studies have demonstrated that agarwood extracts can reduce inflammation and inhibit cholinesterase activity in mouse models of AD (*5*). Given its potential as a neuroprotective agent, agarwood is an appealing candidate for further research. However, its precise mechanisms of action in AD remain unclear. In recent years, network pharmacology has emerged as an innovative approach for investigating drug-disease interactions, providing a comprehensive understanding of the relationship between therapeutics and their molecular targets (*6*). In this study, we applied network pharmacology to identify the target proteins associated with agarwood and elucidate its potential mechanisms in AD.

2. Materials and Methods

2.1. Prediction of active ingredients and targets of agarwood

The active components of agarwood were identified using the Traditional Chinese Medicine Systems Pharmacology Database and Analysis Platform

(TCMSP), applying the screening criteria of oral bioavailability (OB) greater than 30% and drug-likeness (DL) greater than 0.18. The molecular structures and canonical SMILES numbers of the components were obtained from the PubChem database (*http://pubchem.ncbi.nlm.nih.gov*). Target genes of these active components were predicted using the SwissTargetPrediction (*http://swisstargetprediction.ch/*) and SuperPred databases (*https://prediction.charite.de/subpages/target_prediction.php*). Targets were filtered based on a SwissTargetPrediction probability of ≥ 0.60 and a SuperPred probability of ≥ 60%. After compiling the target genes, their IDs were converted using Perl language, and gene symbols were obtained through alignment with the UniProt database.

2.2. Construction of the agarwood active component-target network

A network depicting the interactions between agarwood's active components and their target genes was created using Cytoscape software. The collected data were imported into Cytoscape to visualize the interactions within the network.

2.3. Disease target prediction

Genes associated with AD were identified using "AD" as the keyword, with "Homo sapiens" as the species. These genes were obtained from the GeneCards (*https://www.genecards.org/*), DisGeNET (*http://www.disgenet.org/*), and Online Mendelian Inheritance in Man (OMIM) databases (*http://www.omim.org/*), using a GeneCards score ≥ 50 and a DisGeNET score ≥ 0.10 as the filtering criteria. After eliminating duplicates, the AD-associated genes were consolidated.

2.4. Comparison of drug targets and disease targets

A Venn diagram was used to identify overlapping targets between agarwood's potential therapeutic targets and the disease-related genes associated with AD.

2.5. Biological function and pathway analysis of agarwood-AD common targets

Gene Ontology (GO) and Kyoto Encyclopedia of Genes and Genomes (KEGG) enrichment analyses for the shared targets were performed using the DAVID Bioinformatics Database (*https://david.ncifcrf.gov/home.jsp*). Terms with a *P*-value ≤ 0.05 were collected for GO term clustering, and KEGG pathway enrichment was used to identify statistically significant pathways ($P < 0.05$).

2.6. Construction of the drug-target-disease interaction network

The protein-protein interaction (PPI) data of agarwood's components and their predicted targets were imported into Cytoscape software. Nodes represented drug components and disease-related target genes, with degree values used to filter key components and targets. Additionally, a drug-target-disease interaction network was constructed by importing relevant data into Cytoscape.

2.7. Construction of the PPI network for common targets

The PPI network for the common targets between agarwood and AD was built using the STRING platform (*https://string-db.org/*), with "Homo sapiens" as the species and a minimum interaction confidence of 0.400. The network was then analyzed in Cytoscape, and the main targets were identified based on degree values.

2.8. Expression levels of top ten genes in different brain regions

The AlzData database (*http://www.alzdata.org/*) was utilized to assess the expression levels of the top ten identified genes across various brain regions and individual brain cells.

2.9. Convergent functional genomic (CFG) ranking for target genes

To assess the relevance of the identified target genes for agarwood in AD, we applied the CFG approach. This method integrates data from various sources, including genetic, transcriptomic, and proteomic information, to evaluate the involvement of each gene in AD. The analysis began by selecting the candidate genes identified through network pharmacology. These genes were then cross-referenced with genome-wide association studies (GWAS) and other functional genomics datasets. Each gene was assigned a CFG score, reflecting its cumulative association with AD based on factors such as the number of related genetic variants, known interactions with key proteins, and involvement in inflammatory pathways. This CFG score provided a comprehensive ranking of each gene's potential contribution to AD pathology.

2.10. Expression analysis of hub genes in single cells

Single-cell expression analysis for the hub genes was performed using the GSE67835 dataset from the Gene Expression Omnibus (GEO) database, revealing their expression patterns in different brain cell types.

3. Results

3.1. Screening of active compound targets

A total of eight active compounds from agarwood

were screened from the TCMSP database. The SwissTargetPrediction and SuperPred databases were used to predict the target genes for these compounds. After eliminating duplicates, 511 potential target genes were identified.

3.2. Construction of the target network for agarwood components

A network diagram illustrating the interactions between agarwood's active components and their respective target genes was constructed using Cytoscape software (Figure 1). The network revealed a one-to-many relationship between active compounds and interacting genes, consisting of 52 nodes and 100 edges. DMPEC and norboldine were identified as potential key components in AD treatment.

3.3. Screening of disease targets

Based on the established screening criteria, 123 genes were identified from GeneCards, 268 genes from the OMIM database, and 3,421 genes from the DisGeNET database. After consolidating these data and removing duplicates, 3,611 AD-associated genes were identified.

3.4. Identification of common targets

A Venn diagram comparison revealed 122 overlapping genes between the active components of agarwood and AD-related genes. These common genes represent the potential targets through which agarwood might exert therapeutic effects on AD.

3.5. GO and KEGG enrichment analyses

GO and KEGG enrichment analyses were performed on the 122 common genes identified in the study, using the DAVID database. These analyses revealed significant enrichment in a total of 1,939 GO terms that are relevant to AD treatment.

Among the 176 terms associated with molecular function (MF), the primary activities involved include amide binding, peptide binding, drug binding, protein serine/threonine kinase activity, endopeptidase activity, neurotransmitter receptor activity, protein tyrosine kinase activity, protein phosphatase binding, gated channel activity, and ion channel activity (Figure 2A). These molecular functions highlight the involvement of key signaling and enzyme pathways critical to AD pathology.

In the biological process (BP) category, 1,643 terms

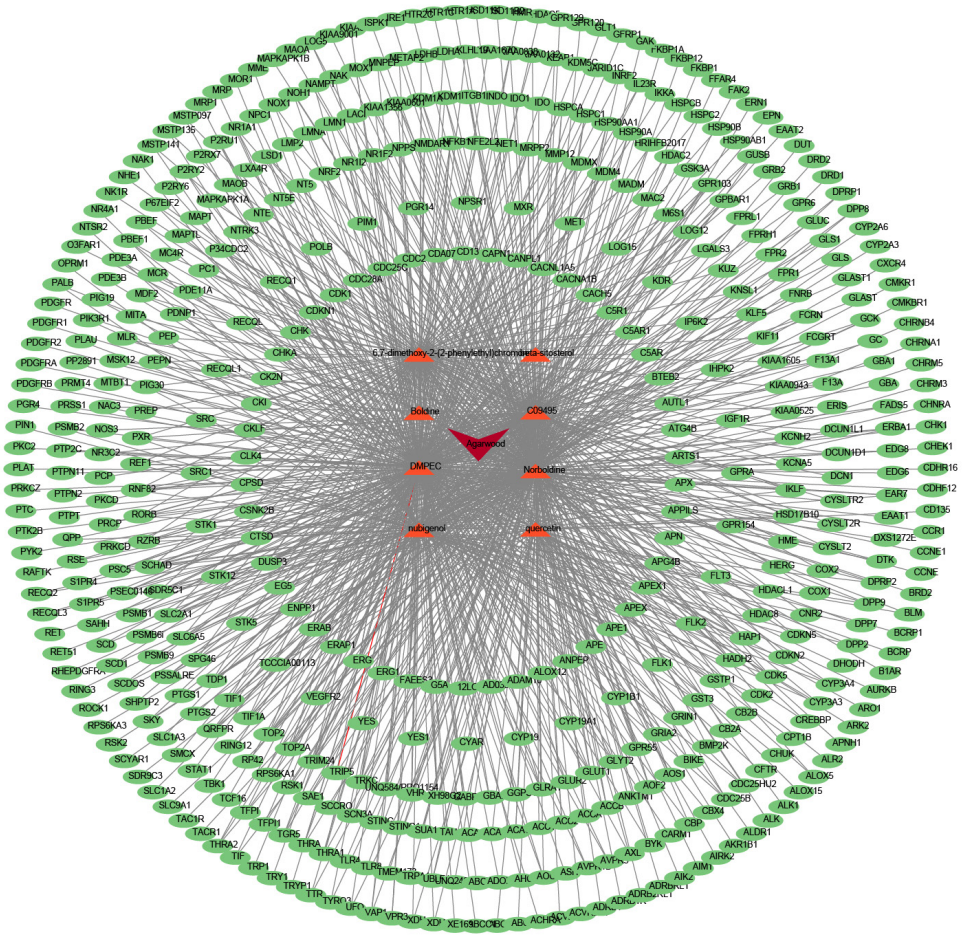

Figure 1. Agarwood components-target network diagram.

were identified. The top 10 processes were responses to drugs, oxygen levels, second-messenger-mediated signaling, oxidative stress, reactive oxygen species (ROS) metabolic processes, radiation, neutrophil degranulation, neutrophil activation involved in immune responses, decreased oxygen levels, and cellular responses to peptides and calcium ion transport (Figure 2B). These processes underscore the role of oxidative stress, immune responses, and calcium signaling in AD pathogenesis, all of which are key areas for potential therapeutic intervention.

For the cellular component (CC) category, 120 terms were identified. The most enriched terms included membrane rafts, membrane microdomains, membrane regions, glutamatergic synapses, secretory granule lumens, cytoplasmic vesicle lumens, vesicle lumens, cell leading edges, dendritic spines, neuron spines, and focal adhesions (Figure 2C). These findings suggest that critical cellular structures involved in signal transduction and synaptic function may play central roles in the progression of AD.

KEGG pathway enrichment analysis revealed 103 associated pathways. The top 10 pathways were neuroactive ligand-receptor interaction, microRNAs in cancer, AD, neurodegeneration pathways common to multiple diseases, the calcium signaling pathway, prostate cancer, the cAMP signaling pathway, the PI3K/Akt signaling pathway, proteoglycans in cancer, Parkinson's disease, and Huntington's disease. These pathways provide further insight into how cellular signaling, neurodegeneration mechanisms, and cancer-related pathways overlap in the context of AD (Figure 2D). In particular, pathways such as the PI3K/Akt and calcium signaling pathways are well-documented in their involvement in neuronal survival, synaptic plasticity, and neuroinflammation, which are critical to the disease process.

By focusing on the most enriched GO terms and KEGG pathways, the analysis reveals how agarwood's active compounds may exert therapeutic effects on AD through modulating biological functions such as protein binding, immune activation, and neuroprotection. These results not only provide potential therapeutic targets for future AD treatments but also highlight the complex interplay between neuroinflammation, oxidative stress, and cellular signaling in AD pathology.

3.6. Drug-component-disease-target network construction

The common target genes between agarwood and AD were imported into Cytoscape software to build a drug-component-disease-target interaction network (Figure 3). This visual model provided insights into how agarwood's

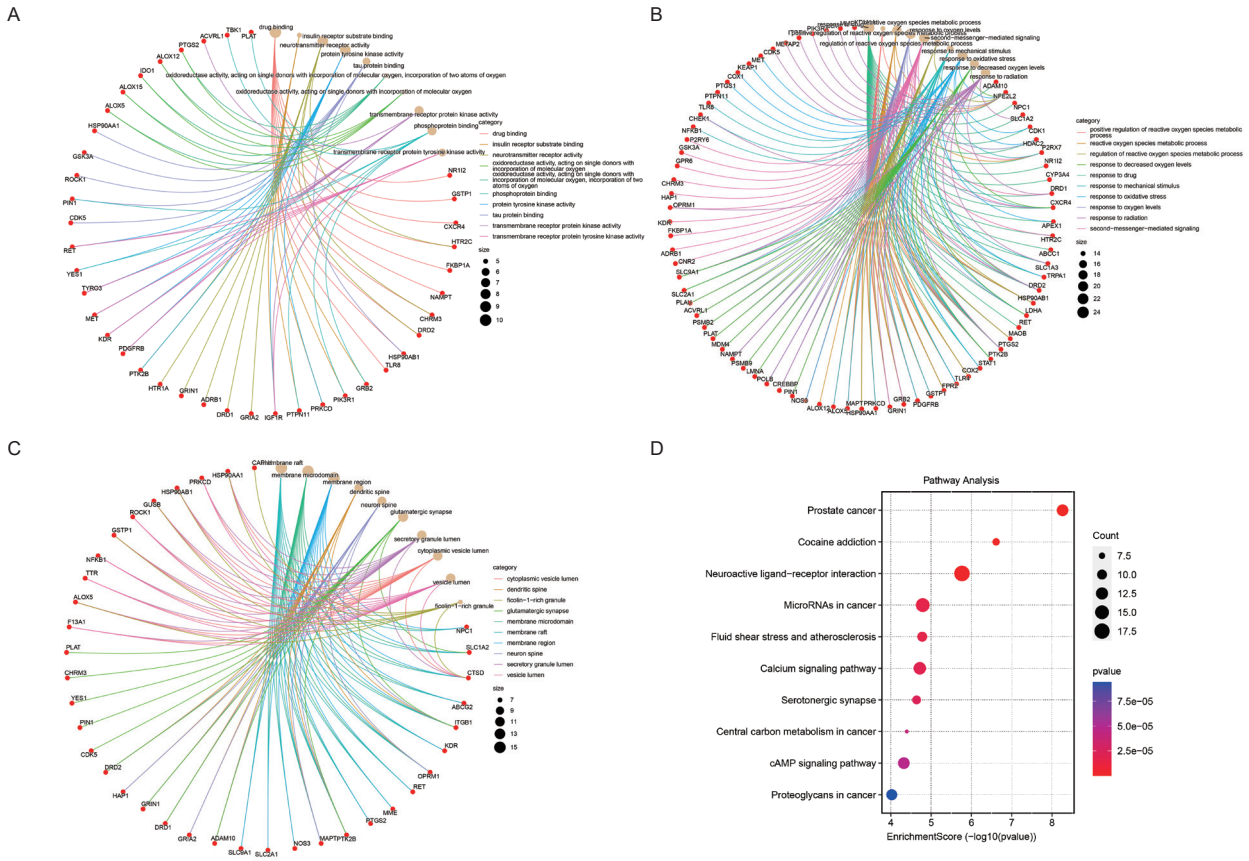

Figure 2. GO and KEGG enrichment analyses of common genes. Significant terms in molecular function **(A)**, biological process **(B)**, cellular component **(C)**, and KEGG pathways **(D)** associated with AD treatment.

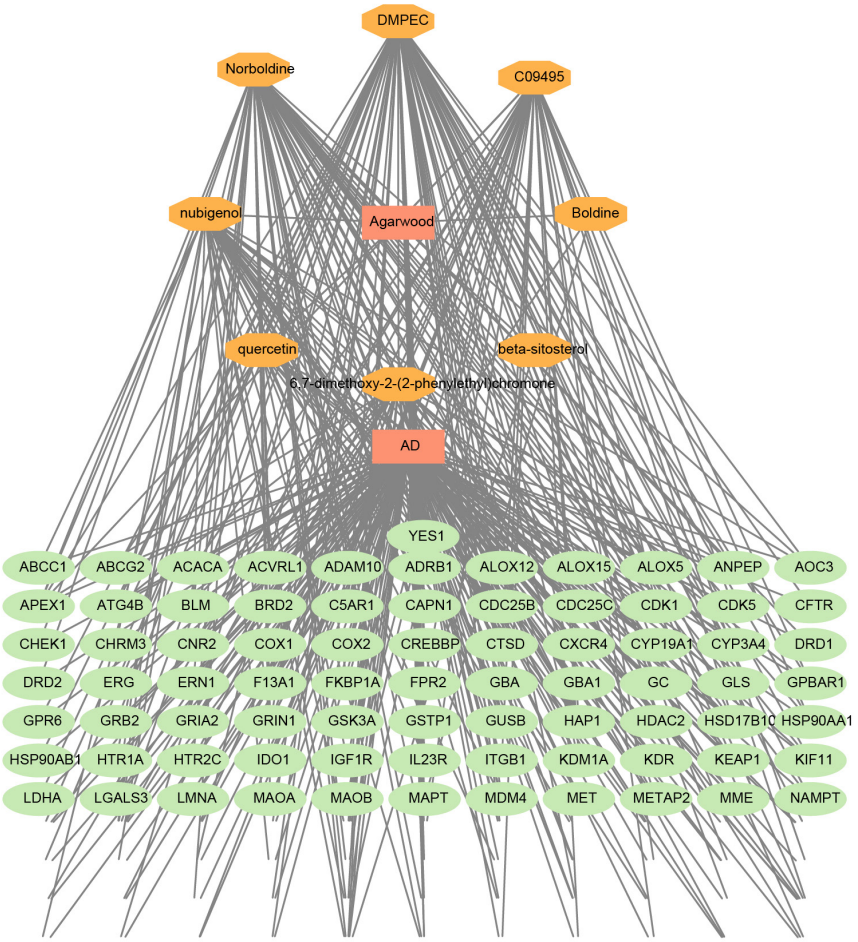

Figure 3. Drug-component-disease-target network diagram.

active components might interact with disease-related targets.

3.7. PPI network analysis

The 122 potential targets of agarwood in AD were further analyzed using the STRING platform, and a PPI network was constructed in Cytoscape after filtering out unconnected targets (Figure 4). The core target interaction network, based on degree values calculated *via* the cytoHubba module, revealed the top 10 hub genes: *HSP90AA1*, *HSP90AB1*, *NFKB1*, *TLR4*, *PTGS2*, *KDR*, *CXCR4*, *IL6*, *EGFR*, and *AKT1*.

3.8. Expression of top 10 genes in different brain regions

To further explore the roles of the ten hub genes (*HSP90AA1*, *HSP90AB1*, *NFKB1*, *TLR4*, *PTGS2*, *KDR*, *CXCR4*, *STAT1*, *PTPN11*, and *GRB2*), we analyzed their expression levels in 1,246 postmortem brain samples, which included 684 from AD patients and 562 from controls. The analysis focused on key brain regions implicated in AD pathology: the entorhinal cortex, hippocampus, temporal cortex, and frontal cortex (Table 1).

In the entorhinal cortex, significant differences were observed in the expression of *GRB2*, *CXCR4*, *KDR*, *TLR4*, *NFKB1* and *HSP90AB1* (Figures 5A, 5D, 5E, 5G-5I). Similarly, in the hippocampus, *PTPN11*, *CXCR4*, *NFKB1* and *HSP90AB1* showed altered expression levels (Figures 5B, 5D, 5H, 5I). In the temporal cortex, genes such as *GRB2*, *PTPN11*, *CXCR4*, *PTGS2*, *TLR4*, *NFKB1*, *HSP90AB1* and *HSP90AA1*, demonstrated differential expression patterns (Figures 5A, 5B, 5D, 5F-5J). Lastly, in the frontal cortex, significant variations were primarily observed for *CXCR4* and *NFKB1* (Figures 5D, 5H).

3.9. CFG ranking for target genes

The CFG analysis ranked the importance of the ten hub genes based on their association with Alzheimer's disease (Table 2). *GRB2* was regulated by five AD-related genetic variants, *HSP90AB1* by four variants, and *CXCR4* by three. According to GWAS, *PTPN11* was associated with three AD variants, while *CXCR4* had one AD-related variant. Additionally, *TLR4* and *PTGS2* were each regulated by two AD variants, and *NFKB1* by one variant.

Further analysis of physical interactions revealed that several of these genes interact with key proteins

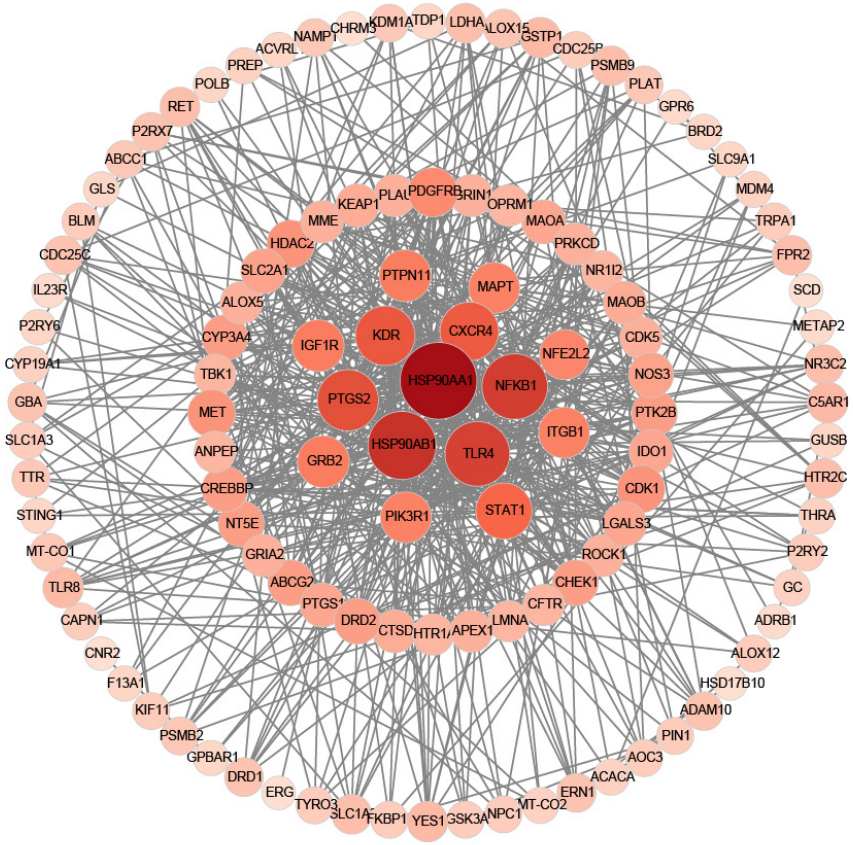

Figure 4. PPI network of agarwood targets in AD.

Table 1. Gene expression in Alzheimer's disease across brain regions

Gene	Entorhinal Cortex			Hippocampus			Temporal Cortex			Frontal Cortex		
	logFC	*P*-value	FDR	logFC	*P*-value	FDR	logFC	*P*-value	FDR	logFC	*P*-value	FDR
HSP90AA1	NA	NA	NA	-0.14	0.096	0.293	-0.36	0.009	0.046	0.11	0.177	0.327
HSP90AB1	-0.6	0.005	0.037	-0.29	0.032	0.155	-0.92	1.75E-06	0.000148231	-0.13	0.095	0.215
NFKB1	0.44	0.002	0.023	0.25	0.039	0.174	0.6	0.001	0.008	0.19	0.002	0.015
TLR4	0.48	0.003	0.027	0.21	0.075	0.256	0.48	0.014	0.063	-0.04	0.708	0.922
PTGS2	-0.07	0.702	0.82	-0.13	0.442	0.679	-0.46	0.01	0.05	-0.19	0.095	0.512
KDR	0.38	0.034	0.125	0.19	0.13	0.349	0.14	0.473	0.682	-0.12	0.458	0.826
CXCR4	0.8	0.0003	0.008	0.56	0.001	0.017	0.55	0.003	0.021	0.5	3.79E-05	0.002
STAT1	-0.17	0.12	0.275	-0.11	0.218	0.465	-0.06	0.61	0.784	0.03	0.631	0.761
PTPN11	NA	NA	NA	0.14	0.029	0.148	-0.31	0.024	0.093	-0.05	0.449	0.61
GRB2	-0.25	0.002	0.02	-0.06	0.308	0.561	-0.26	0.003	0.021	-0.05	0.373	0.537

Notes: logFC: logarithmic fold change, represents the fold change in gene expression, with positive values indicating upregulation and negative values indicating downregulation. FDR: false discovery rate – adjusted *P*-value to account for multiple testing.

implicated in AD pathology, including APP, PSEN1, PSEN2, APOE, and MAPT. For instance: HSP90AA1 interacts with APP, PSEN2, APOE, and MAPT; HSP90AB1 interacts with APP and PSEN1; NFKB1 interacts with APP, PSEN2, and MAPT; TLR4 interacts with PSEN2; PTGS2 interacts with APP, PSEN1, MAPT, and APOE; KDR and STAT1 interact with APOE; CXCR4 interacts with APP and APOE; PTPN11 interacts with APP, PSEN1, MAPT, and APOE; GRB2 interacts with APP, PSEN1, PSEN2, MAPT, and APOE.

The *PTPN11* gene showed differential expression early in the progression of AD, while *NFKB1* and *STAT1* were strongly linked to the development of amyloid-beta (Aβ) pathology. However, none of these hub genes were directly connected to tau pathology. Based on the CFG rankings, *NFKB1*, *CXCR4*, and *PTPN11* were ranked 3, *HSP90AB1*, *STAT1*, *TLR4*, *PTGS2*, and *GRB2* were ranked 2, while *HSP90AA1* and *KDR* were ranked 1. This indicates varying degrees of influence on AD pathology among these target genes.

3.10. Single-cell expression analysis of hub genes

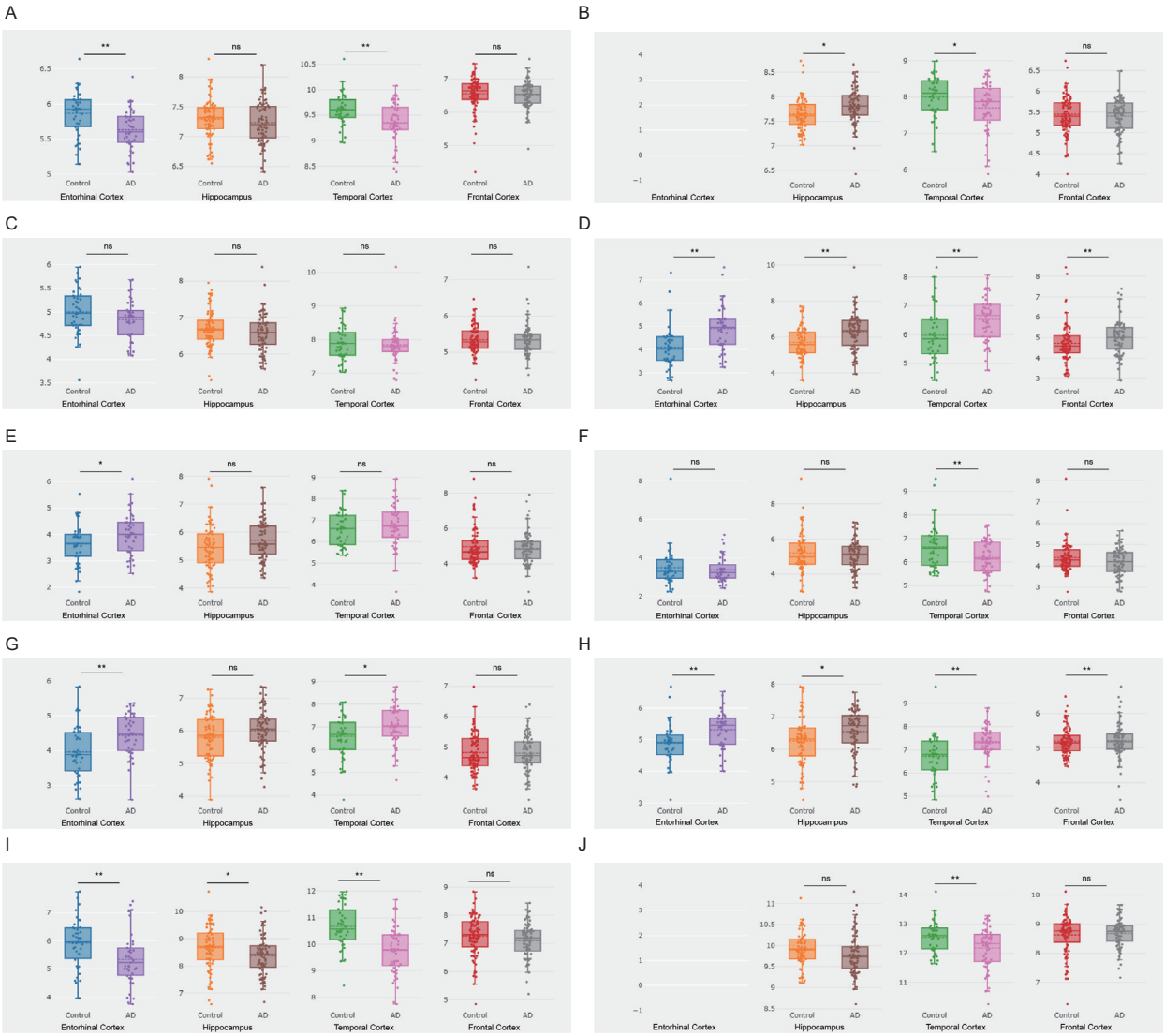

Figure 5. The expression levels of hub genes in different brain regions. Cross-platform nomalized expression level of *GRB2* **(A)**, *PTPN11* **(B)**, *STAT1* **(C)**, *CXCR4* **(D)**, *KDR* **(E)**, *PTGS2* **(F)**, *TLR4* **(G)**, *NFKB1* **(H)**, *HSP90AB1* **(I)**, *HSP90AA1* **(J)**.

Table 2. CFG ranking and evidence for target genes in Alzheimer's disease

Gene	eQTL	GWAS	PPI	Early_DEG	Pathology cor (Aβ)	Pathology cor (tau)	CFG
HSP90AA1	0	0	APP, PSEN2, MAPT, APOE	NA	NA	NA	1
HSP90AB1	4	0	APP, PSEN1	NA	NA	NA	2
NFKB1	1	0	APP, PSEN2, MAPT	NA	0.731,***	0.247, ns	3
TLR4	2	0	PSEN2	NA	NA	NA	2
PTGS2	2	0	APP, PSEN1, MAPT, APOE	NA	NA	NA	2
KDR	0	0	APOE	NA	0.064, ns	0.456, ns	1
CXCR4	3	1	APP, APOE	no	0.104, ns	0.490, ns	3
STAT1	0	0	APOE	NA	0.789,***	0.490, ns	2
PTPN11	0	3	APP, PSEN1, MAPT, APOE	yes	0.175, ns	-0.258, ns	3
GRB2	5	0	APP, PSEN1, PSEN2, MAPT, APOE	NA	0.110, ns	0.138, ns	2

Notes: CFG (convergent functional genomics): The CFG score indicates the functional relevance of a target gene based on various lines of evidence. Each significant piece of evidence contributes one point to the total CFG score, ranging from 0 to 5. Early_DEG: Indicates whether the target gene is differentially expressed in the early stages of AD. "yes" denotes differential expression, "no" indicates no significant differential expression, and "NA" indicates a lack of available data. eQTL: Indicates whether the expression of a target gene is regulated by genetic variants associated with Alzheimer's disease (AD). Genetic variant data are derived from the IGAP GWAS, with significance thresholds set at GWAS $P < 1E-3$ and eQTL $P < 1E-3$. GWAS: Represents a direct association between the target gene and AD in GWAS studies ($P < 0.05$). If a significant association is observed, the value is marked as 1; otherwise, it is 0. Pathology cor (Aβ): Refers to the correlation between target gene expression and AD pathology in Aβ mouse models. "ns" denotes non-significant correlation ($P > 0.05$), ***$P < 0.001$). Pathology cor (tau): Refers to the correlation between target gene expression and AD pathology in tau mouse models. "ns" denotes non-significant correlation ($P > 0.05$). PPI (protein-protein interaction): Indicates significant physical interactions ($P < 0.05$) between the target gene and key AD-related proteins, including APP, PSEN1, PSEN2, APOE, and MAPT. Interacting proteins are listed if a significant interaction is observed.

Figure 6. Expression levels of hub genes in single brain cells. Expression level of *GRB2* **(A)**, *PTPN11* **(B)**, *STAT1* **(C)**, *CXCR4* **(D)**, *KDR* **(E)**, *PTGS2* **(F)**, *TLR4* **(G)**, *NFKB1* **(H)**, *HSP90AB1* **(I)**, *HSP90AA1* **(J)** in single brain cells. OPC, oligodendrocyte precursor cell.

Single-cell expression analysis revealed distinct patterns of hub gene expression across various brain cell types, including neurons, microglia, astrocytes, and oligodendrocytes. These patterns underscore the potential involvement of these genes in AD pathology.

Specifically, the expression levels of different genes in oligodendrocyte precursor cells (OPCs) showed significant variability (Figure 6). Genes such as *HSP90AA1*, *HSP90AB1*, *PTGS2*, and *KDR* exhibited low expression, while *STAT1* and *TLR4* were moderately expressed (Figures 6C, 6E-6G, 6I, 6J). In contrast,

NFKB1, *CXCR4*, and *PTPN11* demonstrated high expression levels in OPCs, suggesting their potential roles in neuroinflammation and immune regulation (Figures 6B, 6D, 6H). Additionally, *GRB2* displayed consistently stable expression levels across OPCs and other cell types, highlighting its ubiquitous regulatory function (Figure 6A).

For endothelial cells, which are critical components of the brain vascular system, gene expression patterns directly influence the functional integrity of the blood-brain barrier (BBB). Analysis revealed high expression levels of *KDR*, *HSP90AA1*, and *HSP90AB1* in endothelial cells (Figures 6E, 6I, 6J). Moderate expression levels were observed for *TLR4*, *CXCR4*, *PTPN11*, and *GRB2*, whereas *NFKB1*, *STAT1*, and *PTGS2* exhibited low expression (Figures 6A-6D, 6F-6H).

4. Discussion

AD is a severe chronic neurodegenerative disorder characterized by memory loss, cognitive decline, behavioral and emotional abnormalities, and ultimately, the inability to perform daily activities independently (*7*). Despite significant advances in AD research, the precise mechanisms underlying its pathogenesis remain elusive. Studies have identified several critical factors contributing to AD progression, including neuroinflammation, Aβ plaque accumulation, tau protein tangles, oxidative stress, and BBB dysfunction (*3*).

Given the complexity of these interconnected pathological mechanisms, traditional single-target therapies have shown limited effectiveness. Consequently, multi-target therapeutic strategies have emerged as a promising approach for combating AD. In this study, we explored the potential mechanisms by which agarwood may modulate key AD-related pathological pathways, particularly in neuroinflammation, neuroprotection, and vascular function regulation.

Neuroinflammation is widely recognized as a central driver of AD onset and progression (*8*). Chronic activation of microglia, astrocytes, and OPCs leads to the release of pro-inflammatory cytokines, chemokines, and ROS. This toxic microenvironment exacerbates neuronal damage and disrupts synaptic function, further contributing to cognitive decline (*9*).

NFKB1 is a pivotal regulator of neuroinflammation (*10*). Studies have shown that its overexpression is closely associated with Aβ accumulation and upregulation of pro-inflammatory genes in AD pathology (*11*). Our findings indicate that NFKB1 is highly expressed in OPCs, suggesting its involvement not only in inflammation signaling but also in amplifying immune responses, which may impact myelin repair processes (*12*). Interestingly, NFKB1 exhibits a dual role: while it contributes to the inflammatory cascade, it may also participate in resolving inflammation by promoting anti-inflammatory pathways. This duality underscores its potential as a therapeutic target. Modulating NFKB1 activity could reduce inflammation while preserving neuronal function, offering a balanced approach to mitigating AD pathology.

STAT1 plays a critical role in promoting the pro-inflammatory (M1) phenotype of microglia and is closely linked to Aβ and tau pathology (*13,14*). In our study, moderate STAT1 expression was observed in both endothelial cells and OPCs, indicating its involvement in immune regulation and vascular function. Agarwood-derived compounds may inhibit excessive STAT1 activation, thereby reducing the expression of iNOS and COX2, key mediators of oxidative stress and neuroinflammation (*15,16*). Moreover, the antioxidant properties of agarwood could further alleviate STAT1-mediated neurotoxicity by mitigating ROS levels. This dual anti-inflammatory and antioxidant effect highlights the potential of agarwood-derived compounds in addressing the multifaceted pathology of AD.

TLR4 is a key pattern recognition receptor that detects damage-associated molecular patterns (DAMPs) such as Aβ (*17,18*). Persistent activation of TLR4 amplifies neuroinflammation and impairs endothelial function, contributing to BBB dysfunction. In our study, moderate TLR4 expression was detected in both OPCs and endothelial cells, suggesting its role as an innate immune sensor involved in amplifying inflammatory signaling (*19*). Agarwood-derived compounds, particularly terpenoids, have demonstrated inhibitory effects on TLR4 signaling (*20*). By suppressing TLR4 activation, these compounds may limit chronic inflammation while preserving the structural and functional integrity of vascular and neuronal systems. This suggests that agarwood has potential as a multi-functional therapeutic agent for mitigating TLR4-driven pathology in AD.

BBB dysfunction is a critical pathological feature of AD. In AD, increased BBB permeability allows peripheral immune cells and toxic molecules to infiltrate the central nervous system (CNS), exacerbating neuroinflammation and neuronal damage. This study identified several key genes, including *KDR* (*VEGFR2*), *HSP90* family proteins, and *TLR4*, that play essential roles in regulating BBB integrity and vascular function.

KDR, a key receptor in the VEGF signaling pathway, promotes angiogenesis and endothelial cell survival under normal conditions(*21*). However, in AD, aberrant VEGF-KDR signaling has been associated with pathological angiogenesis, contributing to BBB dysfunction (*21,22*). This study suggests that agarwood-derived compounds may regulate KDR activity, restoring normal angiogenesis, reducing vascular leakage, and enhancing BBB functional integrity.

HSP90 family proteins, including HSP90AA1 and HSP90AB1, are highly expressed in endothelial cells and play critical roles in mitigating neurotoxicity by

facilitating the autophagic clearance of misfolded proteins such as Aβ and tau (*23,24*). Agarwood's antioxidant and anti-inflammatory properties may synergize with HSP90 family proteins, enhancing its ability to eliminate toxic proteins while minimizing potential adverse effects. This dual action highlights the therapeutic potential of agarwood in protecting endothelial cells from the pathological stressors associated with AD.

Activation of TLR4 in endothelial cells increases the activity of matrix metalloproteinases (MMPs), which degrade tight junction proteins and further compromise BBB integrity (*25*). This process facilitates the infiltration of peripheral inflammatory mediators into the CNS, aggravating neuroinflammation. Agarwood-derived compounds have been shown to inhibit TLR4-related pathways, effectively reducing endothelial inflammation and maintaining BBB barrier function. This suggests that agarwood could play a protective role in preserving vascular and neuronal homeostasis in AD.

OPCs play a pivotal role not only in myelin repair but also in immune regulation (*26,27*). The high expression of *PTPN11* is particularly critical for the differentiation of OPCs into mature oligodendrocytes, a process essential for restoring myelin integrity (*28*). However, in the inflammatory microenvironment of AD, the proliferation, migration, and differentiation of OPCs are significantly impaired (*29*). Agarwood-derived compounds may enhance PTPN11 activity, promoting myelin repair and restoring neuronal signal transmission. Furthermore, OPCs exhibit increased expression of genes involved in antigen processing and presentation through the major histocompatibility complex (MHC)-II pathway. OPCs expressing MHC-II contribute to the activation of memory CD4+ T cells (*30*). In this study, high expression levels of *NFKB1*, *CXCR4*, and *PTPN11* were observed in OPCs, indicating their dual roles in AD-related inflammatory and reparative pathways.

During embryonic development, OPCs are positioned between perivascular cells and neuroglial cells, directly contributing to the formation of the BBB (*31*). Additionally, OPCs regulate the proliferation of perivascular cells and influence the expression of functionally relevant proteins in endothelial cells by releasing regulatory factors (*32*). These findings suggest that OPCs are not only critical for myelin formation and repair but also play a key role in vascular regulation and the maintenance of neurovascular unit homeostasis. This dual functionality underscores the potential of OPCs as therapeutic targets in AD and highlights the importance of agarwood-derived compounds in supporting their protective and reparative roles.

This study, through the construction of drug-target-disease and PPI networks, elucidates the potential mechanisms by which agarwood active compounds may act on multiple targets to influence the progression of AD. The active compounds in agarwood not only target core genes related to neuroinflammation, such as *NFKB1* and *STAT1*, but also demonstrate significant effects in regulating cholinesterase activity and mitigating oxidative stress (*33*). These multi-target actions suggest that agarwood may offer advantages over traditional single-target drugs in AD therapy. By acting through various synergistic mechanisms, agarwood compounds have the potential to alleviate neuroinflammation, inhibit pathological protein aggregation, and improve cognitive function, providing a multidimensional therapeutic strategy for AD.

Despite the promising findings, this study has several limitations that should be acknowledged. First, the study primarily relies on database-driven and bioinformatics analyses, with data sourced from multiple public databases, including TCMSP, GeneCards, STRING, and AlzData. While these databases are supported by extensive data and robust quality control measures, they are still subject to biases and inconsistencies arising from data origin, platform differences, and ongoing updates in gene annotations. Although the databases provide a preliminary framework for exploring the connections between agarwood compounds and AD-related targets, the results lack direct experimental validation. Thus, the reliability of these findings must be further confirmed through *in vitro* and *in vivo* studies.

Second, this study does not fully address the complexity of agarwood components or the pharmacokinetic and pharmacodynamic characteristics of these compounds *in vivo*. Although initial screening of active compounds was conducted using criteria such as OB and DL, these standards may not comprehensively predict the metabolic processes and ultimate biological effects of these compounds in living organisms. Agarwood contains numerous active compounds that may produce metabolic byproducts or interact with each other *in vivo*, and these factors were not extensively examined in this study.

To overcome these limitations, future research should involve animal models and clinical trials to thoroughly investigate the metabolism, bioavailability, and pharmacological effects of individual agarwood compounds as well as their interactions. These studies will provide a more detailed understanding of how agarwood functions as a therapeutic agent and ensure the translatability of these findings to clinical applications.

5. Conclusion

This study, through network pharmacology analysis, PPI network analysis, and single-cell expression analysis, reveals the potential multi-target mechanisms of agarwood in the treatment of AD. Agarwood compounds may modulate key inflammatory factors such as NFKB1, STAT1, and TLR4 to alleviate neuroinflammation; they may enhance expression of HSP90 family proteins and regulate the KDR signaling pathway to improve BBB function; and they may promote the activity of PTPN11

and CXCR4, supporting the repair and remyelination functions of OPCs, providing a multi-dimensional approach for AD therapy. These findings not only offer significant theoretical support for agarwood as a candidate drug for AD treatment but also point the way for the development of novel multi-target therapeutic strategies. With its unique natural medicinal advantages, agarwood has the potential to become an emerging therapy for AD, offering tangible benefits to patients.

Funding: This work was supported by the National Natural Science Foundation of China (No. 82460268), the Hainan Province Clinical Medical Research Center (No. LCYX202410, LCYX202309), and Grants-in-Aid from the Ministry of Education, Science, Sports, and Culture of Japan (24K14216).

Conflict of Interest: The authors have no conflicts of interest to disclose.

References

1. Gu X, Qi L, Qi Q, Zhou J, Chen S, Wang L. Monoclonal antibody therapy for Alzheimer's disease focusing on intracerebral targets. Biosci Trends. 2024; 18:49-65.
2. Collaborators GBDDF. Estimation of the global prevalence of dementia in 2019 and forecasted prevalence in 2050: An analysis for the Global Burden of Disease Study 2019. Lancet Public Health. 2022; 7:e105-e125.
3. Deng Y, Wang H, Gu K, Song P. Alzheimer's disease with frailty: Prevalence, screening, assessment, intervention strategies and challenges. Biosci Trends. 2023; 17:283-292.
4. Tatulian SA. Challenges and hopes for Alzheimer's disease. Drug Discov Today. 2022; 27:1027-1043.
5. Bahrani H, Mohamad J, Paydar MJ, Rothan HA. Isolation and characterisation of acetylcholinesterase inhibitors from Aquilaria subintegra for the treatment of Alzheimer's disease (AD). Curr Alzheimer Res. 2014; 11:206-214.
6. Alshabrmi FM, Aba Alkhayl FF, Rehman A. Novel drug discovery: Advancing Alzheimer's therapy through machine learning and network pharmacology. Eur J Pharmacol. 2024; 976:176661.
7. Ma YN, Hu X, Karako K, Song P, Tang W, Xia Y. Exploring the multiple therapeutic mechanisms and challenges of mesenchymal stem cell-derived exosomes in Alzheimer's disease. Biosci Trends. 2024; 18:413-430.
8. Airapetov M, Eresko S, Ignatova P, Lebedev A, Bychkov E, Shabanov P. A brief summary regarding the roles of interleukin-11 in neurological diseases. Biosci Trends. 2022; 16:367-370.
9. Zhang P, Kishimoto Y, Grammatikakis I, Gottimukkala K, Cutler RG, Zhang S, Abdelmohsen K, Bohr VA, Misra Sen J, Gorospe M, Mattson MP. Senolytic therapy alleviates Abeta-associated oligodendrocyte progenitor cell senescence and cognitive deficits in an Alzheimer's disease model. Nat Neurosci. 2019; 22:719-728.
10. Wang C, Fan L, Khawaja RR, *et al.* Microglial NF-kappaB drives tau spreading and toxicity in a mouse model of tauopathy. Nat Commun. 2022; 13:1969.
11. Xu J, Zhang P, Huang Y, Zhou Y, Hou Y, Bekris LM, Lathia J, Chiang CW, Li L, Pieper AA, Leverenz JB, Cummings J, Cheng F. Multimodal single-cell/nucleus RNA sequencing data analysis uncovers molecular networks between disease-associated microglia and astrocytes with implications for drug repurposing in Alzheimer's disease. Genome Res. 2021; 31:1900-1912.
12. Nicholas RS, Wing MG, Compston A. Nonactivated microglia promote oligodendrocyte precursor survival and maturation through the transcription factor NF-kappa B. Eur J Neurosci. 2001; 13:959-967.
13. Feng W, Zhang Y, Ding S, Chen S, Wang T, Wang Z, Zou Y, Sheng C, Chen Y, Pang Y, Marshall C, Shi J, Nedergaard M, Li Q, Xiao M. B lymphocytes ameliorate Alzheimer's disease-like neuropathology *via* interleukin-35. Brain Behav Immun. 2023; 108:16-31.
14. Rangaraju S, Dammer EB, Raza SA, Rathakrishnan P, Xiao H, Gao T, Duong DM, Pennington MW, Lah JJ, Seyfried NT, Levey AI. Identification and therapeutic modulation of a pro-inflammatory subset of disease-associated-microglia in Alzheimer's disease. Mol Neurodegener. 2018; 13:24.
15. Ma CT, Huang T, Yu JS, Ly TL, Vu Huynh KL, Kwon SW, Park JH, Yang HO. Sesquiterpenoids and hexanorcucurbitacin from Aquilaria malaccensis agarwood with anti-inflammatory effects by inhibiting the STAT1/AKT/MAPK/NLRP3 pathway. RSC Adv. 2024; 14:9391-9405.
16. Ma CT, Lee SB, Cho IH, Yu JS, Huang T, Lee TM, Ly TL, Kwon SW, Park JH, Yang HO. Agarperoxinols A and B: Two unprecedented tricyclic 6/6/7 rearranged humulene-type sesquiterpenoids that attenuated the neuroinflammation in LPS-stimulated microglial models. ACS Omega. 2023; 8:43873-43882.
17. Sangineto M, Ciarnelli M, Cassano T, Radesco A, Moola A, Bukke VN, Romano A, Villani R, Kanwal H, Capitanio N, Duda L, Avolio C, Serviddio G. Metabolic reprogramming in inflammatory microglia indicates a potential way of targeting inflammation in Alzheimer's disease. Redox Biol. 2023; 66:102846.
18. Anwar MM. Oxidative stress-A direct bridge to central nervous system homeostatic dysfunction and Alzheimer's disease. Cell Biochem Funct. 2022; 40:17-27.
19. Srivastava T, Diba P, Dean JM, Banine F, Shaver D, Hagen M, Gong X, Su W, Emery B, Marks DL, Harris EN, Baggenstoss B, Weigel PH, Sherman LS, Back SA. A TLR/AKT/FoxO3 immune tolerance-like pathway disrupts the repair capacity of oligodendrocyte progenitors. J Clin Invest. 2018; 128:2025-2041.
20. Zheng Y, Gao Y, Zhu W, Bai XG, Qi J. Advances in molecular agents targeting toll-like receptor 4 signaling pathways for potential treatment of sepsis. Eur J Med Chem. 2024; 268:116300.
21. Harris R, Miners JS, Allen S, Love S. VEGFR1 and VEGFR2 in Alzheimer's disease. J Alzheimers Dis. 2018; 61:741-752.
22. Singh Angom R, Wang Y, Wang E, Pal K, Bhattacharya S, Watzlawik JO, Rosenberry TL, Das P, Mukhopadhyay D. VEGF receptor-1 modulates amyloid beta 1-42 oligomer-induced senescence in brain endothelial cells. FASEB J. 2019; 33:4626-4637.
23. Salminen A, Ojala J, Kaarniranta K, Hiltunen M, Soininen H. Hsp90 regulates tau pathology through co-chaperone complexes in Alzheimer's disease. Prog Neurobiol. 2011; 93:99-110.
24. Kakimura J, Kitamura Y, Takata K, Umeki M, Suzuki S,

Shibagaki K, Taniguchi T, Nomura Y, Gebicke-Haerter PJ, Smith MA, Perry G, Shimohama S. Microglial activation and amyloid-beta clearance induced by exogenous heat-shock proteins. FASEB J. 2002; 16:601-603.
25. Zhang Y, Liu H, Chen Z, Yu M, Li J, Dong H, Li N, Ding X, Ge Y, Liu C, Ma T, Gui B. TLR4-mediated hippocampal MMP/TIMP imbalance contributes to the aggravation of perioperative neurocognitive disorder in db/db mice. Neurochem Int. 2020; 140:104818.
26. Zou P, Wu C, Liu TC, Duan R, Yang L. Oligodendrocyte progenitor cells in Alzheimer's disease: From physiology to pathology. Transl Neurodegener. 2023; 12:52.
27. Yun W, Choi KA, Hwang I, *et al.* OCT4-induced oligodendrocyte progenitor cells promote remyelination and ameliorate disease. NPJ Regen Med. 2022; 7:4.
28. Ehrman LA, Nardini D, Ehrman S, Rizvi TA, Gulick J, Krenz M, Dasgupta B, Robbins J, Ratner N, Nakafuku M, Waclaw RR. The protein tyrosine phosphatase Shp2 is required for the generation of oligodendrocyte progenitor cells and myelination in the mouse telencephalon. J Neurosci. 2014; 34:3767-3778.
29. Nalivaeva NN, Rybnikova EA. Editorial: Brain hypoxia and ischemia: New insights into neurodegeneration and neuroprotection. Front Neurosci. 2019; 13:770.
30. Falcao AM, van Bruggen D, Marques S, Meijer M, Jakel S, Agirre E, Samudyata, Floriddia EM, Vanichkina DP, Ffrench-Constant C, Williams A, Guerreiro-Cacais AO, Castelo-Branco G. Disease-specific oligodendrocyte lineage cells arise in multiple sclerosis. Nat Med. 2018; 24:1837-1844.
31. Kishida N, Maki T, Takagi Y, Yasuda K, Kinoshita H, Ayaki T, Noro T, Kinoshita Y, Ono Y, Kataoka H, Yoshida K, Lo EH, Arai K, Miyamoto S, Takahashi R. Role of perivascular oligodendrocyte precursor cells in angiogenesis after brain ischemia. J Am Heart Assoc. 2019; 8:e011824.
32. Maki T, Maeda M, Uemura M, Lo EK, Terasaki Y, Liang AC, Shindo A, Choi YK, Taguchi A, Matsuyama T, Takahashi R, Ihara M, Arai K. Potential interactions between pericytes and oligodendrocyte precursor cells in perivascular regions of cerebral white matter. Neurosci Lett. 2015; 597:164-169.
33. Li W, Chen HQ, Wang H, Mei WL, Dai HF. Natural products in agarwood and Aquilaria plants: Chemistry, biological activities and biosynthesis. Nat Prod Rep. 2021; 38:528-565.

Received November 23, 2024; Revised December 15, 2024; Accepted December 18, 2024.

**Address correspondence to:*
Ying Xia, Department of Neurosurgery, Haikou Affiliated Hospital of Central South University Xiangya School of Medicine, Haikou 570208, China.
E-mail: xiaying008@163.com

Peipei Song, National Center for Global Health and Medicine, Tokyo 162-8655, Japan.
E-mail: psong@it.ncgm.go.jp

Released online in J-STAGE as advance publication December 21, 2024.

Brief Report

DOI: 10.5582/ddt.2024.01076

Development of a simple high-performance liquid chromatography-ultraviolet detection method for selpercatinib determination in human plasma

Wataru Suzuki[1,2], Yoshito Gando[1], Takeo Yasu[1,*]

[1] Department of Medicinal Therapy Research, Education and Research Unit for Comprehensive Clinical Pharmacy, Meiji Pharmaceutical University, Tokyo, Japan;
[2] Department of Pharmacy, Cancer Institute Hospital, Japanese Foundation for Cancer Research, Tokyo, Japan.

SUMMARY Selpercatinib is a selective *rearranged during transfection* (*RET*) kinase inhibitor effective for the treatment of *RET*-positive non-small cell lung cancer, thyroid cancer, and other cancers. However, its clinical use requires careful management because of dose-dependent adverse effects and pharmacokinetic interactions. Given the multiple factors influencing selpercatinib blood levels, we hypothesized that establishing a therapeutic drug monitoring system for selpercatinib could help reduce adverse events and optimize efficacy. Therefore, we herein developed a high-performance liquid chromatography-ultraviolet (HPLC-UV) method for measuring selpercatinib blood levels to facilitate therapeutic drug monitoring in clinical practice. Proteins were precipitated with acetonitrile, and selpercatinib and the internal standard (gefitinib) were separated *via* HPLC-UV. The calibration curve was linear over 0.5–8.0 μg/mL with a coefficient of determination (r^2) equaling 0.9996. Intra- and interday validation coefficients were both under 2.80%. The corresponding measurement precision ranged from − 1.50% to 12.60% and − 1.32% to 7.50%, respectively, with recoveries exceeding 94.43%. Thus, this study establishes a simple and sensitive method for quantifying selpercatinib in human plasma. Future studies will analyze plasma samples from patients treated with selpercatinib and utilize this method to explore the relationships among plasma concentration, efficacy, and adverse events to define the therapeutic concentration range.

Keywords targeted kinase inhibitor, clinical settings

1. Introduction

Selpercatinib is an adenosine triphosphate-competitive and highly selective oral small-molecule inhibitor of the *rearranged during transfection* (*RET*) kinase, demonstrating efficacy and safety in the treatment of *RET* fusion-positive lung and thyroid cancers and *RET*-mutant medullary thyroid cancer (*1-3*). In a phase-3 trial involving patients with advanced *RET*-mutant medullary thyroid cancer, the most common adverse events during selpercatinib treatment were hypertension (42.5%), dry mouth (31.6%), diarrhea, and elevated alanine aminotransferase levels. Adverse events led to dose reductions in 38.9% and dose interruptions in 56.0% of patients receiving selpercatinib (*3*). Additionally, chylous effusions, a newly identified treatment-related adverse event, have been reported to occur in a dose-dependent manner in patients with *RET*-mutant thyroid cancer receiving selpercatinib (*4*).

As selpercatinib is metabolized by cytochrome P450 (CYP)3A, its pharmacokinetics are affected by CYP3A inhibitors or inducers (*5,6*). Furthermore, the blood levels of selpercatinib decrease when it is coadministered with drugs that increase intragastric pH, such as proton pump inhibitors (*6*). Whereas the dosage of selpercatinib in children is based on body surface area, no such regimen exists for adults, which leads to possible variations in blood levels depending on body size (*6*). To the best of our knowledge, no studies have examined the association between the blood levels of selpercatinib and its efficacy or adverse events. Given the multiple factors influencing selpercatinib blood levels, we hypothesized that establishing a therapeutic drug monitoring (TDM) system for selpercatinib could help reduce adverse events and optimize efficacy. Therefore, we aimed to develop a method for measuring selpercatinib blood levels to enable TDM in clinical practice.

Currently, only liquid chromatography-tandem mass spectrometry (LC-MS/MS) methods have been reported for selpercatinib quantitation in human plasma (*7*). LC-MS/MS enables rapid, accurate, and sensitive drug quantitation across various biological matrices; however, its high cost and maintenance requirements limit its accessibility in hospitals. High-performance liquid chromatography (HPLC) is more affordable than LC-MS/MS and therefore suitable for routine clinical use. Hence, we developed a high-performance liquid chromatography-ultraviolet (HPLC-UV)-based method for quantifying selpercatinib in human plasma.

2. Materials and Methods

2.1. Reagents and chemicals

Selpercatinib and gefitinib (internal standard, IS) were obtained from MedChemExpress (Monmouth Junction, NJ, USA) and Tokyo Chemical Industry Co., Ltd. (Tokyo, Japan), respectively (Figure 1). HPLC-grade acetonitrile, methanol, distilled water (Kanto Chemical Co., Inc., Tokyo, Japan), dimethyl sulfoxide (Fujifilm Wako, Osaka, Japan), and KH_2PO_4 (Fujifilm Wako, Osaka, Japan) were used to prepare the HPLC mobile phase and stock/working solutions. Human plasma (pooled) collected with ethylenediaminetetraacetic acid (EDTA)-2Na was purchased from Cosmo Bio Co., Ltd. (Tokyo, Japan).

2.2. Equipment and chromatographic conditions

The chromatography system consisted of a Jasco HPLC instrument (Tokyo, Japan) equipped with a pump (PU-4180), a UV detector (UV-4075), and an autosampler (AS-4550). Chromatographic separation was achieved on a Capcell Pak C18 MG II (Osaka Soda, Tokyo, Japan) reversed-phase column (250 mm × 4.6 mm i.d.) with a Capcell Pak C18 MG II guard column (10 mm × 4.0 mm; Osaka Soda, Tokyo, Japan) at ambient temperature. The mobile phase, a mixture of 0.5% KH_2PO_4 (pH 4.5) and acetonitrile (70:30, v/v), was delivered at a flow rate of 1.0 mL/min over a 15 min run. UV detection was performed at 240 nm.

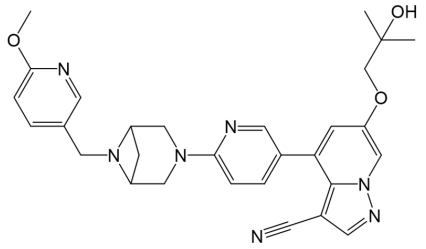

Selpercatinib

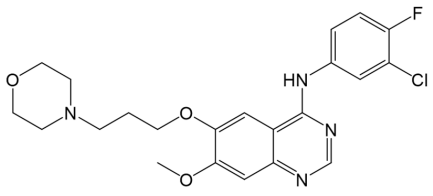

Gefitinib

Figure 1. Chemical structures of selpercatinib and gefitinib.

2.3. Preparation of stock and working solutions

Selpercatinib and IS stock solutions were prepared in dimethyl sulfoxide at a concentration of 1 mg/mL. The selpercatinib stock solution was further diluted with acetonitrile to obtain working solutions with concentrations of 2.5, 5.0, 12.5, 20, 30, and 40 µg/mL. The IS stock solution was diluted with acetonitrile to a working concentration of 10 µg/mL. All stock and working solutions were aliquoted and stored at − 60°C in the dark.

2.4. Sample preparation

Prior to analysis, human plasma and working solutions were thawed and vortexed. A protein precipitation procedure was used to extract selpercatinib and the IS. Blank plasma (50 µL) was spiked with selpercatinib (10 µL), vortexed for 5 s, supplemented with the IS (10 µL) and acetonitrile (180 µL) at − 20°C, and revortexed for 1 min. Subsequently, the sample was centrifuged at 15,000 *g* for 10 min at 4°C, and 10 µL of the supernatant was directly injected into the HPLC system for analysis (Figure 2).

2.5. Specificity

Samples collected from six lots of human plasma were analyzed to determine whether the endogenous matrix of these plasmas eluted near the retention time of selpercatinib or the IS.

2.6. Calibration curves

Accuracy and linearity were evaluated by analyzing a set of standards with concentrations of 0.5-8.0 µg/mL. Precision and accuracy were assessed using samples spiked with selpercatinib at concentrations of 0.5, 1.0, 2.5, 4.0, 6.0, and 8.0 µg/mL.

2.7. Recovery

Recovery was evaluated by comparing the levels of selpercatinib extracted from control plasma samples of the six abovementioned concentrations with those obtained for saline.

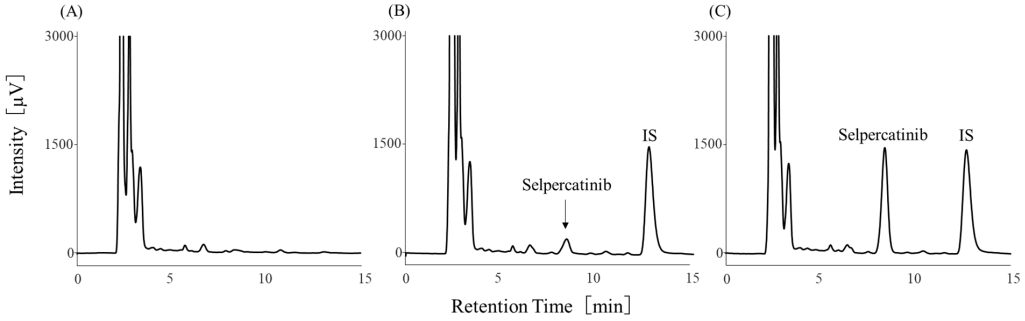

Figure 2. Chromatograms of (A) blank plasma, (B) plasma containing selpercatinib at 0.5 μg/mL, and (C) plasma containing selpercatinib at 4.0 μg/mL.

Table 1. Intra- and interday accuracy and precision of our method

Theoretical selpercatinib concentration (μg/mL)	Intraday (n = 5)			Interday (n = 5)			Recovery (%)
	Detected mean ± SD (μg/mL)	CV (%)	Accuracy (%)	Detected mean ± SD (μg/mL)	CV (%)	Accuracy (%)	
0.5	0.56 ± 0.01	2.08	12.60	0.54 ± 0.02	2.80	7.50	96.51
1.0	0.99 ± 0.02	2.24	−1.50	0.99 ± 0.02	1.53	−1.32	94.43
2.5	2.52 ± 0.06	2.42	0.67	2.48 ± 0.03	1.33	−0.90	96.80
4	4.00 ± 0.06	1.62	−0.02	3.99 ± 0.05	1.35	−0.30	97.30
6	5.94 ± 0.13	2.20	−1.05	5.95 ± 0.04	0.60	−0.87	96.71
8	8.07 ± 0.18	2.22	0.91	8.00 ± 0.11	1.33	−0.05	96.33

CV, coefficient of variation; SD, standard deviation.

Table 2. Stability analysis results (n = 5)

Theoretical selpercatinib concentration (μg/mL)	Stability condition (%)			
	Benchtop mean ± SD	Short-term (24 h) mean ± SD	Long-term (three months) mean ± SD	Freeze and thaw mean ± SD
0.5	99.13 ± 5.95	103.60 ± 5.96	104.71 ± 6.55	105.81 ± 4.29
4.0	95.84 ± 1.67	97.98 ± 1.41	100.26 ± 2.73	98.09 ± 1.13
8.0	97.45 ± 1.28	96.65 ± 0.81	101.12 ± 1.34	99.09± 0.93

2.8. Stability

Analyte stability in human plasma was tested at three different concentrations (0.5, 4.0, and 8.0 μg/mL). For (i) bench-top, (ii) short-term, (iii) long-term, and (iv) freeze-thaw stability evaluations, the samples were stored for (i) 6 h at 22°C, (ii) 4°C for 24 h, and (iii) one month at − 60°C and (iv) subjected to three cycles of freezing at − 60°C or below and thawing at 22°C. The samples were analyzed using a calibration curve prepared with a freshly spiked analyte, and the obtained concentrations were compared with the nominal values.

3. Results and Discussion

We developed an HPLC-UV method to quantify selpercatinib in human plasma, following the analytical validation guidelines of the US Food and Drug Administration. To the best of our knowledge, selpercatinib concentrations in human plasma have previously been determined only using LC-MS/MS (*7*), which is prone to ion suppression and may misinterpret samples containing multiple drugs with similar masses (*8*). Moreover, the high cost and limited availability of LC-MS/MS in general hospitals motivated us to establish an alternative HPLC-UV method.

In our method, linear calibration curves for selpercatinib were obtained over a range of 0.5-8.0 μg/mL. The six-point selpercatinib standard calibration curve was expressed as $y = 0.2464x + 0.0071$ (r^2 = 0.9996). Table 1 lists the intra- and interday coefficients of variation (CVs) and accuracies, with all CVs lying below 2.80%. The intra- and interday accuracies ranged from − 1.50% to 12.60% and − 1.32% to 7.50%, respectively. Protein precipitation with acetonitrile resulted in a high recovery of > 94.43%, whereas no recovery data were provided by Gulikers *et al.* (*7*). The results of stability testing (Table 2) demonstrated

quantifiable results for each concentration (0.5, 4.0, and 8.0 μg/mL) under various clinical conditions.

The representative chromatograms of blank human plasma (Figure 2A) indicated that selpercatinib and the IS were well separated from the coextracted materials under the employed chromatographic conditions, with the respective retention times equaling 8.3 and 12.6 min. No interference from endogenous plasma components was observed at these retention times (Figures 2B and 2C). Additionally, the analysis of six plasma lots confirmed the absence of matrix effects near selpercatinib and IS retention times. The analysis time (15 min) and plasma volume (50 μL) of our method minimally exceed those of a previously reported LC-MS/MS method (9.5 min and 20 μL, respectively) (*7*).

Selpercatinib is administered orally at 160 mg twice daily and has a half-life of 32 h, with the average steady-state C_{max} [coefficient of variation (CV%)] equaling 2,980 (53%) ng/mL (*6*). Unlike the LC-MS/MS method, which can measure plasma concentrations of 50-5,000 ng/mL (*7*), our method has a quantitation limit of 50 ng/mL but is still suitable for assessing plasma concentrations in patients receiving selpercatinib, as selpercatinib trough levels in clinical practice range from 1000 to 4000 ng/mL.

Medullary thyroid cancer is a malignant tumor primarily driven by *RET* gene mutations, particularly in advanced cases with the *RET* M918T mutation (*9*). The plasma inhibitory concentration (IC_{90}) of selpercatinib for the *RET* M918T mutation is 1.1 μg/mL (*10*), suggesting that a trough plasma concentration of ≥ 1.1 μg/mL could serve as a target therapeutic range for selpercatinib. However, the relationship between adverse events and trough or peak plasma concentrations remains unclear.

This study has certain limitations. *RET* fusions are present in a variety of malignancies, including 1-2% of lung cancers, 10-20% of papillary thyroid cancers, and rarely in other solid tumors (*11*). Consequently, our method was not be used to evaluate selpercatinib levels in patient samples. Additionally, we did not assess the selectivity of this method with respect to concomitant medications or their metabolites in patients on selpercatinib. Future studies should confirm selectivity in clinical samples from patients treated with selpercatinib.

In conclusion, we have developed a HPLC-UV method for determining selpercatinib in human plasma. Future studies will examine plasma samples from selpercatinib-treated patients and use the proposed method to investigate the relationships among plasma concentration, efficacy, and adverse events to define the therapeutic target concentration range.

Funding: None.

Conflict of Interest: The authors have no conflicts of interest to disclose.

References

1. Drilon A, Oxnard GR, Tan DSW, *et al*. Efficacy of selpercatinib in *RET* fusion-positive non-small-cell lung cancer. N Engl J Med. 2020; 383:813-824.
2. Wirth LJ, Sherman E, Robinson B, *et al*. Efficacy of selpercatinib in RET-altered thyroid cancers. N Engl J Med. 2020; 383:825-835.
3. Hadoux J, Elisei R, Brose MS, *et al*. Phase 3 trial of selpercatinib in advanced RET-mutant medullary thyroid cancer. N Engl J Med. 2023; 16:1851-1861.
4. Prete A, Gambale C, Cappagli V, Bottici V, Rossi P, Caciagli M, Papini P, Taddei D, Ortori S, Gabbrielli L, Celi A, Materazzi G, Elisei R, Matrone A. Chylous effusions in advanced medullary thyroid cancer patients treated with selpercatinib. Eur J Endocrinol. 2022; 187:905-915.
5. Wang Y, Sparidans RW, Potters S, Şentürk R, Lebre MC, Beijnen JH, Schinkel AH. P-Glycoprotein (ABCB1/MDR1) and BCRP (ABCG2) limit brain accumulation and cytochrome P450-3A (CYP3A) restricts oral exposure of the RET inhibitor selpercatinib (RETEVMO). Pharmaceuticals (Basel). 2021; 14:1087.
6. US Food and Drug Administration (FDA). RETEVMO (selpercatinib) capsules, for oral use. Prescribing information. *https://www.accessdata.fda.gov/drugsatfda_docs/label/2022/213246s008lbl.pdf* (accessed October 1, 2024)
7. Gulikers JL, van Veelen AJ, Sinkiewicz EMJ, de Beer YM, Slikkerveer M, Stolk LML, Tjan-Heijnen VCG, Hendriks LEL, Croes S, van Geel RMJM. Development and validation of an HPLC–MS/MS method to simultaneously quantify brigatinib, lorlatinib, pralsetinib and selpercatinib in human K2-EDTA plasma. Biomed Chromatogr. 2023; 37:e5628.
8. Sauvage FL, Gaulier JM, Lachâtre G, Marquet P. Pitfalls and prevention strategies for liquid chromatography-tandem mass spectrometry in the selected reaction-monitoring mode for drug analysis. Clin Chem. 2008; 54:1519-1527.
9. Romei C, Ciampi R, Casella F, Tacito A, Torregrossa L, Ugolini C, Basolo F, Materazzi G, Vitti P, Elisei R. RET mutation heterogeneity in primary advanced medullary thyroid cancers and their metastases. Oncotarget. 2018; 9:9875-9884.
10. Subbiah V, Velcheti V, Tuch BB, *et al*. Selective RET kinase inhibition for patients with RET-altered cancers. Ann Oncol. 2018; 29:1869-1876.
11. Stransky N, Cerami E, Schalm S, Kim JL, Lengauer C. The landscape of kinase fusions in cancer. Nat Commun. 2014; 5:4846.

Received November 2, 2024; Revised November 28, 2024; Accepted December 3, 2024.

**Address correspondence to:*
Takeo Yasu, Department of Medicinal Therapy Research, Education and Research Unit for Comprehensive Clinical Pharmacy, Meiji Pharmaceutical University, 2-522-1, Noshio, Kiyose, Tokyo 204-8588, Japan.
E-mail: yasutakeo-tky@umin.ac.jp

Released online in J-STAGE as advance publication December 8, 2024.

Brief Report

DOI: 10.5582/ddt.2024.01077

Expression of *c-fos* in cortical neuron cultures under dynamic magnetic field is not suppressed by calcium channel blockers

Takashi Shibata[1,2,*], Daisuke Ihara[3], Yuji Kirihara[4], Tohru Yagi[4], Akiko Tabuchi[3], Satoshi Kuroda[1]

[1] Department of Neurosurgery, University of Toyama, Japan;
[2] Department of Neurosurgery, Toyama Nishi General Hospital, Japan;
[3] Laboratory of Molecular Neurobiology, Graduate School of Medicine and Pharmaceutical Sciences, University of Toyama, Toyama, Japan;
[4] Department of Mechanical Engineering, Institute of Science Tokyo, Tokyo, Japan.

SUMMARY Previously, we developed a dynamic magnetic field (DMF) device using neodymium magnets that induced *c-fos* expression in cortical neurons, while *activity-regulated cytoskeleton-associated protein* (*Arc*), and *brain-derived neurotrophic factor* (*BDNF*) remained unaffected. The precise signal transduction pathway for *c-fos* induction under DMF was unclear. This study aimed to investigate the mechanism of immediate early gene (IEG) induction using calcium channel blockers (CCBs). Six experiments were conducted with cortical neurons, employing an NMDA receptor antagonist and an L-type voltage-dependent calcium channel blocker as CCBs. Neuronal cultures were exposed to DMF, CCBs, or both, and IEG expression (*Arc*, *c-fos*, *BDNF*) was measured through polymerase chain reaction. Results showed a tendency for increased *c-fos* expression with DMF exposure, which was unaffected by CCBs. In contrast, *Arc* and *BDNF* were not induced under DMF exposure but were significantly inhibited by CCBs. These findings suggest that *c-fos* induction under DMF involves a distinct pathway, potentially relevant to stress resistance and drug discovery.

Keywords dynamic magnetic field, immediate early gene, cortical neurons, calcium channel blockers, *c-fos*

1. Introduction

We developed a dynamic magnetic field (DMF) device based on Arago's disc principle (*1,2*). This DMF device, using a rotating magnet, generates both electromagnetic and Lorentz forces (Figure 1). When rat cortical neurons were cultured under DMF with rotating neodymium magnets, *c-fos* expression was induced, while a transcription factor; *activity-regulated cytoskeleton-associated protein* (*Arc*), and *brain-derived neurotrophic factor* (*BDNF*) were not (*2*). This selective induction suggests a distinct signaling pathway for *c-fos*, though the physiological mechanism remains unclear.

c-fos functions as a marker for neuronal activation (*3*) and is essential for neuronal excitability and survival (*4*). Its molecular evolution might contribute to stress resistance, such as from heat shock and ultraviolet (UV) irradiation (*5,6*), as well as to the establishment of long-term memory in engram cells (*7*). *c-fos* acts as a signaling hub, playing a central role in both calcium-dependent and calcium-independent pathways, including the cyclic adenosine monophosphate (cAMP)-dependent protein kinase A (PKA)-activated cAMP response element-binding protein (CREB) and the stress-responsive p38 pathways (*8,9*). Understanding the unique signaling pathways of *c-fos* not only helps unravel the evolution from ancestral neurons to engram neurons but also holds potential for new drug discovery, enhancing neuronal survival, growth, and stress resistance.

In this study, to investigate *c-fos*'s unique signaling pathway, we examined the induction of immediate early genes (IEGs) in primary cortical neurons using calcium channel blockers (CCBs), N-methyl-D-aspartate (NMDA) receptor antagonist amino-5-phosphonovaleric acid (APV), and the L-type voltage-dependent calcium channel (VDCC) blocker (nicardipine). This research explores the distinct DMF response pathway in cortical neurons that might contribute to *c-fos* expression.

2. Materials and Methods

2.1. DMF exposure system

The device comprises a stand for holding a cell culture container, a rotating component made of acrylic resin with a circular surface embedded with permanent

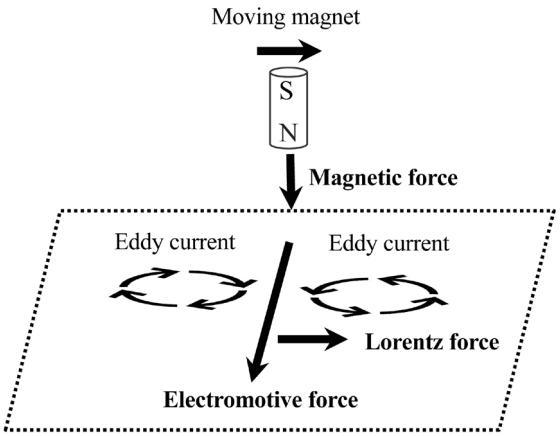

Figure 1. Principle of Arago's Disk through Dynamic Magnetic Field (DMF) exposure. When a magnet approaches an object, such as a neuron, the magnetic force arising from its magnetic flux induces electromotive force, leading to the flow of eddy currents. This process also generates mechanical force within the neuron.

magnets (NeoMag Co., Ltd., Tokyo, Japan) and a control device to manage the motor mounted at the center of the rotating part, as previously described (*2*). The dish stand, made of aluminum, has a 35.5 mm hole that fits a 35 mm diameter dish. The height of the stand is adjustable to ensure the dish does not touch the magnets. In our experiment, we set the minimum distance between the dish and the magnets to 3 mm. The circular surface includes ten rectangular neodymium magnets evenly spaced from the center, with their N poles facing the dish. The surface exhibits a magnetic flux density of 484 mT (length 40 × width 6 × height 11 mm, magnetization direction along the 11mm dimension). The circular surface is driven by a Direct-current (DC) motor (Pololu Co., Ltd, USA: item #4863, 20.4:1 metal gearmotor 25 Depth x65 Length mm Motor Power 12 Volt with 48 count per revolution encoder), controlled by a microcontroller (Arduino CC, Italy: Arduino Uno R3) and a motor driver (Pololu Co., Ltd, USA : Dual TB9051FTG Motor Driver Shield for Arduino) to regulate the motor speed. Speed is controlled using PID (proportional, integral, differential) control, by supplying voltage to the motor, measuring the speed, and adjusting the target RPM (revolutions per minute) every 0.3 seconds to achieve the desired speed. The ten default magnets on the circular surface correspond to low speed (30.0 rpm), middle speed (60 rpm), and high speed (240 rpm), with the speed adjustment knob set to achieve frequencies of 5 Hz, 10 Hz, and 40 Hz, respectively. These speeds can be modified to expose cells to frequencies in the delta band (0.5-4 Hz), theta band (4-8 Hz), alpha band (8-13 Hz), beta band (14-30 Hz), gamma band (30-80 Hz), and high-frequency band above 80 Hz.

2.2. DMF exposure

Primary cultures of cortical neurons were obtained from Sprague-Dawley rats at embryonic day 17 and cultured until day 10 (Japan SLC, Shizuoka, Japan), following the method detailed by previous papers (*2,10*). The preparation and treatment of these cells were conducted under the University of Toyama's Animal Care and Experimentation Committee guidelines, approval number A2022PHA-6. In brief, the cerebral cortex was extracted from embryonic brains, treated with trypsin and DNase I, and the resulting dissociated cells were seeded at a density of 2.0×10^6 cells on poly-L-lysine (PLL) coated dishes (AGC Techno Glass Co., Ltd., Shizuoka, Japan) for Reverse Transcription Polymerase Chain Reaction (RT-PCR). Half of the culture medium was refreshed every 3 days. PLL, a positively charged synthetic polymer, enhances cell adhesion by attracting negatively charged molecules on the cell surface.

This research comprised 6 experiments with a total of 24 dish samples. Each experiment involved 4 conditions: a vehicle control condition, a condition treated with the NMDA receptor antagonist (APV) and the L-type calcium channel blocker nicardipine (Nica), a no-magnetic-exposure control condition, and a condition exposed to a DMF. Gene expression was evaluated immediately after 3 consecutive days of exposure, comparing 4 groups: vehicle condition without DMF, vehicle condition with DMF, APV + Nica without DMF, and APV + Nica with DMF. The APV + Nica exposure (APV: 200 μM, Nica: 5 μM) was administered 10 minutes before the first day of DMF exposure.

Preliminary experiments showed that γ-band (40 Hz) exposure for 6 hours per day suppressed the effect (data not shown). Hence, the neurons were exposed to a rotating magnetic field of 484 mT at 40 Hz for 1 hour daily over 3 consecutive days. The exposure setup was inside an incubator (MCO-5AC-PJ. PHC Co., Ltd., Tokyo, Japan) with controlled temperature (37°C), humidity (95%), and CO_2 concentration (10%). A microcomputer-controlled the rotation speed of the magnetic disks outside the incubator.

The study focused on the expression of IEGs such as *c-fos, Arc*, and *BDNF* (exon IV-IX and CDS), which are activity-dependent and essential for neuronal morphology and function (*11*). Gene expressions were normalized to *glyceraldehyde-3-phosphate dehydrogenase* (*GAPDH*), a stable housekeeping gene. RT-PCR procedures and primer sequences for *c-fos*, *Arc*, *BDNF* exon IV-IX, *BDNF* CDS, and *GAPDH* are described as previous paper (*2*).

2.3. Statistical analysis

All data are presented as the median (interquartile range). Statistical analyses were performed using BellCurve for Excel version 4.05 (Social Survey Research Information Co., Ltd.). The expression levels of IEGs in cultured cortical neurons were compared using one-way analysis of variance (ANOVA) followed by Bonferroni's multiple comparisons test for *c-fos*, *Arc*, *BDNF* CDS, and *BDN*F

exon IV-IX. This comparison assessed the increase in IEGs due to DMF exposure and the suppression of IEGs due to CCBs exposure. Differences with a *P*-value < 0.05 were considered statistically significant.

3. Results and Discussion

In this study, primary cultured rat cortical neurons were exposed to a rotating neodymium magnet for three consecutive days, one hour per day, under continuous 40 Hz DMF exposure. The results showed that the group median and interquartile range of *c-fos* mRNA expression without DMF was 6.6 (3.4-9.4) (E-3/GAPDH), compared to 7.6 (5.6-15.7) (E-3/GAPDH) with DMF. For *Arc* mRNA, the group median and interquartile range without DMF were 9.2 (4.9-23) (E-4/GAPDH), and 14.5 (7.9-23) (E-4/GAPDH) with DMF. *BDNF* gene expression analysis focused on *BDNF* exon IV-IX mRNA, regulated in a neuronal activity-dependent manner, and *BDNF* CDS (*12,13*). The group median and interquartile range of *BDNF* CDS mRNA expression without DMF was 16.3 (9.2-25) (E-3/GAPDH) and 15.8 (11.8-31.6) (E-3/GAPDH) with DMF. For *BDNF* exon IV-IX mRNA, the group median and interquartile range were 4.4 (1.8-6.2) (E-3/GAPDH) without DMF, and 5.2 (2.4-6.9) (E-3/GAPDH) with DMF.

Comparing IEG expression levels with and without DMF exposure revealed a slight increase in *c-fos* mRNA expression upon DMF exposure, consistent with our previous findings (*2*), though it did not reach statistical significance under stringent Bonferroni multiple comparison testing. *Arc* and *BDNF* mRNA expressions (both CDS and exons IV-IX) did not show increased expression upon DMF exposure, with no significant differences observed.

Under conditions involving CCBs (APV + Nica), median and interquartile ranges for *c-fos* mRNA expression were 5.3 (3.9-11.9) (E-3/GAPDH) without DMF and 5.4 (4.1-16.4) (E-3/GAPDH) with DMF. For *Arc* mRNA, the group median and interquartile range were 4.1 (2-8.5) (E-4/GAPDH) without DMF and 5.1 (2.8-7.5) (E-4/GAPDH) with DMF. *BDNF* CDS mRNA expression showed median and interquartile ranges of 5.3 (4.7-8.8) (E−3/GAPDH) without DMF and 6 (4.4-9.5) (E−3/GAPDH) with DMF. Lastly, *BDNF* exon IV-IX mRNA expression was 7.1 (5-13.4) (E-4/GAPDH) without DMF and 7.8 (3.8-12.7) (E-4/GAPDH) with DMF. No significant induction of *c-fos* mRNA, *Arc* mRNA, or *BDNF* mRNA (both CDS and exons IV-IX) was detected with DMF exposure (Bonferroni multiple comparison test, $P > 0.05$). However, when exposed to CCBs, *Arc* mRNA and *BDNF* mRNA (both CDS and exons IV-IX) were significantly inhibited (Bonferroni multiple comparison test, $P < 0.05$), while *c-fos* mRNA was not significantly affected (Bonferroni multiple comparison test, $P > 0.05$) (Figure 2).

In this study, two major findings were revealed. 1) Slight induction of *c-fos* mRNA by DMF exposure: Cultured cortical neurons exposed to DMF showed a slight increase in *c-fos* mRNA expression. This pattern was reproducible and consistent with previous our study (*2*). However, no corresponding increase in the expression of *Arc* or *BDNF* (both CDS and exon IV-IX) was observed under DMF exposure. 2) Differential

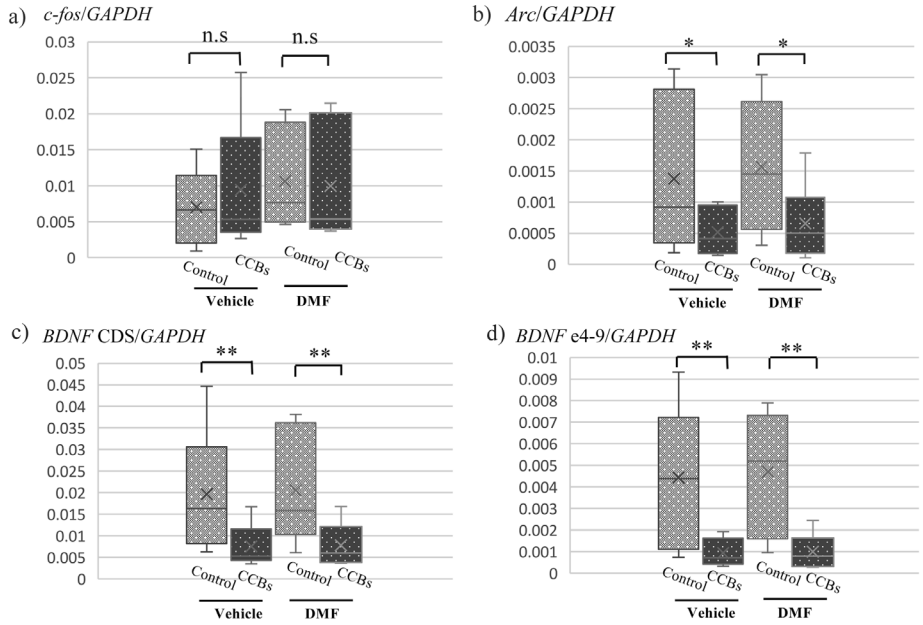

Figure 2. Inhibitory effect of calcium blockers (CCBs: APV + Nica) on the expression of immediate early genes (IEGs) under vehicle conditions or dynamic magnetic fields (DMF) conditions. a) *c-fos* mRNA b) *Arc* mRNA c) *BDNF* CDS mRNA d) *BDNF* e4-9 mRNA. The box plots exhibit the normalized group median and quartile range of IEGs in cultured cortical cells. The Y-axis represents the IEG mRNA normalized to *GAPDH*. Error bars indicate the maximum and minimum values. Statistical significance denoted by asterisks (*) (**) indicates *P*-values less than 0.05, and *P*-values less than 0.01, respectively, based on the Bonferroni multiple comparison test.

effects on gene expression by CCBs under DMF: Under DMF exposure with CCBs, *Arc* mRNA and *BDNF* mRNA (both CDS and exon IV-IX) were significantly inhibited, while *c-fos* mRNA was not. These results suggest that the selective induction of *c-fos* under DMF is different from the calcium signaling pathways required for *Arc* and *BDNF* expression and might play a different role, such as in stress resilience, distinct from the roles of *Arc* and *BDNF* in neuronal plasticity and maturation.

The hypothetical pathway of *c-fos* induction in a DMF environment is summarized in Figure 3. Induction of *c-fos* mRNA is usually promoted by calcium influx through NMDA receptors and voltage-dependent calcium channels (*14*). However, since *c-fos* mRNA expression was not inhibited under NMDA receptor antagonist and L-type calcium channel blocker exposure in this study, alternative pathways of *c-fos* induction need to be investigated. Potential *c-fos* signaling pathways include calcium-dependent pathways through T-type channels or Transient receptor potential (TRP) channels, or calcium-independent pathways through cAMP/PKA/CREB or p38 stress pathways (*8,9*). T-type VDCC are known for low-threshold pacemaker activity and have been reported to induce mesenchymal stem cell proliferation under a static magnetic field (*15*). Additionally, TRP channels, which respond to environmental stimuli such as temperature and mechanical forces (*16*), might also respond to stress from DMF as they detect environmental stress.

The evolutionary significance of *c-fos* is not yet fully understood. Unlike pseudogenes that evolve rapidly due to neutral mutations (*17*), genes expressed in the brain evolve slowly under selective pressure (*18,19*). The stability of the *c-fos* gene might arise from forming a stable activator protein-1 (AP-1) complex with c-Jun, reducing its sensitivity to mutational pressure during adaptive evolution (*20*). Therefore, *c-fos* has been repeatedly utilized for various functions by serving as a master switch that could convert short-term responses to long-term responses (*21*), controlling cell proliferation, apoptosis, and deoxyribonucleic acid (DNA) repair (Figure 3). During the evolution from unicellular to multicellular organisms 600-950 million years ago, *c-fos* might have played a role similar to tumor suppressor genes that promote multicellularity (*22,23*). Under environmental selective pressures such as UV radiation (*6*), gravity (*24*), *c-fos* might have evolved to enhance stress resistance in early eukaryotic cells and help neurons adapt to environmental challenges. Increased levels of *c-fos* expression might also confer stress resistance, as demonstrated by increased resilience in mice with high levels of Fos protein (*25*). Therefore, *c-fos* induction might contribute to stress resistance, especially under extreme environmental conditions.

There are several limitations to this study: 1) The underlying mechanism of slight *c-fos* induction under DMF exposure remains unknown. In the DMF device, we hypothesized the presence of voltage-dependent, mechanical force, and magnetic-dependent ion channels

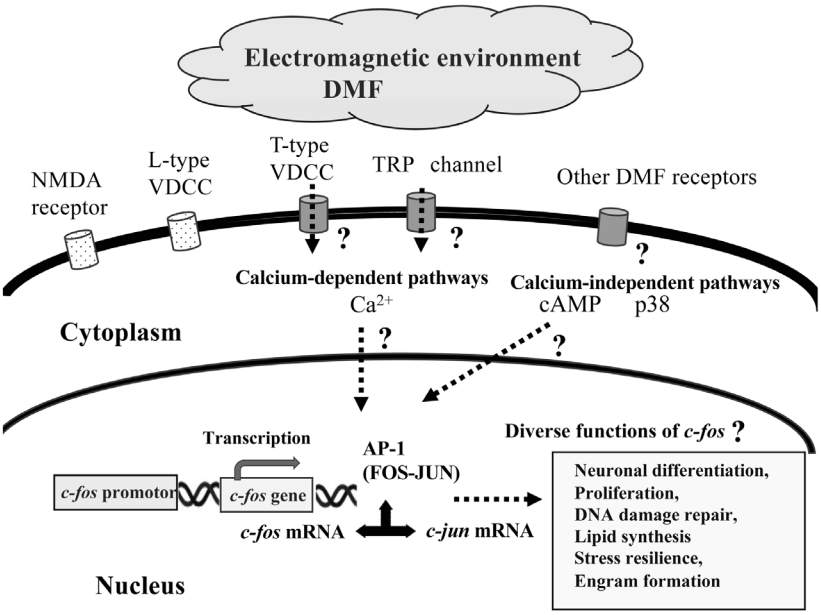

Figure 3. The hypothetical pathway of c-fos induction in a DMF environment. The transduction pathway responsible for inducing *c-fos* in the DMF environment might involve mechanisms beyond the calcium-dependent pathway through L-type voltage-dependent calcium channels and NMDA receptors. Instead, hypothetical transduction pathways, such as other calcium-dependent pathways (*e.g.*, T-type VDCC, TRP channels) or calcium-independent pathways (*e.g.*, cAMP, p38), might exist. These pathways could potentially contribute to the acquisition of diverse and significant functions by the c-*fos* gene during neuronal evolution in electromagnetic environments. Abbreviations: DMF: dynamic magnetic field, TRP: transient receptor potential, NMDA: N-methyl-D-aspartate, VDCC: voltage-dependent calcium channel. The question mark (?) indicates an unresolved issue.

as DMF sensors (*2*), but no ion channels activated by DMF have been discovered, and the physiological mechanisms of DMF effects on neurons are unclear. 2) The magnetic field strength used in this study (484 mT) was much stronger than the geomagnetic field (30-50 μT). Therefore, it is necessary to investigate the strength, frequency, and exposure duration of the DMF that could induce both *Arc* and *BDNF*, which are more beneficial for neurons. Neurons could mature into engram cells by inducing *Arc* mRNA, which is essential for the formation of neural circuits, synaptic plasticity, and memory retention (26,27), and *BDNF*, which supports neuronal survival and synaptic complexity (*28,29*).

Many animals, from honeybees and salmon to migratory birds, utilize geomagnetic field for navigation (*30*). However, little is known about the effects of geomagnetic field on the evolution of neurons. In the future, by using this device to expose neurons to a DMF environment (approximately 30-50 μT) for an extended period, it might be possible to elucidate how neurons adapt to such conditions. Understanding the *c-fos* induction signaling pathways in neurons under DMF conditions is crucial for comprehending how neurons have evolved in electromagnetic field (*i.e.* brainwave) environments. Furthermore, elucidating the signaling pathways involved in these processes could contribute to the discovery of various drugs that enhance stress resistance and promote synaptic maturation.

Acknowledgements

We thank Professor Hisao Nishijo, Faculty of Human Sciences, University of East Asia, Yamaguchi, Japan for their warm support throughout this research.

Funding: This study was supported by Grants-in-Aid from the Research Center for Idling Brain Science, University of Toyama, Japan.

Conflict of Interest: The authors have no conflicts of interest to disclose.

References

1. Arago F. Ceuvres Completes De Francois Arago, Paris: Gide et J. Baudry. 1856; 4:424. (in French)
2. Shibata T, Ihara D, Kirihara Y, Yagi T, Tabuchi A, Kuroda S. Enhancing *c-fos* mRNA expression in primary cortical cell cultures with a dynamic magnetic fields device. IEEJ Trans Electr Electron Eng. 2023; 29:1932-1938.
3. Barth AL, Gerkin RC, Dean KL. Alteration of neuronal firing properties after *in vivo* experience in a FosGFP transgenic mouse. J Neurosci. 2004; 24:6466-6475.
4. Zhang J, Zhang D, McQuade JS, Behbehani M, Tsien JZ, Xu M. c-fos regulates neuronal excitability and survival. Nat Genet. 2002; 30:416-420.
5. Chen C, Xie Y, Stevenson MA, Auron PE, Calderwood SK. Heat shock factor 1 represses Ras-induced transcriptional activation of the *c-fos* gene. J Biol Chem. 1997; 272:26803-26806.
6. Haas S, Kaina B. c-Fos is involved in the cellular defence against the genotoxic effect of UV radiation. Carcinogenesis. 1995; 16:985-991.
7. Miyashita T, Kikuchi E, Horiuchi J, Saitoe M. Long-term memory engram cells are established by c-Fos/CREB transcriptional cycling. Cell Rep. 2018; 25:2716-2728.
8. Schuck S, Soloaga A, Schratt G, Arthur JS, Nordheim A. The kinase MSK1 is required for induction of c-fos by lysophosphatidic acid in mouse embryonic stem cells. BMC Mol Biol. 2003; 4:6.
9. Guan R, Lv J, Xiao F, Tu Y, Xie Y, Li L. Potential role of the cAMP/PKA/CREB signalling pathway in hypoxic preconditioning and effect on propofol-induced neurotoxicity in the hippocampus of neonatal rats. Mol Med Rep. 2019; 20:1837-1845.
10. Fukuchi M, Tabuchi A, Kuwana Y, Watanabe S, Inoue M, Takasaki I, Izumi H, Tanaka A, Inoue R, Mori H, Komatsu H, Takemori H, Okuno H, Bito H, Tsuda M. Neuromodulatory effect of Gαs- or Gαq-coupled G-protein-coupled receptor on NMDA receptor selectively activates the NMDA receptor/Ca^{2+}/calcineurin/cAMP response element-binding protein-regulated transcriptional coactivator 1 pathway to effectively induce brain-derived neurotrophic factor expression in neurons. J Neurosci. 2015; 35:5606-5624.
11. Okuno H. Regulation and function of immediate-early genes in the brain: beyond neuronal activity markers. Neurosci Res. 2011; 69:175-186.
12. Timmusk T, Palm K, Metsis M, Reintam T, Paalme V, Saarma M, Persson H. Multiple promoters direct tissue-specific expression of the rat *BDNF* gene. Neuron. 1993; 10:475-489.
13. Tao X, Finkbeiner S, Arnold DB, Shaywitz AJ, Greenberg ME. Ca^{2+} influx regulates BDNF transcription by a CREB family transcription factor-dependent mechanism. Neuron. 1998; 20:709-726.
14. Lara Aparicio SY, Laureani Fierro ÁJ, Aranda Abreu GE, Toledo Cárdenas R, García Hernández LI, Coria Ávila GA, Rojas Durán F, Aguilar MEH, Manzo Denes J, Chi-Castañeda LD, Pérez Estudillo CA. Current opinion on the use of c-Fos in neuroscience. NeuroSci. 2022; 3:687-702.
15. Wu H, Li C, Masood M, Zhang Z, González-Almela E, Castells-Garcia A, Zou G, Xu X, Wang L, Zhao G, Yu S, Zhu P, Wang B, Qin D, Liu J. Static magnetic fields regulate T-type calcium ion channels and mediate mesenchymal stem cells proliferation. Cells. 2022; 11:2460.
16. Zhang M, Ma Y, Ye X, Zhang N, Pan L, Wang B. TRP (transient receptor potential) ion channel family: structures, biological functions and therapeutic interventions for diseases. Signal Transduct Target Ther. 2023; 8:261.
17. Kimura M. The neutral theory of molecular evolution. Cambridge University Press, Cambridge. 1983.
18. Kuma K, Iwabe N, Miyata T. Functional constraints against variations on molecules from the tissue level: slowly evolving brain-specific genes demonstrated by protein kinase and immunoglobulin supergene families. Mol Biol Evol. 1995; 12:123-130.
19. Tuller T, Kupiec M, Ruppin E. Evolutionary rate and gene expression across different brain regions. Genome Biol. 2008; 9:R142.
20. Shah K, Tyagi S. Barriers to transmission of transcriptional

noise in a c-fos c-jun pathway. Mol Syst Biol. 2013; 9:687.
21. Velazquez FN, Caputto BL, Boussin FD. c-Fos importance for brain development. Aging (Albany NY). 2015; 7:1028-1029.
22. Hanschen ER, Marriage TN, Ferris PJ, *et al*. The Gonium pectorale genome demonstrates co-option of cell cycle regulation during the evolution of multicellularity. Nat Commun. 2016;7:11370.
23. Etienne O, D'Astolfo DS, Silvestre DC, Boussin FD, Caputto BL. Brain development is impaired in *c-fos*$^{-/-}$ mice. Oncotarget. 2015; 6:16883-16901.
24. Fuller PM, Jones TA, Jones SM, Fuller CA. Evidence for macular gravity receptor modulation of hypothalamic, limbic and autonomic nuclei. Neuroscience. 2004; 129:461-471.
25. Inaba H, Li H, Kawatake-Kuno A, Dewa KI, Nagai J, Oishi N, Murai T, Uchida S. GPCR-mediated calcium and cAMP signaling determines psychosocial stress susceptibility and resiliency. Sci Adv. 2023; 9:eade5397.
26. Nikolaienko O, Patil S, Eriksen MS, Bramham CR. Arc protein: A flexible hub for synaptic plasticity and cognition. Semin Cell Dev Biol. 2018; 77:33-42.
27. Zhang H, Bramham CR. Arc/Arg3.1 function in long-term synaptic plasticity: Emerging mechanisms and unresolved issues. Eur J Neurosci. 2021; 54:6696-6712.
28. Kirschenbaum B, Goldman SA. Brain-derived neurotrophic factor promotes the survival of neurons arising from the adult rat forebrain subependymal zone. Proc Natl Acad Sci U S A. 1995; 92:210-214.
29. Yamada K, Mizuno M, Nabeshima T. Role for brain-derived neurotrophic factor in learning and memory. Life Sci. 2002; 70:735-744.
30. Lohmann KJ, Goforth KM, Mackiewicz AG, Lim DS, Lohmann CMF. Magnetic maps in animal navigation. J Comp Physiol A Neuroethol Sens Neural Behav Physiol. 2022; 208:41-67.

Received November 5, 2024; Revised November 28, 2024; Accepted December 8, 2024.

**Address correspondence to:*
Takashi Shibata, Department of Neurosurgery, Toyama University Hospital, Japan, 2530 Sugitani, Toyama 930-0194, Japan.
E-mail: sibata@dj8.so-net.ne.jp

Released online in J-STAGE as advance publication December 11, 2024.

Letter to the Editor

DOI: 10.5582/ddt.2024.01081

Clinical characteristics and aetiological analysis of combined central and pulmonary cryptococcal infection: Clinical cases

Yi Su, Yiyi Qian, Qingqing Wang, Yao Zhang, Bijie Hu, Jue Pan

Zhongshan Hospital, Fudan University, Shanghai, China.

SUMMARY This paper presents a summary of seven cases of combined pulmonary and central cryptococcal infection and analyses of their clinical features, treatment and prognosis. No clear correlation was identified between the intracranial cryptococcal capsular antigen titre and either the intracranial pressure or the amount of protein in the cerebrospinal fluid. Pulmonary lesions may develop in any of the lung lobes and manifest in multiple forms. Infection at the central level is predominantly meningitis. As the central cerebrospinal fluid (CSF) capsular antigen titre can be considerably elevated even when serum capsular antigen titres are markedly low, lumbar puncture and subsequent analysis are essential for every case of pulmonary cryptococcal infection. Patients with renal insufficiency or who refused intravenous treatment opted for oral fluconazole therapy, and their prognoses were favourable.

Keywords Pulmonary cryptococcosis, cryptococcal meningitis, imaging characteristics, treatment, prognosis

Letter to the Editor:

Cryptococcosis is a major cause of morbidity and mortality worldwide. *Cryptococcus neoformans* was listed at the top of the WHO fungal pathogens priority list in 2022 (*1*). Cryptococcosis often involves the central nervous system (CNS) or the lungs and can disseminate to any organ.

While numerous studies have examined the clinical characteristics of pulmonary cryptococcosis and central cryptococcosis (*2-5*), cases involving the coexistence of pulmonary and central cryptococcosis warrant further investigation. This paper presents a summary of seven cases of combined pulmonary and central cryptococcosis, allowing an analysis of their clinical features.

Patients were deemed eligible if they were admitted to the Infectious Diseases Department at Zhongshan Hospital, Fudan University, between January 1, 2012, and September 30, 2024. Data regarding patient demographics, clinical features, laboratory results, pathogenic findings, treatments, and outcomes were obtained from the Zhongshan Hospital Information System. This project was approved by the Ethics Committee of Zhongshan Hospital (Ethics approval number B2024-276), and informed consent was obtained from all the subjects or their legal guardians. All research was performed in accordance with relevant guidelines and the Declaration of Helsinki. All the data were reviewed by two physicians (QQW and YS), and any discrepancies in interpretation between the primary reviewers were resolved by a third researcher (JP and BJH). The data that support the findings of this study are available from the corresponding author.

Patients with confirmed and clinical cases of cryptococcosis were included. Confirmed cryptococcosis was identified as a positive *Cryptococcus* culture from any site. Clinical cryptococcosis was identified as positive histopathology or cryptococcal antigen results and clinical or radiographic evidence of disease (*6*). The treatment duration refers to the period between medication initiation to medication discontinuation. Improvement days denote the period between medication initiation and improvements observed on chest imaging and review of lumbar puncture results. The morphological features on CT scans can be categorized as solitary nodules/masses, multiple nodules/masses, consolidation, or diffuse infiltrates (nodules/masses with consolidation) (*5*).

C. neoformans spores or yeast cells are ubiquitous in the environment and are inhaled by immunosuppressed or immunocompromised individuals. The yeast cells become dehydrated and cause respiratory system infections. In the event of a defective immune response, *C. neoformans* can disseminate to various parts of the body, such as the brain, kidney, and bone marrow. Various studies on cryptococcal infection and dissemination indicate that after pulmonary infection, it disseminates to the brain and

can cross the blood-brain barrier (BBB) *via* paracytosis, transcytosis and the Trojan horse strategy (*7,8*).

During our investigation, we identified a single female patient with positive cultures for both pulmonary and intracranial cryptococcal infections. Furthermore, the presence of a *Cryptococcus* infection at multiple sites in two patients without an underlying disease was a cause for concern. No clear correlation was identified between the intracranial cryptococcal capsular antigen titre and either intracranial pressure or amount of protein in the cerebrospinal fluid in this study (Table 1).

The relationship between the *Cryptococcus* capsular antigen assay and intracranial infection has always been worthy of further exploration. According to recent guidelines for managing a *Cryptococcus* infection, lumbar puncture examination for every patient with pulmonary cryptococcosis (*9*). However, in the past 10 years in our Infectious Diseases Department, according to the literature we reviewed, lumbar puncture has not been routinely performed for patients without central nervous system symptoms, with lesions relatively limited to the lung, and with a serum *Cryptococcus* capsular antigen titre ≤ 1:160 (*10*). In the seven patients included in this study, no correlation was detected between the serum and cerebrospinal fluid (CSF) capsular antigen levels. Notably, the central CSF capsular antigen titre can be elevated even when the serum capsular antigen titre is markedly low. Consequently, lumbar puncture and subsequent analysis are necessary for every case of pulmonary cryptococcal infection.

The morphological features on CT scans can be categorized as solitary nodules/masses, multiple nodules/masses, consolidation, or diffuse infiltrates (nodules/masses with consolidation) (*11*). Immunocompetent patients mainly present solitary nodules, whereas immunocompromised patients present multiple nodules/masses, consolidation, or diffuse infiltrates (*12*). In our 7 patients with pulmonary and central cryptococcal infections, lung imaging revealed any of the four forms described above. The main cranial MRI findings were basal meningeal enhancement (44.6%), dilated Virchow–Robin space/pseudocyst, "dirty" cerebrospinal fluid sign, hydrocephalus, acute/subacute cerebral infarct, cryptococcoma, and hazy brain base in HIV-negative adults (*13,14*). Among our 7 patients, one presented with white matter lesions, which are rarely reported in HIV-negative patients, and 5 patients had no brain parenchymal involvement (*15*) (Figure 1).

Compared with CSF samples, lower respiratory tract samples presented less microorganisms. The mNGS positivity rate was higher in lower respiratory tract specimens than in conventional cultures. Conversely, the culture results were more positive in the CSF samples than in the mNGS samples. The sensitivity structure exhibited sensitivity to triazoles and amphotericin B (Figure 2).

Patients 1 and Patient 4 were eventually cured. In

Table 1. Patient characteristics and laboratory indicators

No.	Sex	Age	Underlying disease	WBC (*10^9)	Lymphocytes (*10^9)	CRP (mg/L)	IL_2 (U/mL)	IL_6 (pg/mL)	CD4 (cell/uL)	Serum capsular antigen titre	Titer	Pressure (mmH_2O)	WBC ($/mm^3$)	Sugar (mmol/L)	Chloride (mmol/L)	Protein (g/L)	Other Infections
1	M	67	DM+IgG4+ Autoimmune Pancreatitis	5.26	0.4	18.4	1341	7	385	1:2560	1:2	60	1	10.9	125	0.53	
2	M	33	Kidney Transplant +Hepatitis B	7.73	0.75	17.2	1086	15.4	258	1:80	1:10	130	125	1.7	123	0.51	Cryptococcus Laryngeal Infection
3	M	65	MDS	2.4	1.5	4.8	386	4.8	/	1:320	1:320	300	72	2.9	126	1.7	Pulmonary Acinetobacter Baumannii Infection
4	M	45	DM	6	1	1.5	292	2.8	354	1:1280	1:40	>400	23	3.8	119	0.49	
5	M	47	None	5.13	0.3	5.7	/	/	/	1:2560	1:2560	170	120	2.7	117	3.53	
6	M	47	Antiphospholipid Syndrome	12.38	0.5	8.2	933	5	43	1:10	1:640	190	51	3	121	0.59	Pulmonary Nocardia Infection
7	F	26	None	9.23	2.5	2.7	432	4.3	1066	>1:2560	1:2	170	0	3.8	125	0.18	

WBC: White blood cell count. CRP: highly sensitive C-reactive protein. DM: Diabetes mellitus. MDS: Myelodysplastic Syndrome.

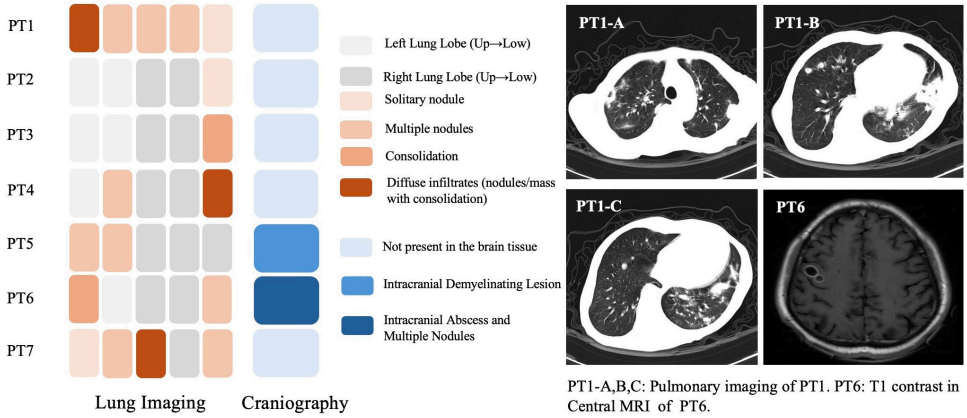

Figure 1. Imaging of pulmonary lesions and intracranial lesions in 7 patients with cryptococcal disease.

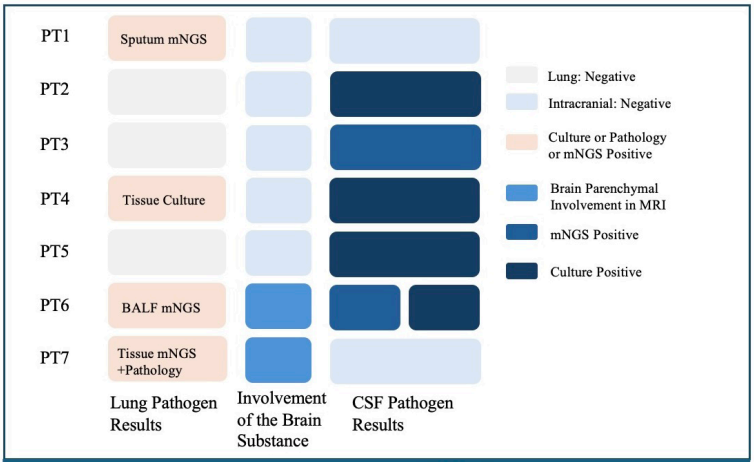

No.	Source of Strain	MIC/RAD				
		Fluconazole	Voriconazole	Itraconazole	Flucytosine	Amphotericin B
2	CSF	4	≤0.125	0.125	≤0.5	≤4
4-1	Lung Tissue	4	≤0.125	0.125	≤0.5	≤4
4-2	CSF	4	≤0.125	0.125	≤0.5	≤4
5	CSF	≤1	≤0.125	≤0.06	≤0.5	≤4
6	CSF	4	≤0.125	≤0.06	≤0.5	≤4

CSF: Cerebrospinal Fluid. MIC: Minimum Inhibitory Concentration.

Figure 2. Microbiological findings and antifungal drug sensitivity results.

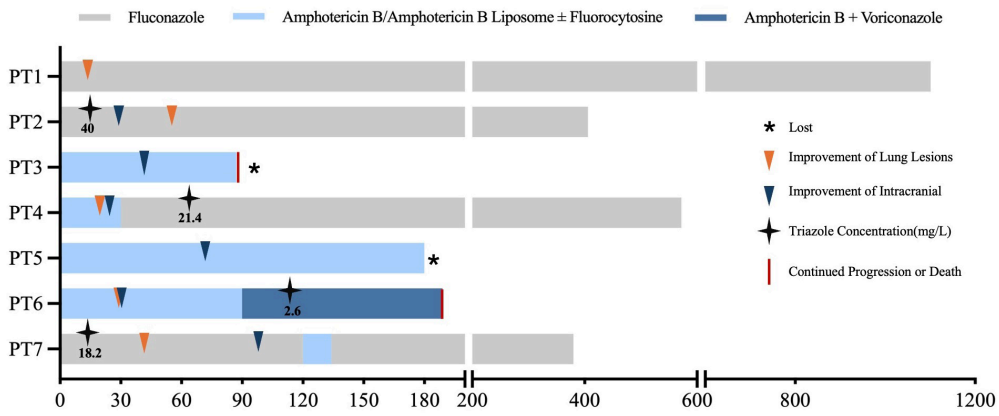

Figure 3. Treatment regimen and duration, time to signs of improvement, drug concentration detection and prognoses.

Patient 2, the fluconazole dosage was adjusted to 0.3 g per day due to the presence of his renal insufficiency, which was administered continuously. Patient 3 was automatically discharged from the hospital because of haematological disorders, a progressive decline in their general condition, and continued progression of lung lesions during the course of the disease. Patient 5 was stable after a six-month period of hospitalization with amphotericin B. He was discharged on oral fluconazole therapy and subsequently lost to follow-up. Patient 6 was successfully treated for cryptococcosis but ultimately died of COVID-19 pneumonia. At the time of this report, Patient 7 has been on medication for 380 days (Figure 3).

According to the guidelines, an intravenous regimen of amphotericin B or liposomal formulations is recommended as the first-line treatment, and oral fluconazole is used as a secondary option (*9,16*). Oral fluconazole may be considered for patients in better overall health because of the prolonged duration of intravenous amphotericin B administration. Three patients with renal insufficiency and who refused intravenous treatment opted for oral fluconazole therapy, and their prognoses were favourable.

Acknowledgements

We would like to thank all the study participants whose data were used in this study. Furthermore, we are most grateful for the assistance and support of clinicians, laboratory technicians and radiologists at Zhongshan Hospital, Fudan University.

Funding: This work was supported by grants from the National Key Research and Development Program of China (2021YFC 2300400) and the Fund of Zhongshan Hospital Fudan University (2021ZSFZ15).

Conflict of Interest: The authors have no conflicts of interest to disclose.

References

1. WHO. WHO fungal priority pathogens list to guide research, development and public health action. Geneva: World Health Organization, 2022.
2. Shokouhi S, Hakamifard A. Meningitis caused by *Cryptococcus neoformans* in an apparently immunocompetent patient. J Investig Med High Impact Case Rep. 2022; 10:23247096221111779.
3. Tugume L, Ssebambulidde K, Kasibante J, Ellis J, Wake RM, Gakuru J, Lawrence DS, Abassi M, Rajasingham R, Meya DB, Boulware DR. Cryptococcal meningitis. Nat Rev Dis Primers. 2023; 9:62.
4. Howard-Jones AR, Sparks R, Pham D, Halliday C, Beardsley J, Chen SC. Pulmonary cryptococcosis. J Fungi (Basel). 2022; 8:1156.
5. Kohno S, Kakeya H, Izumikawa K, Miyazaki T, Yamamoto Y, Yanagihara K, Mitsutake K, Miyazaki Y, Maesaki S, Yasuoka A, Tashiro T, Mine M, Uetani M, Ashizawa K. Clinical features of pulmonary cryptococcosis in non-HIV patients in Japan. J Infect Chemother. 2015; 21:23-30.
6. Baddley JW, Perfect JR, Oster RA, Larsen RA, Pankey GA, Henderson H, Haas DW, Kauffman CA, Patel R, Zaas AK, Pappas PG. Pulmonary cryptococcosis in patients without HIV infection: factors associated with disseminated disease. Eur J Clin Microbiol Infect Dis. 2008; 27:937-943.
7. May RC, Stone NRH, Wiesner DL, Bicanic T, Nielsen K. *Cryptococcus*: from environmental saprophyte to global pathogen. Nat Rev Microbiol. 2016; 14:106-117.
8. Vu K, Eigenheer RA, Phinney BS, Gelli A. *Cryptococcus neoformans* promotes its transmigration into the central nervous system by inducing molecular and cellular changes in brain endothelial cells. Infect Immun. 2013; 81:3139-3147.
9. Chang C, Harrison TS, Bicanic T, *et al*. Global guideline for the diagnosis and management of cryptococcosis: an initiative of the ECMM and ISHAM in cooperation with the ASM. Lancet Infect Dis. 2024; 24:S1473-3099.
10. Gassiep I, Aye C, Armstrong M, Emeto TI, Heather CS, Norton RE. Correlation between serum cryptococcal antigen titre and meningitis in immunocompetent patients. J Med Microbiol. 2018; 67:1515-1518.
11. Bongomin F, Oladele RO, Gago S, Moore CB, Richardson MD. A systematic review of fluconazole resistance in clinical isolates of *Cryptococcus* species. Mycoses. 2018; 61:290-297.
12. Su Y, Zhang Y, Wang Q, Hu B, Pan J. Imaging of pulmonary cryptococcosis with consolidations or diffuse infiltrates suggests longer clinical treatment in non-HIV patients. Biosci Trends. 2024; 18:476-481.
13. Zhang C, Tan Z, Tian F. Impaired consciousness and decreased glucose concentration of CSF as prognostic factors in immunocompetent patients with cryptococcal meningitis. BMC Infect Dis. 2020; 20:69.
14. Tsai WC, Lien CY, Lee JJ, Lin WC, Hsu CW, Huang CR, Tsai NW, Chang CC, Lu CH, Chang WN. The prognostic factors of HIV-negative adult cryptococcal meningitis with a focus on cranial MRI-based neuroimaging findings. J Clin Neurosci. 2018; 55:57-61.
15. Qu J, Lv X. Cryptococcal meningitis in apparently immunocompetent patients. Crit Rev Microbiol. 2024; 50:76-86.
16. Guidelines for the Diagnosis, Prevention and Management of Cryptococcal Disease in HIV-Infected Adults, Adolescents and Children: Supplement to the 2016 Consolidated Guidelines on the Use of Antiretroviral Drugs for Treating and Preventing HIV Infection. World Health Organization; 2018 Mar. PMID: 30285342.

Received November 10, 2024; Revised December 2, 2024; Accepted December 8, 2024.

**Address correspondence to:*
Jue Pan, Zhongshan Hospital, Fudan University, Shanghai 200032, China.
E-mail: pjzjzy@163.com

Released online in J-STAGE as advance publication December 11, 2024.

DD&T
Drug Discoveries & Therapeutics

Guide for Authors

1. Scope of Articles

Drug Discoveries & Therapeutics (Print ISSN 1881-7831, Online ISSN 1881-784X) welcomes contributions in all fields of pharmaceutical and therapeutic research such as medicinal chemistry, pharmacology, pharmaceutical analysis, pharmaceutics, pharmaceutical administration, and experimental and clinical studies of effects, mechanisms, or uses of various treatments. Studies in drug-related fields such as biology, biochemistry, physiology, microbiology, and immunology are also within the scope of this journal.

2. Submission Types

Original Articles should be well-documented, novel, and significant to the field as a whole. An Original Article should be arranged into the following sections: Title page, Abstract, Introduction, Materials and Methods, Results, Discussion, Acknowledgments, and References. Original articles should not exceed 5,000 words in length (excluding references) and should be limited to a maximum of 50 references. Articles may contain a maximum of 10 figures and/or tables. Supplementary Data are permitted but should be limited to information that is not essential to the general understanding of the research presented in the main text, such as unaltered blots and source data as well as other file types.

Brief Reports definitively documenting either experimental results or informative clinical observations will be considered for publication in this category. Brief Reports are not intended for publication of incomplete or preliminary findings. Brief Reports should not exceed 3,000 words in length (excluding references) and should be limited to a maximum of 4 figures and/or tables and 30 references. A Brief Report contains the same sections as an Original Article, but the Results and Discussion sections should be combined.

Reviews should present a full and up-to-date account of recent developments within an area of research. Normally, reviews should not exceed 8,000 words in length (excluding references) and should be limited to a maximum of 10 figures and/or tables and 100 references. Mini reviews are also accepted, which should not exceed 4,000 words in length (excluding references) and should be limited to a maximum of 5 figures and/or tables and 50 references.

Policy Forum articles discuss research and policy issues in areas related to life science such as public health, the medical care system, and social science and may address governmental issues at district, national, and international levels of discourse. Policy Forum articles should not exceed 3,000 words in length (excluding references) and should be limited to a maximum of 5 figures and/or tables and 30 references.

Case Reports should be detailed reports of the symptoms, signs, diagnosis, treatment, and follow-up of an individual patient. Case reports may contain a demographic profile of the patient but usually describe an unusual or novel occurrence. Unreported or unusual side effects or adverse interactions involving medications will also be considered. Case Reports should not exceed 3,000 words in length (excluding references).

Communications are short, timely pieces that spotlight new research findings or policy issues of interest to the field of global health and medical practice that are of immediate importance. Depending on their content, Communications will be published as "Comments" or "Correspondence". Communications should not exceed 1,500 words in length (excluding references) and should be limited to a maximum of 2 figures and/or tables and 20 references.

Editorials are short, invited opinion pieces that discuss an issue of immediate importance to the fields of global health, medical practice, and basic science oriented for clinical application. Editorials should not exceed 1,000 words in length (excluding references) and should be limited to a maximum of 10 references. Editorials may contain one figure or table.

News articles should report the latest events in health sciences and medical research from around the world. News should not exceed 500 words in length.

Letters should present considered opinions in response to articles published in *Drug Discoveries & Therapeutics* in the last 6 months or issues of general interest. Letters should not exceed 800 words in length and may contain a maximum of 10 references. Letters may contain one figure or table.

3. Editorial Policies

For publishing and ethical standards, *Drug Discoveries & Therapeutics* follows the Recommendations for the Conduct, Reporting, Editing, and Publication of Scholarly Work in Medical Journals issued by the International Committee of Medical Journal Editors (ICMJE, *https://icmje.org/recommendations*), and the Principles of Transparency and Best Practice in Scholarly Publishing jointly issued by the Committee on Publication Ethics (COPE, *https://publicationethics.org/resources/guidelines-new/principles-transparency-and-best-practice-scholarly-publishing*), the Directory of Open Access Journals (DOAJ, *https://doaj.org/apply/transparency*), the Open Access Scholarly Publishers Association (OASPA, *https://oaspa.org/principles-of-transparency-and-best-practice-in-scholarly-publishing-4*), and the World Association of Medical Editors (WAME, *https://wame.org/principles-of-transparency-and-best-practice-in-scholarly-publishing*).

Drug Discoveries & Therapeutics will perform an especially prompt review to encourage innovative work. All original research will be subjected to a rigorous standard of peer review and will be edited by experienced copy editors to the highest standards.

Ethical Approval of Studies and Informed Consent: For all manuscripts reporting data from studies involving human participants or animals, formal review and approval, or formal review and waiver, by an appropriate institutional review board or ethics committee is required and should be described in the Methods section. When your manuscript contains any case details, personal information and/or images of patients or other individuals, authors must obtain appropriate written consent, permission and release in order to comply with all applicable laws and regulations concerning privacy and/or security of personal information. The consent form needs to comply with the relevant legal requirements of your particular jurisdiction, and please do not send signed consent form to *Drug Discoveries & Therapeutics* to respect your patient's and any other individual's privacy. Please instead describe the information clearly in the Methods (patient consent) section of your manuscript while retaining copies of the signed forms in the event they should be needed. Authors should also state that the study conformed to the provisions of the Declaration of Helsinki (as revised in 2013, *https://wma.net/what-we-do/medical-ethics/declaration-of-helsinki*). When reporting experiments on animals, authors should indicate whether the institutional and national guide for the care and use of laboratory animals was followed.

Reporting Clinical Trials: The ICMJE (*https:// icmje.org/recommendations/browse/publishing-and-editorial-issues/clinical-trial-registration.html*) defines a clinical trial as any research project that prospectively assigns people or a group of people to an intervention, with or without concurrent comparison or control groups, to study the relationship between a health-related intervention and a health outcome. Registration of clinical trials in a public trial registry

at or before the time of first patient enrollment is a condition of consideration for publication in *Drug Discoveries & Therapeutics*, and the trial registration number will be published at the end of the Abstract. The registry must be independent of for-profit interest and publicly accessible. Reports of trials must conform to CONSORT 2010 guidelines (*https://consort-statement.org/consort-2010*). Articles reporting the results of randomized trials must include the CONSORT flow diagram showing the progress of patients throughout the trial.

Conflict of Interest: All authors are required to disclose any actual or potential conflict of interest including financial interests or relationships with other people or organizations that might raise questions of bias in the work reported. If no conflict of interest exists for each author, please state "There is no conflict of interest to disclose".

Submission Declaration: When a manuscript is considered for submission to *Drug Discoveries & Therapeutics*, the authors should confirm that 1) no part of this manuscript is currently under consideration for publication elsewhere; 2) this manuscript does not contain the same information in whole or in part as manuscripts that have been published, accepted, or are under review elsewhere, except in the form of an abstract, a letter to the editor, or part of a published lecture or academic thesis; 3) authorization for publication has been obtained from the authors' employer or institution; and 4) all contributing authors have agreed to submit this manuscript.

Initial Editorial Check: Immediately after submission, the journal's managing editor will perform an initial check of the manuscript. A suitable academic editor will be notified of the submission and invited to check the manuscript and recommend reviewers. Academic editors will check for plagiarism and duplicate publication at this stage. The journal has a formal recusal process in place to help manage potential conflicts of interest of editors. In the event that an editor has a conflict of interest with a submitted manuscript or with the authors, the manuscript, review, and editorial decisions are managed by another designated editor without a conflict of interest related to the manuscript.

Peer Review: *Drug Discoveries & Therapeutics* operates a single-anonymized review process, which means that reviewers know the names of the authors, but the authors do not know who reviewed their manuscript. All articles are evaluated objectively based on academic content. External peer review of research articles is performed by at least two reviewers, and sometimes the opinions of more reviewers are sought. Peer reviewers are selected based on their expertise and ability to provide quality, constructive, and fair reviews. For research manuscripts, the editors may, in addition, seek the opinion of a statistical reviewer. Every reviewer is expected to evaluate the manuscript in a timely, transparent, and ethical manner, following the COPE guidelines (*https://publicationethics.org/files/cope-ethical-guidelines-peer-reviewers-v2_0.pdf*). We ask authors for sufficient revisions (with a second round of peer review, when necessary) before a final decision is made. Consideration for publication is based on the article's originality, novelty, and scientific soundness, and the appropriateness of its analysis.

Suggested Reviewers: A list of up to 3 reviewers who are qualified to assess the scientific merit of the study is welcomed. Reviewer information including names, affiliations, addresses, and e-mail should be provided at the same time the manuscript is submitted online. Please do not suggest reviewers with known conflicts of interest, including participants or anyone with a stake in the proposed research; anyone from the same institution; former students, advisors, or research collaborators (within the last three years); or close personal contacts. Please note that the Editor-in-Chief may accept one or more of the proposed reviewers or may request a review by other qualified persons.

Language Editing: Manuscripts prepared by authors whose native language is not English should have their work proofread by a native English speaker before submission. If not, this might delay the publication of your manuscript in *Drug Discoveries & Therapeutics*.

The Editing Support Organization can provide English proofreading, Japanese-English translation, and Chinese-English translation services to authors who want to publish in *Drug Discoveries & Therapeutics* and need assistance before submitting a manuscript. Authors can visit this organization directly at *https://www.iacmhr.com/iac-eso/support.php?lang=en. IAC-ESO* was established to facilitate manuscript preparation by researchers whose native language is not English and to help edit works intended for international academic journals.

Copyright and Reuse: Before a manuscript is accepted for publication in *Drug Discoveries & Therapeutics*, authors will be asked to sign a transfer of copyright agreement, which recognizes the common interest that both the journal and author(s) have in the protection of copyright. We accept that some authors (*e.g.*, government employees in some countries) are unable to transfer copyright. A JOURNAL PUBLISHING AGREEMENT (JPA) form will be e-mailed to the authors by the Editorial Office and must be returned by the authors by mail, fax, or as a scan. Only forms with a hand-written signature from the corresponding author are accepted. This copyright will ensure the widest possible dissemination of information. Please note that the manuscript will not proceed to the next step in publication until the JPA Form is received. In addition, if excerpts from other copyrighted works are included, the author(s) must obtain written permission from the copyright owners and credit the source(s) in the article.

4. Cover Letter

The manuscript must be accompanied by a cover letter prepared by the corresponding author on behalf of all authors. The letter should indicate the basic findings of the work and their significance. The letter should also include a statement affirming that all authors concur with the submission and that the material submitted for publication has not been published previously or is not under consideration for publication elsewhere. The cover letter should be submitted in PDF format. For an example of Cover Letter, please visit: Download Centre (*https://www.ddtjournal.com/downcentre)*.

5. Submission Checklist

The Submission Checklist should be submitted when submitting a manuscript through the Online Submission System. Please visit Download Centre (*https://www.ddtjournal.com/downcentre)* and download the Submission Checklist file. We recommend that authors use this checklist when preparing your manuscript to check that all the necessary information is included in your article (if applicable), especially with regard to Ethics Statements.

6. Manuscript Preparation

Manuscripts are suggested to be prepared in accordance with the "Recommendations for the Conduct, Reporting, Editing, and Publication of Scholarly Work in Medical Journals", as presented at *http://www.ICMJE.org*.

Manuscripts should be written in clear, grammatically correct English and submitted as a Microsoft Word file in a single-column format. Manuscripts must be paginated and typed in 12-point Times New Roman font with 24-point line spacing. Please do not embed figures in the text. Abbreviations should be used as little as possible and should be explained at first mention unless the term is a well-known abbreviation (*e.g.* DNA). Single words should not be abbreviated.

Title page: The title page must include 1) the title of the paper (Please note the title should be short, informative, and contain the major key words); 2) full name(s) and affiliation(s) of the author(s), 3) abbreviated names of the author(s), 4) full name, mailing address, telephone/fax numbers, and e-mail address of the corresponding author; 5) author contribution statements to specify the individual contributions of all authors to this manuscript, and 6) conflicts of interest (if you have an actual or potential conflict of interest to disclose, it must be included as a footnote on the title page of the manuscript; if no conflict of interest

exists for each author, please state "There is no conflict of interest to disclose").

Abstract: The abstract should briefly state the purpose of the study, methods, main findings, and conclusions. For article types including Original Article, Brief Report, Review, Policy Forum, and Case Report, a one-paragraph abstract consisting of no more than 250 words must be included in the manuscript. For Communications, Editorials, News, or Letters, a brief summary of main content in 150 words or fewer should be included in the manuscript. For articles reporting clinical trials, the trial registration number should be stated at the end of the Abstract. Abbreviations must be kept to a minimum and non-standard abbreviations explained in brackets at first mention. References should be avoided in the abstract. Three to six key words or phrases that do not occur in the title should be included in the Abstract page.

Introduction: The introduction should provide sufficient background information to make the article intelligible to readers in other disciplines and sufficient context clarifying the significance of the experimental findings.

Materials/Patients and Methods: The description should be brief but with sufficient detail to enable others to reproduce the experiments. Procedures that have been published previously should not be described in detail but appropriate references should simply be cited. Only new and significant modifications of previously published procedures require complete description. Names of products and manufacturers with their locations (city and state/country) should be given and sources of animals and cell lines should always be indicated. All clinical investigations must have been conducted in accordance with the Declaration of Helsinki (as revised in 2013, *https://wma.net/what-we-do/medical-ethics/declaration-of-helsinki*). All human and animal studies must have been approved by the appropriate institutional review board(s) and a specific declaration of approval must be made within this section.

Results: The description of the experimental results should be succinct but in sufficient detail to allow the experiments to be analyzed and interpreted by an independent reader. If necessary, subheadings may be used for an orderly presentation. All Figures and Tables should be referred to in the text in order, including those in the Supplementary Data.

Discussion: The data should be interpreted concisely without repeating material already presented in the Results section. Speculation is permissible, but it must be well-founded, and discussion of the wider implications of the findings is encouraged. Conclusions derived from the study should be included in this section.

Acknowledgments: All funding sources (including grant identification) should be credited in the Acknowledgments section. Authors should also describe the role of the study sponsor(s), if any, in study design; in the collection, analysis, and interpretation of data; in the writing of the report; and in the decision to submit the paper for publication. If the funding source had no such involvement, the authors should so state.

In addition, people who contributed to the work but who do not meet the criteria for authors should be listed along with their contributions.

References: References should be numbered in the order in which they appear in the text. Citing of unpublished results, personal communications, conference abstracts, and theses in the reference list is not recommended but these sources may be mentioned in the text. In the reference list, cite the names of all authors when there are fifteen or fewer authors; if there are sixteen or more authors, list the first three followed by *et al*. Names of journals should be abbreviated in the style used in PubMed. Authors are responsible for the accuracy of the references. The EndNote Style of *Drug Discoveries & Therapeutics* could be downloaded at **EndNote** (*https://www.ddtjournal.com/examples/Drug_Discoveries_Therapeutics.ens*).

Examples are given below:

Example 1 (Sample journal reference):

Nakata M, Tang W. Japan-China Joint Medical Workshop on Drug Discoveries and Therapeutics 2008: The need of Asian pharmaceutical researchers' cooperation. Drug Discov Ther. 2008; 2:262-263.

Example 2 (Sample journal reference with more than 15 authors):

Darby S, Hill D, Auvinen A, *et al*. Radon in homes and risk of lung cancer: Collaborative analysis of individual data from 13 European case-control studies. BMJ. 2005; 330:223.

Example 3 (Sample book reference):

Shalev AY. Post-traumatic stress disorder: Diagnosis, history and life course. In: Post-traumatic Stress Disorder, Diagnosis, Management and Treatment (Nutt DJ, Davidson JR, Zohar J, eds.). Martin Dunitz, London, UK, 2000; pp. 1-15.

Example 4 (Sample web page reference):

World Health Organization. The World Health Report 2008 – primary health care: Now more than ever. *https://apps.who.int/iris/handle/10665/43949* (accessed September 23, 2022).

Tables: All tables should be prepared in Microsoft Word or Excel and should be arranged at the end of the manuscript after the References section. Please note that tables should not in image format. All tables should have a concise title and should be numbered consecutively with Arabic numerals. If necessary, additional information should be given below the table.

Figure Legend: The figure legend should be typed on a separate page of the main manuscript and should include a short title and explanation. The legend should be concise but comprehensive and should be understood without referring to the text. Symbols used in figures must be explained. Any individually labeled figure parts or panels (A, B, *etc*.) should be specifically described by part name within the legend.

Figure Preparation: All figures should be clear and cited in numerical order in the text. Figures must fit a one- or two-column format on the journal page: 8.3 cm (3.3 in.) wide for a single column, 17.3 cm (6.8 in.) wide for a double column; maximum height: 24.0 cm (9.5 in.). Please make sure that artwork files are in an acceptable format (TIFF or JPEG) at minimum resolution (600 dpi for illustrations, graphs, and annotated artwork, and 300 dpi for micrographs and photographs). Please provide all figures as separate files. Please note that low-resolution images are one of the leading causes of article resubmission and schedule delays.

Units and Symbols: Units and symbols conforming to the International System of Units (SI) should be used for physicochemical quantities. Solidus notation (*e.g*. mg/kg, mg/mL, mol/mm^2/min) should be used. Please refer to the SI Guide *www.bipm.org/en/si/* for standard units.

Supplemental data: Supplemental data might be useful for supporting and enhancing your scientific research and *Drug Discoveries & Therapeutics* accepts the submission of these materials which will be only published online alongside the electronic version of your article. Supplemental files (figures, tables, and other text materials) should be prepared according to the above guidelines, numbered in Arabic numerals (*e.g*., Figure S1, Figure S2, and Table S1, Table S2) and referred to in the text. All figures and tables should have titles and legends. All figure legends, tables and supplemental text materials should be placed at the end of the paper. Please note all of these supplemental data should be provided at the time of initial submission and note that the editors reserve the right to limit the size

and length of Supplemental Data.

7. Online Submission

Manuscripts should be submitted to *Drug Discoveries & Therapeutics* online at *https://www.ddtjournal.com/login*. Receipt of your manuscripts submitted online will be acknowledged by an e-mail from Editorial Office containing a reference number, which should be used in all future communications. If for any reason you are unable to submit a file online, please contact the Editorial Office by e-mail at *office@ddtjournal.com*

8. Accepted Manuscripts

Page Charge: Page charges will be levied on all manuscripts accepted for publication in *Drug Discoveries & Therapeutics* (Original Articles / Brief Reports / Reviews / Policy Forum / Communications: $140 per page for black white pages, $340 per page for color pages; News / Letters: a total cost of $600). Under exceptional circumstances, the author(s) may apply to the editorial office for a waiver of the publication charges by stating the reason in the Cover Letter when the manuscript online.

Misconduct: *Drug Discoveries & Therapeutics* takes seriously all allegations of potential misconduct and adhere to the ICMJE Guideline (*https://icmje.org/recommendations*) and COPE Guideline (*https://publicationethics.org/files/Code_of_conduct_for_journal_editors.pdf*). In cases of suspected research or publication misconduct, it may be necessary for the Editor or Publisher to contact and share submission details with third parties including authors' institutions and ethics committees. The corrections, retractions, or editorial expressions of concern will be performed in line with above guidelines.

(As of December 2022)

Drug Discoveries & Therapeutics
Editorial and Head Office
Pearl City Koishikawa 603,
2-4-5 Kasuga, Bunkyo-ku,
Tokyo 112-0003, Japan.
E-mail: office@ddtjournal.com